INVESTIGATION OF HERPES SIMPLEX-1 LATENCY IN VIVO AND IN VITRO

Sándor Dósa

Ph. D. Thesis

Szeged

2016

Supervisor:
Dr. Valéria Endrész, Ph.D.

Department of Medical Microbiology and Immunobiology, Faculty of Medicine, University of Szeged
Department of Pathology, College of Medicine, University of Illinois at Chicago
Department of Pathology, Faculty of Medicine, University of Szeged

Publications directly related to the subject of the dissertation

I. Valyi-Nagy K, **Dósa S**, Kovacs SK, Bacsa S, Voros A, Shukla D, Folberg R, Valyi-Nagy T. Identification of virus resistant tumor cell subpopulations in three-dimensional uveal melanoma cultures. Cancer Gene Ther., 17(4):223-234 (2010)

IF: 3.74

II. **Dósa S**, Castellanos K, Bacsa S, Gagyi E, Kovacs SK, Valyi-Nagy K, Shukla D, Dermody TS, Valyi-Nagy T. Chronic progressive deficits in neuron size, density and number in the trigeminal ganglia of mice latently infected with herpes simplex virus. Brain Pathol., 21(5):583-593 (2011)

IF: 3.99

Other publications

I. Rakonczay Z Jr, Hegyi P, **Dósa S**, Ivanyi B, Jarmay K, Biczo G, Hracsko Z, Varga IS, Karg E, Kaszaki J, Varro A, Lonovics J, Boros I, Gukovsky I, Gukovskaya AS, Pandol SJ, Takacs T. A new severe acute necrotizing pancreatitis model induced by L-ornithine in rats. Critical Care Medicine, 36(7):2117-2127 (2008)

IF: 6.59

II. Kovacs SK, Tiwari V, Prandovszky E, **Dosa S**, Bacsa S, Valyi-Nagy K, Shukla D, Valyi-Nagy T. Expression of herpesvirus entry mediator (HVEM) in the cornea and trigeminal ganglia of normal and HSV-1 infected mice. Current Eye Research, 34:896-904 (2009)

IF: 1.51

III. Biczó G, Hegyi P, Sinervirta R, Berczi S, **Dósa S**, Siska A, Iványi B, Venglovecz V, Takács T, Alhonen L, Rakonczay Z Jr. Characterization of polyamine homeostasis in l-ornithine-induced acute pancreatitis in rats. Pancreas, 39(7):1047-1056 (2010)

IF: 2.60

IV. Biczó G, Hegyi P, Berczi S, **Dósa S**, Hracskó Z, Varga IS, Iványi B, Venglovecz V, Wittmann T, Takács T, Rakonczay Z Jr. Inhibition of arginase activity ameliorates L-arginine-induced acute pancreatitis in rats. Pancreas, 39(6):868-874 (2010)

IF: 2.60

V. Bacsa S, Karasneh G, **Dósa S**, Liu J, Valyi-Nagy T, Shukla D. Syndecan-1 and syndecan-2 play key roles in herpes simplex virus type-1 infection. J Gen Virol, 92(Pt 4):733-743 (2011)

IF: 3.36

VI. Biczó G, Hegyi P, **Dósa S**, Balla Z, Venglovecz V, Iványi B, Wittmann T, Takács T, Rakonczay Z Jr. Aliphatic, but not imidazole, basic amino acids cause severe acute necrotizing pancreatitis in rats. Pancreas, 40(3):486-487 (2011)

IF: 2.38

VII. Biczó G, Hegyi P, **Dósa S**, Shalbuyeva N, Berczi S, Sinervirta R, Hracskó Z, Siska A, Kukor Z, Jármay K, Venglovecz V, Varga IS, Iványi B, Alhonen L, Wittmann T, Gukovskaya A, Takács T, Rakonczay Z. The Crucial Role of Early Mitochondrial Injury in L-Lysine-Induced Acute Pancreatitis. Antioxid Redox Signal, 15(10):2669-81 (2011)

IF: 8.45

VIII. Pallagi P, Balla Z, Singh AK, **Dósa S**, Iványi B, Kukor Z, Tóth A, Riederer B, Liu Y, Engelhardt R, Jármay K, Szabó A, Janovszky A, Perides G, Venglovecz V, Maléth J, Wittmann T, Takács T, Gray MA, Gácser A, Hegyi P, Seidler U, Rakonczay Z Jr. The Role of Pancreatic Ductal Secretion in Protection against Acute Pancreatitis in Mice. Crit Care Med., (2013)

IF: 6.1

TABLE OF CONTENTS

List of abbreviations

ANOVA	analysis of variance
BHK	baby hamster kidney cells
BSA	bovine serum albumin
CNS	central nervous system
C918	Human primary uveal melanoma cells of high invasive potential
DMEM	Dulbecco's modified Eagle's medium
EMEM	Eagle's Minimal Essential Medium
ECM	extracellular matrix
GFP	green fluorescence protein
HSE	herpes simplex encephalitis
HSV-1	herpes simplex virus type 1
HSV-2	herpes simplex virus type 2
LATs	latency-associated transcripts
mAbs	monoclonal antibodies
M.O.I.	multiplicity of infection
OCM1	Human primary uveal melanoma cells of low invasive potential
pAbs	polyclonal antibodies
PBS	phosphate buffered saline
P.F.U.	plaque forming unit
p.i.	post infection
P/S	penicillin/streptomycin
SD	standard deviation
TG	trigeminal ganglia
wt	wild type

1. INTRODUCTION

Amongst human diseases caused by pathogen microorganisms, viral pathogens play a significant part. From clinical point of view, a viral infection can follow different patterns in time. An acute infection generally means that the infected individual shows symptoms which last a short period – generally few days/weeks – and after that the infective virus is eliminated completely by the host´s immune system. A chronic or persistent infection in general can be defined as an infection that is present in a given individual for a long time interval. The presence of the virus can be theoretically equilibrial, increasing, decreasing or intermittent. However, these clinical aspects describe only the time course but does not define the under lying mechanisms behind these events. It is important to notice that the same virus can cause divergent patterns in different individuals [1].

On the cellular level a viral infection can be abortive when some viral components are synthesized but no infective virus is assembled and/or released. An infection is defined productive when new infectious viruses are produced. This results generally in the death of the host cell while a large amount of the newly formed viruses are spread towards the surroundings and stand ready for a new infection. This type of infection called lytic infection results in the lysis of infected cells due to production of viral progeny. The vast majority of the viruses possess only this lytic life cycle, the best examples are the influenza viruses causing seasonal cold and the rotaviruses causing gastrointestinal infections [1].

However, there are some viral families and species which have the ability to maintain a different route in the lifecycle. In this case there is no immediate lysis of the host cells. The viral genome can exist in the host cell for a longer period of time, sometimes for a lifetime and can persist even during the host cell´s replication. The characteristic hallmark of this type of viral cycle is the reversibility where under certain circumstances the expression of the viral genome can be activated resulting in the productive lytic cycle. This different way in the life cycle called latent (dormant) life cycle or infection [2]. The establishment of this latent infection depends on various factors of the host, including the immunological status which is crucial in determining whether latency shall be the outcome of the primary infection, as well as how often a probable subsequent reactivation occurs.

The clinical and epidemiological significance of viral latency is highly important since this type of infection serves as potential reservoir from which dissemination of the pathogen to a new host can occur. On the other hand, such infections could play a role in the development of some human malignant and benign tumors and thirdly, because the

reactivation of the latent virus might cause acute or chronic progressive disorders in the original host [2].

This type of "carrier state" can take different forms. During latency, the viral genome can exist as a provirus integrated in the host genome, called proviral latency. In this form of latency the viral genome does not replicate directly, but is passively duplicated when the host cell divides. The proviral latency appears frequently in cells with the potential for persistent proliferation [3]. Another form of latency is known as the episomal latency, where viral genes are floating in the cytoplasm or in the nucleus of the host cell as distinct objects and the genetic material can form either linear or circular plasmid structures without the integration into the genome of the host cell. The episomal latency can occur even in cells with limited self-renewing potential and long life expectancy. Both types of latency have advantages and disadvantages for the virus. In case of proviral latency, the passive replication of the viral genome is beneficial but during the entry into the nucleus the viral genome must face and avoid several defense mechanisms that are activated against it by the host cell. During episomal latency the effect of dilution could represent a problem in proliferating cells and vital genes are more exposed to ribozymes and to the antiviral defensive pathways of the host in the cytoplasm and/or in the nucleoplasm.

The possible consequences of latency show divergent patterns. The most common form of the outcome is the reactivation following different, yet not clearly characterized activator signals (i.e. stress, sunlight) to cause an acute infection and production of viral progeny. A less frequent but more severe consequence is the transformation of the latently infected cell which results in a virus induced formation of malignant or benign tumors. The transformation can be caused by viral gene products which may exert their effect by interfering with particular cellular proteins or by insertional mutagenesis [4]. Some of the most extensively studied virus families known to maintain latency include *Adenoviridae, Parvoviridae, Retroviridae, Papillomaviridae, Polyomaviridae* and *Herpesviridae* among others.

The family of *Herpesviridae* forms a large and diverse group that includes a considerable number of animal viruses. Herpesviruses can cause infections in vertebrates from catfish to humans. Furthermore one species has been discovered in invertebrates (Pacific oyster) [5]. *Herpesviridae* show a broad range of pathogenic properties and can cause from mild to life-threatening disorders. Based on their biological properties the family of *Herpesviridae* can be further divided into the three subfamilies of *Alphaherpesvirinae, Betaherpesvirinae,* and *Gammaherpesvirinae* [5, 6].

Herpesviruses are defined based on morphological criteria. They share a common structure of an icosahedral capsid, containing 162 capsomeres, the tegument which is a layer consisting of 22 proteins that surrounds the capsid and a lipid bilayer envelope derived from the host cell membrane in which most cell proteins have been replaced by viral membrane proteins. As a core they contain a large, linear, double-stranded DNA genome [6, 7] (Fig. 1).

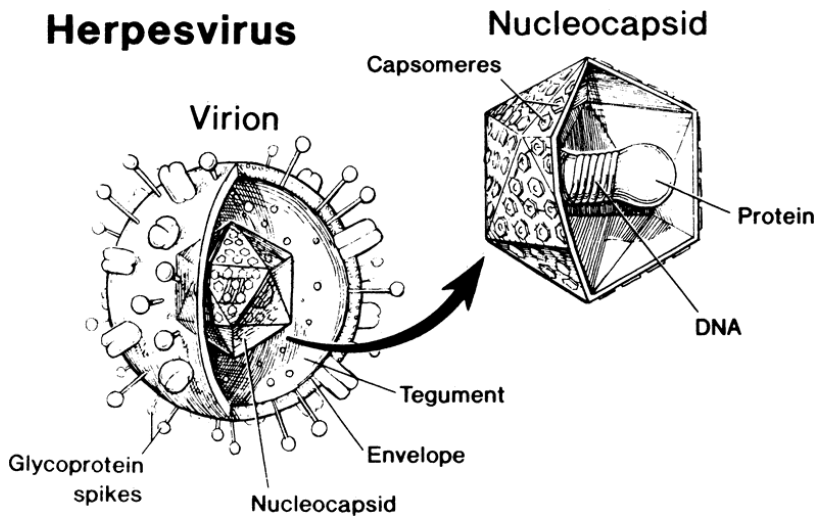

Figure 1. The schematic morphology and structure of herpes viruses [8].

The herpes simplex viruses (HSV): type-1 (HSV-1) and type-2 (HSV-2) belong to the *Alphaherpesvirinae* subfamily of the *Herpesviridae* family, which are defined by their ability to form a relatively short reproductive cycle, rapidly spread in culture, efficiently destruct infected cells and by the capacity to establish latent infections primarily – but not exclusively – in sensory ganglia [9].

The HSV-1 – which was the subject of our investigations – is a neurotropic virus that establishes latency in sensory neurons innervating the site of primary infection and has the capacity to sustain a life-long latent infection and it can also be reactivated from those neurons in a periodical manner [10].

Regarding HSV-1 the primary site of infection is generally the oronasal mucosa, the primary infection is often acquired in early childhood. The infection is frequently asymptomatic, but it may present as vesicles on the mucosa and finally form ulcers at the site of the infected area [11, 12]. Following a productive infection of the epithelial cells, the virus enters the terminal axons and the nucleocapsid is transported to the nucleus of the neuron by

retrograde axonal transport. Once the virus reaches the ganglia where the bodies of the neurons reside either lytic or latent pathway of viral gene expression is triggered [13] (Fig. 2).

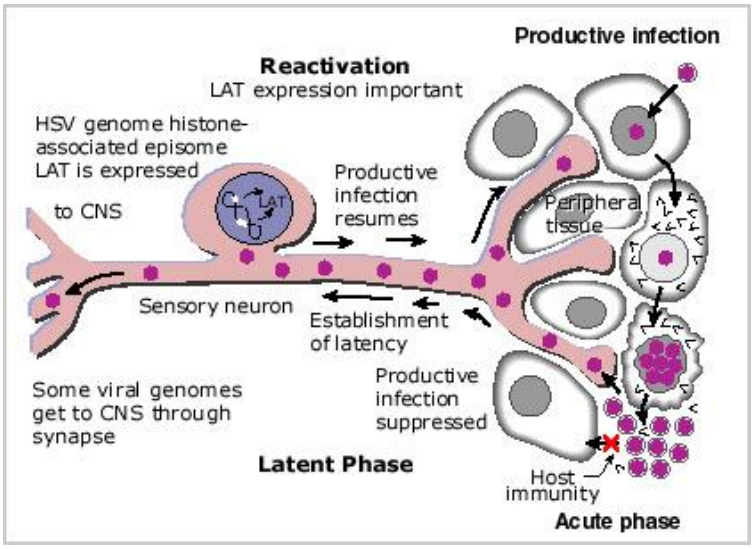

Figure 2. Schematic representation of HSV latent infection and reactivation [14].

Not all of the neurons are equally susceptible in the sensory ganglia to productive infection and specific types of neurons are more likely to harbor latent HSV- infection based, in part, on the differential presence of regulatory RNAs or regulatory proteins [15, 16].

Rarely the ganglionitis is followed by herpes simplex encephalitis (HSE), which is the most common fatal sporadic encephalitis. HSE is characterized by severe destruction of the frontal and the temporal lobe with the adjacent structures, including the amygdala and the hippocampus. If left untreated, the mortality rate is as high as 70% with a high rate of neurological sequelae [17, 18]. HSV-1 DNA is detectable at a relatively high frequency at various sites of the adult human central nervous system (CNS) including the brainstem, olfactory bulbs and the temporal lobe [19-22], although it is not clear whether the virus can get reactivated in the CNS.

During latent HSV infection in the trigeminal ganglia (TG), there is little detectable viral protein and infectious virus production [20, 23]. HSV transcripts during latency are restricted to neurons, with *in situ* hybridization signals that are strongest over nuclei [24-26]. Abundant transcription from the viral genome appears to be restricted to the latency-associated transcripts (LATs) that map to repeat sequences flanking the unique long region

[24-27]. Interestingly, HSV latency in human TG is associated with chronic inflammation [28]. It is unknown whether the latent HSV-1 infection itself or the repeated reactivation events in the human TG are behind the significant injury of the peripheral nervous system characterized by even neuronal loss.

Virus mediated oncolytic therapy including the application of HSV-1, is a promising novel modality of tumor therapy with potential usefulness against a wide variety of malignancies [29-33]. Oncolytic HSV-1 therapy is dependent on virus replication in tumor cells and is augmented by host antiviral and infection-induced anti-tumor immune responses [34-37]. In spite of significant progress, oncolytic virotherapy faces significant challenges. Although traditional two-dimensional (2D) monolayer cultures of many types of tumor cells are efficiently destroyed by a variety of HSV-1 vectors *in vitro*, tumor destruction is often incomplete *in vivo* [29, 34]. Factors limiting the effectiveness of HSV-1 oncolytic therapy *in vivo* remain incompletely understood. However, observations indicate that potential problems include the impairment of intratumoral virus spread by the extracellular matrix (ECM), decreased expression of viral entry receptors by different tumor cell populations, activation of intracellular tumor defenses to viral infection, and quick virus clearance by the host immune system [34, 38-41]. It is clear that many aspects of the complex virus–host interactions that determine the effectiveness of HSV-1 oncolytic therapy are difficult to impossible to study in traditional 2D tissue culture systems.

The behavior of cells *in vivo* is controlled by their interactions with neighboring cells and with the ECM [42-44]. Cancer cells grown in three-dimensional (3D) cultures in a polymeric ECM closely mimic the biology of tumor development *in vivo* and numerous studies indicate that 3D cultures are superior to traditional 2D monolayer cultures for studies of key cellular behaviors such as differentiation, proliferation, invasion, and apoptosis [45-48]. Cancer cells grown in 3D culture are more resistant to chemotherapeutic agents and radiation than cells in 2D culture and 3D tumor cell cultures are useful for preclinical evaluation of the cytotoxic effect of anticancer agents [46, 48, 49]. It is well established that multiple cell types within individual tumors have differential sensitivities to drugs. Although 3D cultures provide an excellent experimental system to study mechanisms of tumor cell resistance to drugs and radiation, very few studies have used 3D tumor cell cultures in the context of viral oncolytic therapy [50-52]. Earlier work in our laboratory indicated that 3D cultures of uveal melanoma cells show increased resistance to HSV-1 relative to 2D cultures [52]. Specifically, destruction of 95% of tumor cells in 3D cultures occurred several days later than in 2D cultures after HSV-1 inoculation. These findings suggested that HSV-1 inoculation

of 3D uveal melanoma cultures could provide a useful model to study mechanisms of ECM-mediated tumor resistance to HSV-1 oncolytic therapy.

The goal of our work was to investigate the effect of the HSV-1 latent infection using two model systems.

First, we examined the role of the HSV-1 latent infection in mouse TG-s. Since HSV-1 latent infection is relatively common in the bipolar neurons in peripheral ganglia we aimed to explore the significance of the latent infection and anticipated chronic progressive alterations in mean neuron diameter, mean neuron nucleus diameter, TG volume, and mean number of neurons per TG. Using morphometric studies we tested whether HSV-1 latent infection has an effect on those above mentioned quantitative indicators in healthy adult mice. Studies have shown chronic behavioral and neurological deficits and chronic pain in these animals [53-59] but chronic progressive quantitative alterations remained poorly understood. Therefore we performed *in vivo* studies using mice to determine the effect of HSV-1 latent infection on mean neuron diameter, mean neuron nucleus diameter, TG volume, and mean number of neurons per TG.

Our second aim was to explore virus resistance of distinct tumor cell subpopulations in 3D tumor cell cultures and the mechanisms of ECM-mediated virus resistance of tumor cells. So far very few studies have used 3D tumor cell cultures in the context of viral oncolytic therapy. These studies have indicated that tumor cells grown in 3D cultures are also more resistant to viral, including HSV-1 and adenovirus-mediated oncolytic therapy, than cells grown in 2D culture [46, 48]. Therefore we performed *in vitro* studies using HSV-1 and uveal melanoma cells in 2D and 3D cultures to identify any differences in growth pattern and the outcome of the HSV-1 infection.

2. AIMS

2.1 To investigate the HSV-1 latency and the consequent quantitative alterations on morphologic level using *in vivo* model

- To examine the effect of latent HSV-1 infection on mean neuron diameter, neuronal nucleus diameter, neuron density and neuron number in trigeminal ganglia derived from adult BALB/c mice in association with neuronal injury.

2.2 To explore HSV-1 latency in tumor cells and the effect of extracellular matrix concerning latently infected tumor cells

- To explore whether 3D tumor cell cultures can be used to identify morphologically distinct tumor cell populations that have increased resistance to HSV-1.

- To examine whether 3D tumor cell cultures can be used to learn about mechanisms of ECM mediated tumor cell resistance to HSV-1 oncolytic therapy.

3. MATERIAL AND METHODS

3.1 Investigation of HSV-1 latency and the consequent quantitative alterations on morphologic level using *in vivo* model

3.1.1 Viruses

Wild-type HSV-1 strain 17+ having non-syncycial plaque morphology [60] was obtained from Nigel Fraser (University of Pennsylvania, Philadelphia, PA). Virus stocks were propagated in complementing cell lines and stored at -80 ºC. Yields of infectious virus titer (P.F.U. ml^{-1}) were determined by plaque assay in baby hamster kidney (BHK) 21 clone 13 cells.

3.1.2 Animals

Female BALB/c mice (obtained from Harlan Laboratories, Indianapolis, IN) were bred and raised in conventional animal housing. Animal husbandry and experimental procedures were performed in accordance with NIH Public Health Service policy and approved by the Vanderbilt University School of Medicine Institutional Animal Care and Use Committee.

3.1.3 Inoculation of mice

Four to six-week-old female BALB/c mice were inoculated with 1 x 10^5 plaque-forming units (P.F.U.) of HSV-1 17+ per eye after superficial corneal scarification with a sterile hypodermic needle under Metofen anesthesia. Control mice were inoculated with an equivalent volume of sterile tissue culture medium using the same inoculation technique (mock infection). Mice were followed daily for signs and symptoms of disease. Groups of mice consisting of five randomly chosen HSV-1-infected or mock-infected mice per treatment were euthanized at 1, 12 and 31 weeks after inoculation (at 5, 17 and 35 weeks of age) and TG were aseptically removed. TG were excised by cutting the trigeminal root at its entrance into the brainstem, the mandibular branch at least 1 mm distally to the ganglion and the maxillary branch at the level of the orbital fissure. Tissues were fixed in paraformaldehyde–lysine–

periodate fixate and embedded in paraffin. Before the final embedding step, TG were randomly rotated along their longitudinal axis, embedded in paraffin and sectioned. Multiple sections encompassing the complete thickness of the tissue blocks were processed for hematoxylin and eosin staining for histologic evaluation, immunohistochemistry, *in situ* hybridization and morphometric studies.

3.1.4 Immunohistochemical detection of HSV-1 proteins

Multiple 6-µm-thick tissue sections derived from representative portions of the paraffin-embedded TG tissues were deparaffinized with xylene and dehydrated through a series of graded ethanols. Endogenous peroxidase activity was quenched using a 0.3% H_2O_2-methanol bath followed by several washes with phosphate buffered saline (PBS). HSV-1 antigens were detected using a 1:1000 dilution of a polyclonal anti-HSV-1 antiserum raised in a rabbit (DAKO). Tissue sections were incubated with primary antibody at 43°C for 32 minutes before the addition of biotinylated anti-rabbit immunoglobulin secondary antibody, avidin-horseradish peroxidase, and 3,3'-diaminobenzidine tetrahydrochloride (0.04%) in 0.05M Tris-HCL (pH 7.4) and 0.025% H_2O_2 as a chromogen (Ventana Medical Systems). Before staining, the binding of secondary antibodies and conjugates was blocked by appropriate reagents provided by the manufacturer.

3.1.5 *In situ* hybridization for HSV-1-LAT gene expression

In situ hybridization was performed using a nick-translated ^{35}S-labeled DNA probe specific for HSV-1 latency-associated transcript (LAT) (Bst2±Bst2 fragment) and 6-µm-thick tissue sections [61]. Prior to hybridization, ^{35}S-labeled nick-translated DNA probes were denatured in a boiling water bath for 5 min, cooled on ice, and diluted with hybridization mix (2x saline-sodium citrate (SSC) [lx SSC is 0.15 M NaCl plus 0.015 M sodium citrate], 1 mM Tris, pH 7.4, 1 mM EDTA, lx Denhardt solution [0.02% polyvinylpyrrolidone, bovine serum albumin, and Ficoll], 10% dextran sulfate, 45% formamide, and 100 mg of polyadenylic acid, 1 mg of mouse brain RNA, and 1 mg of mouse brain DNA per ml). The probe concentration was adjusted to contain 1 ng of DNA per 5 µl (ca. 10^5 cpm per tissue section). The hybridization mixture including probe was heated for 30 seconds at 100 °C and cooled on ice; 10 mM dithiothreitol was added, and the complete mixture was prehybridized at 45°C for at least 1 h. Portions of the prehybridized probe solution (5 µl) were placed on tissue sections

and covered with baked, siliconized cover slips and paraffin oil. After hybridization at 50°C for 48 to 65 h, the paraffin oil was removed by two 5-min incubations in chloroform. Cover slips were removed by gently shaking the slides in wash solution, and non-hybridized probe was removed by extensive washing for 2 days at 37°C in 10 mM Tris-HCl, pH 7.4/2x SSC/50% formamide/1 mM EDTA followed by 1 h at 55°C in 2x SSC, then rinsed in 2x SSC, and dehydrated in graded ethanol solutions containing 300 mM ammonium acetate. Following dehydration in ethanol ammonium acetate (0.3 M), slides were dipped in NTB2 nuclear track emulsion (Kodak) that was diluted 1:1 with 0.6 M ammonium acetate. After 2 to 4 days of exposure at 4°C, slides were developed with D19 (Kodak) and stained with hematoxylin and eosin. The specific activities of the nicktranslated ^{35}S-labeled probes were 1 x 10^8 to 2 x 10^8 cpm/µg.

3.1.6 Determination of mean neuron diameter, neuron nucleus diameter, neuron density, TG volume, and neuron number per TG

For the determination of mean neuron diameter and mean neuron nucleus diameter, multiple 6-µm-thick tissue sections derived from representative portions of the paraffin-embedded TG tissues were stained with hematoxylin, scanned at 200x magnification using the ImageScope® System (Aperio Technologies, Inc.) and analyzed with the aid of Aperio image analysis software. The largest diameter and the largest nuclear diameter of 100 randomly chosen neurons in each TG were measured manually by an observer blinded to the nature and time of inoculation. For each time point and treatment group, measurements were made for 7 to 12 TG sections derived from five mice yielding 700 to 1200 measurements per group. Mean neuron diameter and neuronal nucleus diameter and standard deviations were calculated for each treatment type (HSV-1-inoculated or mock-inoculated) and each time point (1, 12 and 31 weeks after inoculation).

For neuronal cell density measurements, multiple 20-µm-thick sections derived from representative portions of the paraffin embedded TG tissues were cut, stained with hematoxylin and viewed using a 60x objective under an Olympus BH-2 microscope (Olympus Optical Co. Ltd.; magnification: 600x). For each time point and treatment group (infected or mock), five TG (randomly selected left or right) from five mice were examined using at least three sections of each TG. Neurons were identified by morphology based on the detection of nucleoli and Nissl substance [62]. Neuronal cell density determinations were made with the aid of image analysis software (ImageJ, Research Service Branch, National Institute of Mental

Health, Bethesda, MD, USA), digital video camera (Sony) and a computer system according to a published stereological optical dissector method [62]. The dimensions of the dissector used were 50 x 50 μm in the *x*- and the *y*-axis. The guard area (the top and bottom of the histological section in which neurons were not counted to avoid errors) was 5 μm; the optimal dissector's height was 15 μm. Nuclei were used as counting units. Neuronal density, that is the number of neurons per unit volume of TG (neurons per volume, n_v), was determined with an optical dissector method using Tandrup's review concerning dorsal root ganglion as a guiding principle [62]. The total value of n_v for a TG was then determined from:

$$n_v = \frac{\Sigma Q}{p \cdot \Sigma a(frame) \cdot h}$$

where ΣQ- is the sum of the dissector neurons in the total dissector volumes, $a_{(frame)}$ is the area of the counting frame, h is the height of the optical dissector and p is the number of points per dissector. Neuron density was determined for each examined TG separately, and mean neuron density and standard deviation per treatment group was then calculated.

The volume of TG was calculated using image analysis software (ImageJ) and digital video camera (Sony) to draw manually the contour of each analyzed TG section at a magnification of 5x and to measure automatically its area in mm^2. One of every 10 sections derived from the whole thickness of the TG was analyzed. The total volume of ganglia was calculated by multiplying the surface area by the thickness of the section and by the number of sections included in the interval between the analyzed sections and summarizing the calculated volumes for the whole TG. Mean TG volume and standard deviation for each treatment group (HSV-1-inoculated or mock-inoculated and 1, 12 and 31 weeks after inoculation) was then calculated.

The number of neurons per TG was calculated based on neuron density and TG volume as follows: $N = n_v \times V$, where N corresponds to neuron number per TG, n_v stands for neuron density and V for TG volume. Calculation was performed separately for five TG in each treatment group. Mean neuron number per TG and standard deviation for each treatment group (HSV-1-inoculated or mock-inoculated and 1, 12 and 31 weeks after inoculation) was then calculated.

3.1.7 Statistical analyses

Statistical analyses were performed with the STATISTICA software (version 8.0) for Windows. Normality was tested using the Kolmogorov–Smirnov test. All variables were distributed normally. Homogeneity of variance was determined using F-test and Levene's test was considered violated when this test yielded $p < 0.05$. All variances were homogeneous. Data were assessed using independent samples T-test and repeated measures analysis of variance (ANOVA) followed by Scheffe's post-hoc test. Differences between the means were considered statistically significant if $p < 0.05$. The results are expressed as means ± standard deviation (SD) values.

3.2 Investigation of HSV-1 latency in tumor cells and the effect of extracellular matrix concerning latently infected tumor cells

3.2.1 Viruses

Wild-type (wt) HSV-1 strain KOS and recombinant HSV-1 strain K26GFP was provided by P. Desai (Johns Hopkins University, Baltimore, MD, USA). Jellyfish green fluorescence protein (GFP) was fused in-frame with the UL35 ORF generating the K26GFP virus whose capsids express GFP [63]. Cells infected with HSV-1 strain K26GFP exhibit punctate nuclear fluorescence at early times in the replication cycle and at later times during infection, a generalized cytoplasmic and nuclear fluorescence, including fluorescence at the cell membranes can be observed [63]. K26GFP was shown to grow in cell culture as well as wild type (wt) virus [63]. Virus stocks were propagated in complementing cell lines and stored at -80 ºC. Yields of infectious virus titer (P.F.U. ml^{-1}) were determined by plaque assay in Vero cells.

3.2.2 Cells

Human primary uveal melanoma cells of low (OCM1) and high (C918) invasive potential were provided by Robert Folberg (University of Illinois at Chicago, Chicago, IL, USA). OCM1 and C918 cells were maintained in Eagle's Minimal Essential Medium (EMEM; BioWhittaker Inc.) supplemented with heat inactivated 15% fetal bovine serum

(FBS; Fisher) and 100 mg l^{-1} of penicillin/streptomycin (P/S) without the addition of exogenous extracellular matrix (ECM) molecules or growth factors.

3.2.3 Two-dimensional and three-dimensional uveal melanoma cultures

Melanoma cells were grown on six-well plates in EMEM either in the presence (three-dimensional; 3D cultures) or in the absence (two-dimensional; 2D cultures) of ECM rich in laminin (Matrigel, BD Biosciences). For 3D cultures, Matrigel was poured onto tissue culture plates to a depth of approximately 0.2 mm followed by polymerization for 1 h at 37 °C before placement of melanoma cells on the Matrigel surface. Cultures were incubated in repeatedly refreshed culture medium for up to 4 weeks and observed daily under an inverted microscope (Leica).

3.2.4 Determination of susceptibility of uveal melanoma cells to wt HSV-1 (KOS) and HSV-1 K26GFP-mediated destruction in 2D and 3D cultures

C918 and OCM1 uveal melanoma cells were grown on six-well tissue culture plates in the presence (3D cultures) or absence of Matrigel (2D cultures). After 3-4 days, when in the 3D cultures C918 cells formed prominent vasculogenic mimicry patterns and OCM-1 cells formed cell aggregates on the Matrigel surface and both cell lines showed invasion of tumor cells into the Matrigel matrix, the tissue culture medium was removed and one of the following inocula was gently placed on the surface of the cultures: (i) 0.5 ml of sterile PBS (mock infection); (ii) wt HSV-1 (strain KOS) with a calculated multiplicity of infection (M.O.I.) of 0.5 plaque forming units (PFU) per cell diluted in PBS to a final volume of 0.5 ml; (iii) HSV-1 K26GFP with a calculated M.O.I. of 0.5 PFU per cell diluted in PBS to a final volume of 0.5 ml. After incubation for 1 h, the original inocula were removed and fresh tissue culture medium (3 ml) was added to each well and further incubated in repeatedly refreshed culture medium for up to 4 weeks. During this 4-week period, cultures were observed daily under an inverted fluorescence microscope (Leica) for evidence of viral cytopathic effects and green fluorescent protein (GFP) expression. The day when at least 95% of the melanoma cells were destroyed was noted. Cell death was confirmed by the uptake of the charged cationic dye Trypan blue (0.2%) by >95% of residual cells after incubation of cultures with Trypan blue (0.2%) for 10 min at 37 °C.

3.2.5 Determination of HSV-1 spread through Matrigel

C918 and OCM1 uveal melanoma cells were grown on 12-well tissue culture plates in monolayers (2D cultures). When the cultures reached approximately 70% confluency, culture media were removed and either 0.5 ml of a 1:1 mixture of PBS and Matrigel or 0.5 ml of PBS was layered on the cells. Cultures were then incubated at 37 °C for 1 h to allow Matrigel to polymerize and form an approximately 1 mm thick layer matrix on the cells. Next, cultures were either inoculated with 0.5 ml HSV-1 K26GFP diluted in PBS to a calculated M.O.I. of 0.5 PFU per cell or were mock infected with 0.5 ml PBS by gently layering these solutions on the cultures making sure that the Matrigel surface was not violated. After further incubation at 37 °C for 1 h, additional 2 ml of fresh tissue culture media was added to each well. Cultures were then further incubated for up to 2 weeks at 37 °C with fresh culture medium added to the cultures every 2 days. During this 2-week period, cultures were observed regularly under an inverted fluorescence microscope (Leica) for evidence of GFP expression.

3.2.6 Placement and culturing of earlier HSV-1 inoculated uveal melanoma cells in 2D or 3D environments

C918 and OCM1 uveal melanoma cells were grown on 12-well tissue culture plates in monolayers (2D cultures). When the cultures reached approximately 70% confluency, culture media were removed and the cells were exposed at 37 °C to one of the following inocula: (i) 0.5 ml of sterile PBS (mock infection) or (ii) HSV-1 K26GFP with a calculated M.O.I. of 0.5 P.F.U. per cell diluted in PBS to a final volume of 0.5 ml. After incubation for 1 h, the original inocula were removed and the monolayers were washed in sterile PBS twice and 1 ml of sterile PBS was added to each well. Cells were than scraped off using sterile, disposable cell scrapers. Cell suspensions were than centrifuged and cell pellets were resuspended in culture medium. Equal volumes (0.25 ml) of the cell suspensions were then used to either establish new 2D cultures in 12-well tissue culture plates or 3D cultures as follows. For 3D cultures, Matrigel was poured onto tissue culture plates to a depth of approximately 0.2 mm followed by polymerization for 1 h at 37 °C. Cell suspensions of HSV-1 K26GFP or mock-infected uveal melanoma cells were mixed with Matrigel 1:1 (0.25:0.25 ml) and poured on the Matrigel-coated wells. Finally, 2 ml of fresh culture medium was added. 2D and 3D cultures were then further incubated for up to 4 weeks at 37 °C with fresh culture medium added to the cultures every 2 days. During this 4-week period, cultures were observed regularly under an

inverted fluorescence microscope (Leica) for evidence of GFP expression and the percentage of GFP-expressing cells was determined by counting the number of GFP-positive and GFP-negative cells in 16 high power microscopic fields for each studied type of treatment at selected time points.

4. RESULTS

4.1 Investigation of HSV-1 latency and the consequent quantitative alterations at morphologic level using *in vivo* model

4.1.1 Characterization of TG tissues derived from mice at 1, 12 and 31 weeks following corneal HSV-1 inoculation

To obtain TG tissues at various stages of HSV-1 infection, mice were inoculated on the cornea with either HSV-1 or sterile tissue culture medium. A minority of HSV-1-infected mice demonstrated signs of encephalitis (agitation or paralysis), and 13% of the animals died within 3 weeks of infection. Animals surviving beyond 3 weeks of virus inoculation demonstrated no signs of encephalitis and developed normally. Groups of five randomly chosen HSV-1-infected or mock-infected mice were euthanized at 1, 12 and 31 weeks after inoculation. TG were aseptically removed from euthanized animals, and tissues were processed for immunohistochemical staining for HSV-1 antigen and *in situ* hybridization for LAT expression to document acute or latent HSV-1 infection and to evaluate for histopathologic evidence of inflammation (Fig. 3–5).

No HSV-1 protein expression was detected in the TG of mock-infected mice at any time point (Fig. 3A, C, and E). In five animals euthanized 1 week after HSV-1 inoculation, HSV-1 proteins were detected in all 10 TG by immunostaining (Fig. 3B), consistent with replication of HSV-1. HSV-1 proteins were detected in numerous cells that by morphological criteria were neurons and non-neuronal cells. In TG derived from animals euthanized at 12 and 31 weeks after corneal HSV-1 inoculation, HSV-1 protein expression was not detected in the TG derived from four out of five mice tested (Fig. 3D, F).

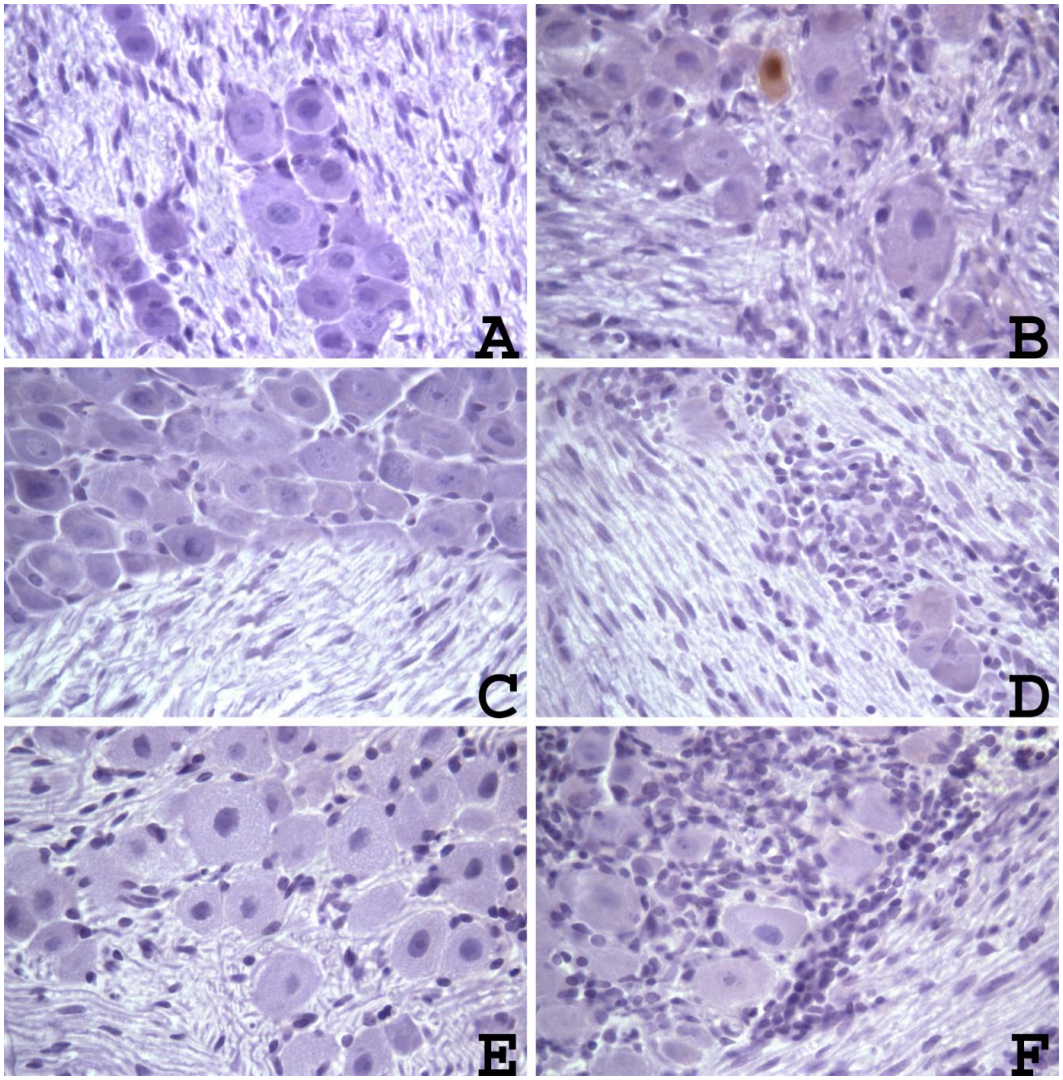

Figure 3. HSV-1 protein expression in murine TG tissues following corneal inoculation of HSV-1 or sterile medium (mock-infection) as detected by immunohistochemistry. Brown staining indicates HSV-1 proteins. HSV-1 protein expression was not detected in TG derived from mock-infected mice at 1 (A), 12 (C) or 31 (E) weeks after mock inoculation. HSV-1 protein expression in a neuron in a TG derived from a mouse 1 week after corneal HSV-1 inoculation (B). HSV-1 protein expression was not detected in TG derived from mice 12 (D) or 31 (F) weeks after corneal HSV-1 inoculation. Magnification = 400x.

One TG section at each time point demonstrated very rare non-neuronal cells that stained for HSV-1 proteins (data not shown). Abundant LAT RNA expression was detected by *in situ* hybridization in TG tissues of HSV-1-infected mice euthanized at 12 and 31 weeks after virus inoculation (Fig. 4).

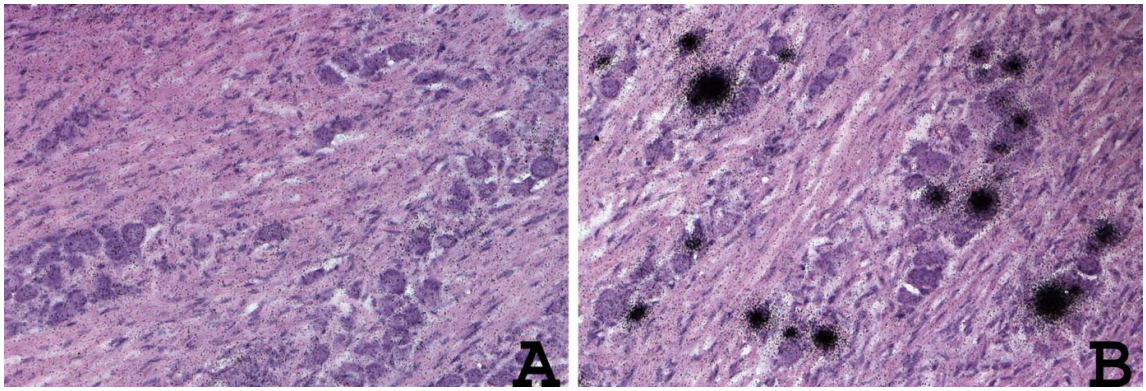

Figure 4. Detection of HSV-1 LAT in the TG of mice by *in situ* hybridization. Accumulation of dark grains indicates LAT accumulation. There was no evidence of LAT expression in TG derived from a mouse 31 weeks after corneal mock inoculation (A). Numerous LAT-positive cells in TG tissue derived from a mouse 31 weeks after corneal HSV-1 inoculation (B). Magnification = 200x.

Sections of TG stained with hematoxylin and eosin at 1, 12, and 31 weeks after HSV-1 inoculation revealed chronic inflammatory changes (Fig. 5B, D, and F). Inflammation was not detected in the TG of mock-infected animals (Fig. 5A, C, and E). These findings indicate that mice examined at 1 week after virus inoculation were productively infected with HSV-1, whereas those examined at 12 and 31 weeks after inoculation were latently infected with the virus. Marginal HSV-1 expression in one mouse each at 12 and 31 weeks after virus inoculation is consistent with rare focal HSV-1 reactivation. In addition, both acute and latent HSV-1 infection in the murine TG was associated with inflammation.

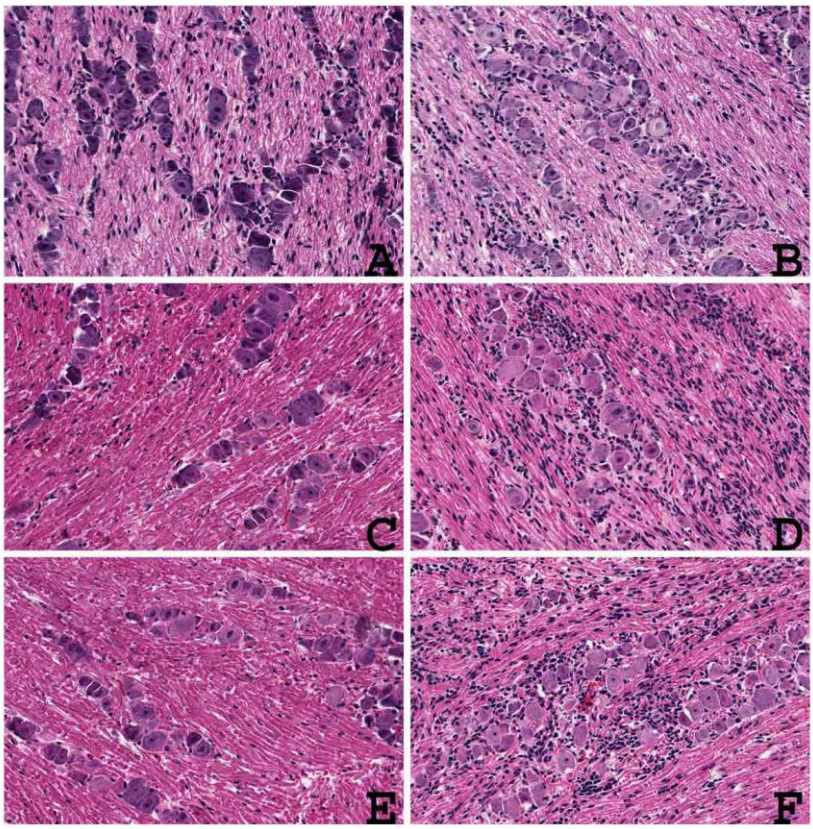

Figure 5. Inflammation in murine TG tissues following corneal inoculation of HSV-1. No evidence of inflammation in hematoxylin and eosin stained sections of TG derived from mice at 1 (A), 12 (C), or 31 (E) weeks after corneal mock inoculation. Chronic inflammation in hematoxylin and eosin stained sections of TG derived from mice at 1 (B), 12 (D), and 31 (F) weeks after corneal HSV-1 inoculation. Magnification = 100x

4.1.2 Mean neuron diameter, mean neuronal nucleus diameter, and the number of neurons increase in the TG of mock-infected BALB/c mice

Mean neuron diameter and mean neuronal nucleus diameter gradually increased in the TG of control mice between 1 and 31 weeks after mock infection (between 6 and 36 weeks of age) (Tab. 1). Specifically, mean neuron diameters at 6, 17, and 36 weeks of age were 22.74 ± 5.2 µm (n=700), 22.98 ± 4.9 µm (n=700) and 25.16 ± 5.0 µm (n=900), respectively. Mean neuronal nucleus diameters at 6, 17, and 36 weeks of age were 9.15 ± 2.2 µm (n=700), 9.27 ± 1.8 µm (n=700), and 10.33 ± 2.0 µm (n=900), respectively. Increases in mean neuron diameter and neuronal nucleus diameter did not differ statistically between 6 and 17 weeks ($p=0.3782$ and 0.2794, respectively), but were significantly different at 6 and 36 weeks and 17

and 36 weeks ($p<0.0001$). These findings are consistent with growth of TG neurons during the observation interval.

Neuron density in the TG decreased while TG volume increased in mock-infected mice during the period of observation. The combination of these changes resulted in a gradual increase in the mean number of neurons per TG between 6 and 36 weeks of age (Tab. 1, Fig. 6A, B, C). Neuron density was $5.64 \pm 0.2 \times 10^{-5}$ neurons per μm^3 at 6 weeks of age (n=5) and decreased to $4.59 \pm 0.2 \times 10^{-5}$ neurons per μm^3 by 17 weeks (n=5, p=0.000191). Neuron density was $4.51 \pm 0.1 \times 10^{-5}$ neurons per μm^3 at 36 weeks of age (n=5), which was similar to that of 16 weeks (p=0.99) but significantly less than at 6 weeks of age (p=0.000082). Mean TG volume was 0.33 ± 0.03 mm^3 at 6 weeks of age (n=5), 0.53 ± 0.04 mm^3 at 17 weeks (n=5), and 0.89 ± 0.04 mm^3 at 36 weeks of age (n=5) (Tab. 1, Fig. 6B). These increases were statistically significant (6 to 16 weeks: p=0.000006; 17 to 36 weeks: p=0.000005; 6 to 36 weeks: p=0.0000001). The mean number of neurons per TG was 18600 ± 1000 (n=5), 24250 ± 1800 (n=5), and 40950 ± 3100 (n=5) at 6, 17, and 36 weeks of age, respectively (Tab. 1, Fig. 6C). These increases were statistically significant (6 to 16 weeks: p=0.00054; 17 to 36 weeks: p=0.000013; 6 to 36 weeks: p=0.000001). Thus, TG volume and neuron number per TG increase, while neuron density decreases in the TG of mice between 6 and 36 weeks of age.

Age (weeks)	Inocu-lation	HSV-1 protein	HSV-1 LAT	Inflam-mation	Neuron diameter (µm ±SD)	Neuron nucleus diameter (µm ± SD)	Neurondensity (per μm^3 ± SD ‡)	TG volume (mm^3 ± SD)	Neuron number/TG (thousand ± SD)
6	Mock	-	-	-	22.74 ± 5.2	9.15 ± 2.2	5.64 ± 0.2	0.33 ± 0.03	18.6 ± 1.0
17	Mock	-	-	-	22.98 ± 4.9	9.27 ±1.8	4.59 ± 0.2	0.53 ± 0.04	24.25 ± 1.8
36	Mock	-	-	-	25.16 ± 5.0	10.33 ± 2.0	4.51 ± 0.1	0.89 ± 0.04	40.95 ± 3.1
6	HSV-1	+	+	+	23.94 ± 5.2	9.58 ± 2.0	5.15 ± 0.1	0.33 ± 0.03	17.0 ± 1.4
17	HSV-1	-†	+	+	22.25 ± 4.6	9.07 ± 1.8	4.18 ± 0.2	0.53 ± 0.03	21.28 ± 2.2
36	HSV-1	-†	+	+	23.55 ± 5.4	9.76 ± 2.0	3.91 ± 0.2	0.86 ± 0.04	33.62 ± 1.6

Table 1. Expression of HSV-1 protein and LAT, inflammation and changes in neuron diameter, neuron nucleus diameter, neuron density, trigeminal ganglion (TG) volume and neuron number in the TG of BALB/c mice following corneal inoculation of either HSV-1 or sterile medium (mock-inoculation) at 5 weeks of age.

† 1 out of 10 TG studied demonstrated weak HSV-1 protein expression in a few cells. ‡ Results are multiplied by 10^{-5}. HSV-1 protein = herpes simplex virus-1 protein expression as detected by immunohistochemistry; HSV-1

LAT = herpes simplex virus-1 latency associated transcript expression as detected by in situ hybridization; SD = standard deviation; TG = trigeminal ganglion; N = total number of neurons.

4.1.3 Productive HSV-1 infection in the TG of mice is associated with increased mean neuron diameter and neuronal nucleus diameter and decreased neuron density

In the TG of mice euthanized 1 week after corneal HSV-1 inoculation, mean neuron diameter and mean neuronal nucleus diameter were greater than that detected in TG derived from mice 1 week after mock infection (Tab. 1). Specifically, mean neuron diameter 1 week after HSV-1 inoculation was 23.94 ± 5.2 μm (n = 1200) vs. 22.74 ± 5.2 μm (n = 700) in age-matched mock-infected controls (Tab. 1, p = 0.0001), a 5.27% increase (Tab. 2). Mean neuronal nucleus diameter 1 week after HSV-1 inoculation was 9.58 ± 2.0 μm (n = 1200) vs. 9.15 ± 2.2 μm (n = 700) detected in controls (Tab. 1, p = 0.0001), representing a 4.7% increase (Tab. 2). These changes in mean neuron diameter and neuronal nucleus diameter are consistent with the cytopathic effects associated with HSV-1 replication in a subset of the ganglionic neurons. Indeed, analysis of TG sections derived from mice 1 week following virus inoculation and immunostained for HSV-1 proteins indicated that mean neuron diameter and neuronal nucleus diameter were significantly greater in HSV-1 protein expressing neurons than in HSV-1 antigen–negative neurons ($p < 0.001$). Specifically, mean neuron diameter and neuronal nucleus diameter measurements were 31.10 ± 6.36 μm (n = 27) and 14.22 ± 2.32 μm (n = 12), respectively, in HSV-1 antigen–positive neurons, while mean neuron diameter and neuronal nucleus diameter were measured at 25.93 ± 4.32 μm (n = 50) and 11.66 ± 1.5 μm (n = 50), respectively, in HSV-1 antigen–negative neurons.

Mean neuron density was 8.69% less ($5.15 \pm 0.1 \times 10^{-5}$ neurons per μm^3, n = 5) in TG derived from HSV-1-inoculated mice than in mock-infected controls ($5.64 \pm 0.2 \times 10^{-5}$ neurons per μm^3, n = 5) 1 week after inoculation (Tab. 1 and 2, Fig. 6A, p = 0.002646). Mean TG volume was similar [0.33 ± 0.3 mm^3 (n = 5) vs. 0.33 ± 0.3 mm^3 (n = 5)] in HSV-1- and mock-infected mice at 1 week after inoculation (Tab. 1, Fig. 6B). The mean number of neurons per TG was 17 000 ± 1400 (n = 5) in virus-infected vs. 18 600 ± 1000 (n = 5) in mock-infected TG (Tab. 1, Fig. 6C), an 8.61% decrease (Tab. 2). This decreasing tendency in neuron number per TG did not reach statistical significance (p = 0.082395). Collectively, these findings are consistent with neuron destruction by productive HSV-1 infection in the TG.

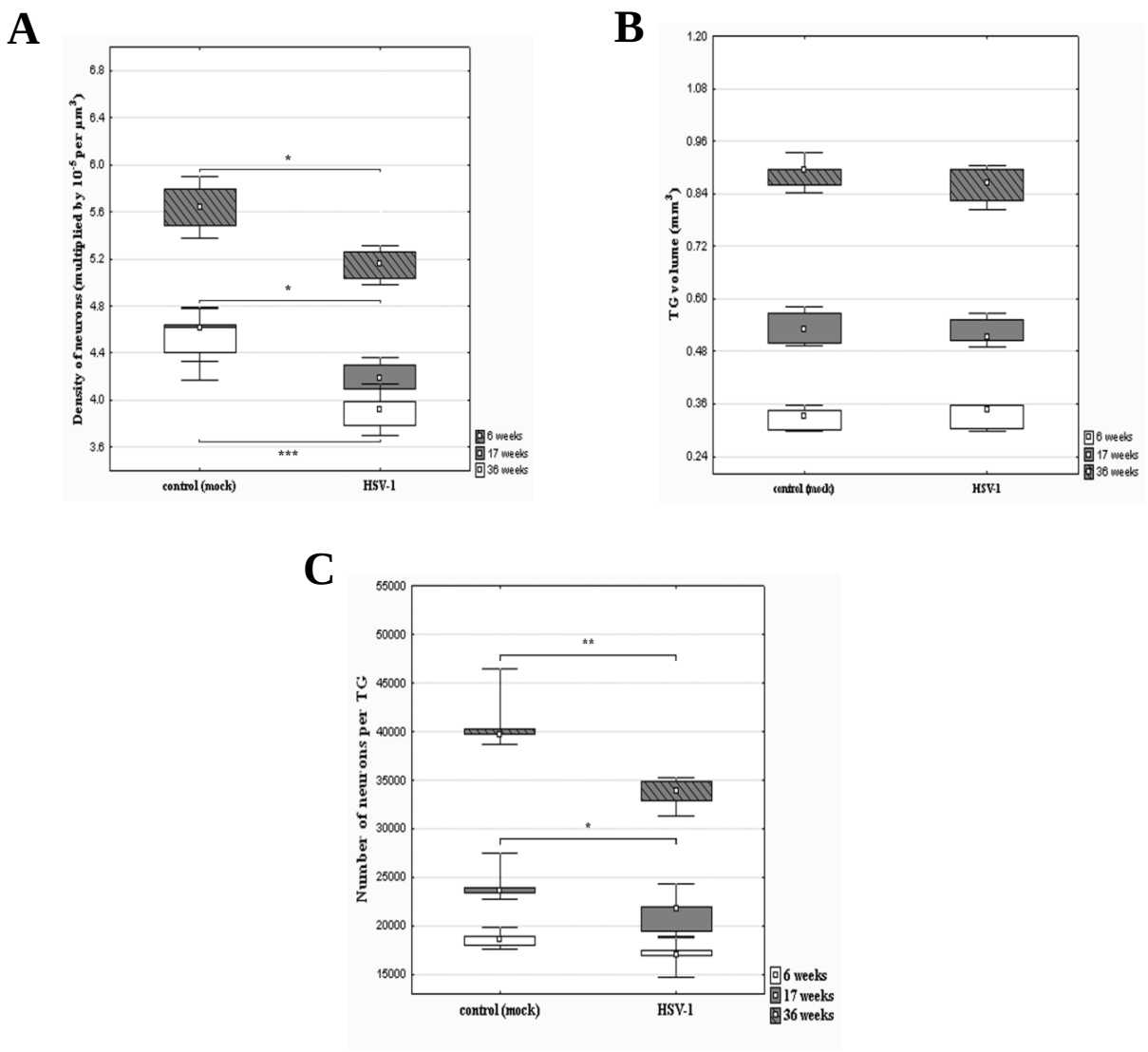

Figure 6. Median and range of neuron density per TG (A), TG volume (B) and neuron number per TG (C) in mice euthanized 1, 12 and 31 weeks after corneal inoculation of HSV-1 or sterile medium (mock) at 6, 17 and 36 weeks of age. TG number (n) was 5 for all time points and treatment groups. Rectangles represent 25% to 75% quartiles. *$p < 0.05$; **$p < 0.001$; ***$p < 0.0001$.

Age	6 weeks	17 weeks	36 weeks
Neuron diameter (infected/control)	+5.27%	-3.17%	-6.4%
Neuron nucleus diameter (infected/control)	+4.7%	-2.15%	-5.5%
Neuron density (infected/control)	-8.69%	-8.94%	-13.3%
Neuron number per TG (infected/control)	-8.61%	-12.25%	-17.9%

Table 2. Percentage of change in mean neuron diameter, mean neuronal nucleus diameter, neuron density and mean neuron number per TG in HSV-1-infected mice relative to age-matched mock-infected control.

4.1.4 Latent HSV-1 infection in the TG of mice is associated with decreased mean neuron diameter, neuronal nucleus diameter and neuron density and number

In the TG of mice euthanized 12 weeks after corneal HSV-1 inoculation (at 17 weeks of age), mean neuron diameter, mean neuronal nucleus diameter, neuron density and mean neuron number per TG were all significantly less than those in age-matched mock-infected control mice (Tab. 1 and 2, Fig. 6A, C). Specifically, mean neuron diameter at 12 weeks after HSV-1 inoculation was 22.25 ± 4.6 µm (n=1000) vs. 22.98 ± 4.9 µm (n=700) detected in age-matched mock-infected controls (Tab. 1, p=0.0023), a 3.17% decrease (Tab. 2). Mean neuronal nucleus diameter at 12 weeks after HSV-1 inoculation was 9.07 ± 1.8 µm (p=1000) vs. 9.27 ± 1.8 µm (p=700) in controls (Tab. 1, p=0.0249), a 2.15% reduction (Tab. 2). Neuron density was 8.94% less ($4.18 \pm 0.2 \times 10^{-5}$ neurons per μm^3, n=5) in TG derived from HSV-1-infected mice in comparison with those from mock-infected mice ($4.59 \pm 0.2 \times 10^{-5}$ neurons per μm^3, n=5) at 12 weeks after inoculation (Tab. 1, Fig. 6A, p=0.00458). Mean TG volume did not differ significantly (0.53 ± 0.03 vs. 0.53 ± 0.04 mm^3, n=5 for each) in HSV-1- and mock-infected mice at 12 weeks after inoculation (Tab. 1, Fig. 6B). However, the mean number of neurons per TG was significantly less in HSV-1-infected mice than in mock-infected mice at 12 weeks after inoculation (Tab. 1, Fig. 6C). Specifically, the total number of neurons was 21280 ± 2200 (n=5) in virus-infected vs. 24250 ± 1800 (n=5) in mock-infected TG (Tab. 1, Fig. 6C; p=0.04718), a 12.25% decrease (Tab. 2). Thus, neuron size and number are decreased in the TG of mice 12 weeks after HSV-1 corneal inoculation.

In the TG of mice euthanized 31 weeks after corneal HSV-1 inoculation (at 36 weeks of age), mean neuron diameter, mean neuronal nucleus diameter, neuron density, and mean

neuron number per TG were all significantly less than those detected in age-matched mock-infected control mice (Tab. 1, Figs. 6A, B). Specifically, mean neuron diameter at 31 weeks after HSV-1 inoculation was 23.55 ± 5.4 μm (n=1000) vs. 25.16 ± 5.0 μm (n=900) in age-matched mock-infected controls (Tab. 1, p=0.0001), a 6.4% decrease (Tab. 2). Mean neuronal nucleus diameter at 31 weeks after HSV-1 inoculation was 9.76 ± 2.0 μm (n=1000) vs. 10.33 ± 2.0 μm(n=900) in controls (Tab. 1, p=0.0001), a 5.5% reduction (Tab. 2). Neuron density was 13.3% less ($3.91 \pm 0.2 \times 10^{-5}$ neurons per μm^3, n=5) in TG derived from HSV-1-infected mice in comparison with those from mock-infected mice ($4.51 \pm 0.1 \times 10^{-5}$ neurons per μm^3, n=5) at 31 weeks after inoculation (Tab. 1, Fig. 6A, p=0.000054). Mean TG volume did not differ significantly (0.86 ± 0.04, n=5 vs. 0.89 ± 0.04 mm^3, n=5) in HSV-1- and mock-infected mice at 31 weeks after inoculation (Tab. 1, Fig. 6B). However, like the TG from mice at 12 weeks after HSV-1 inoculation, the number of neurons per TG was significantly less in HSV-1-infected mice than in mock-infected mice at 31 week after inoculation (Tab. 1, Fig. 6C). Specifically, the total number of neurons was 33.620 ± 1600 (n=5) in virus-infected vs. 40950 ± 3100 (n=5) in mock-infected TG (Tab. 1, p=0.0016), a 17.9% relative decrease (Tab. 1, Fig. 6C).

Deficits in mean neuron diameter, neuron nucleus diameter, neuron density, and neuron number per TG relative to age-matched mock-infected controls were all more substantial at 31 weeks that at 12 weeks after corneal virus inoculation (Tab. 2). As only latent HSV-1 infection was detected in TG neurons at 12 and 31 weeks after corneal virus inoculation, the progressive deficits in neuron size, density, and number between these times are consistent with chronic progressive neural injury during latent HSV-1 infection.

4.2 Investigation of HSV-1 latency in tumor cells and the effect of extracellular matrix concerning latently infected tumor cells

4.2.1 OCM1 and C918 uveal melanoma cells form several morphologically distinct cell populations under 3D culture conditions

To define in detail the growth pattern of uveal melanoma cells in 2D and 3D cultures, OCM1 and C918 cells were grown either in the presence or absence of laminin-rich ECM (Matrigel). In the absence of Matrigel (2D cultures), both OCM1 and C918 grew in monolayers (Fig. 7A, B). In the presence of Matrigel, both cell lines developed 3D structures (Fig. 7C–H; Fig. 8A–D; Fig. 9A–D). When OCM1 cells were placed on the Matrigel surface, cells first formed aggregates that were loosely attached to the Matrigel surface (Fig. 7C; Fig. 8A). As the cell aggregates were growing further, their attachment to the Matrigel surface became wider and firmer and single tumor cells began to invade the Matrigel matrix (Fig. 8A, B). During further growth, individual tumor cells invaded the matrix deeply and some of these cells formed multicellular spheroids showing a smooth surface and consisting of cells tightly attached to each other (Fig. 7E; Fig. 8C). Tumor cell aggregates on the Matrigel surface also showed similar spheroid formation at their bottom portion that completely immersed in the Matrigel matrix (Fig. 8B, C). Many of the tumor cell spheroids were stable for days to weeks, whereas others showed outgrowth of individual cells into the matrix. Cells invading the matrix (Fig. 7G) eventually reached the bottom of the tissue culture plate and grew under the matrix in monolayers (Fig. 8D). The growth of OCM1 cells within the Matrigel matrix did not cause massive destruction of the matrix until the end of the 4-week observation period.

When C918 cells were placed on the Matrigel surface, the cells started to grow on the matrix surface in a single layer and formed circular vasculogenic mimicry patterns that surrounded round matrix surfaces free of tumor cells (Fig. 7D; Fig. 9A). Next, individual tumor cells started to grow into the Matrigel at the line defined by the vasculogenic mimicry patterns (Fig. 7F; Fig. 9B). Cells invading the matrix migrated to the bottom of the culture plate and formed monolayers there (Fig. 7H; Fig. 9C, D). Interestingly, the formation of monolayers at the bottom of the well was restricted to areas under the Matrigel surfaces not colonized by cells but were surrounded by vasculogenic mimicry patterns (Fig. 9C). Next, individual tumor cells invaded the matrix underlying cell monolayers on the Matrigel surface (Fig. 9D). Tumor cell growth and matrix invasion eventually caused a loss of Matrigel in areas surrounded by vasculogenic mimicry patterns (Fig. 9D).

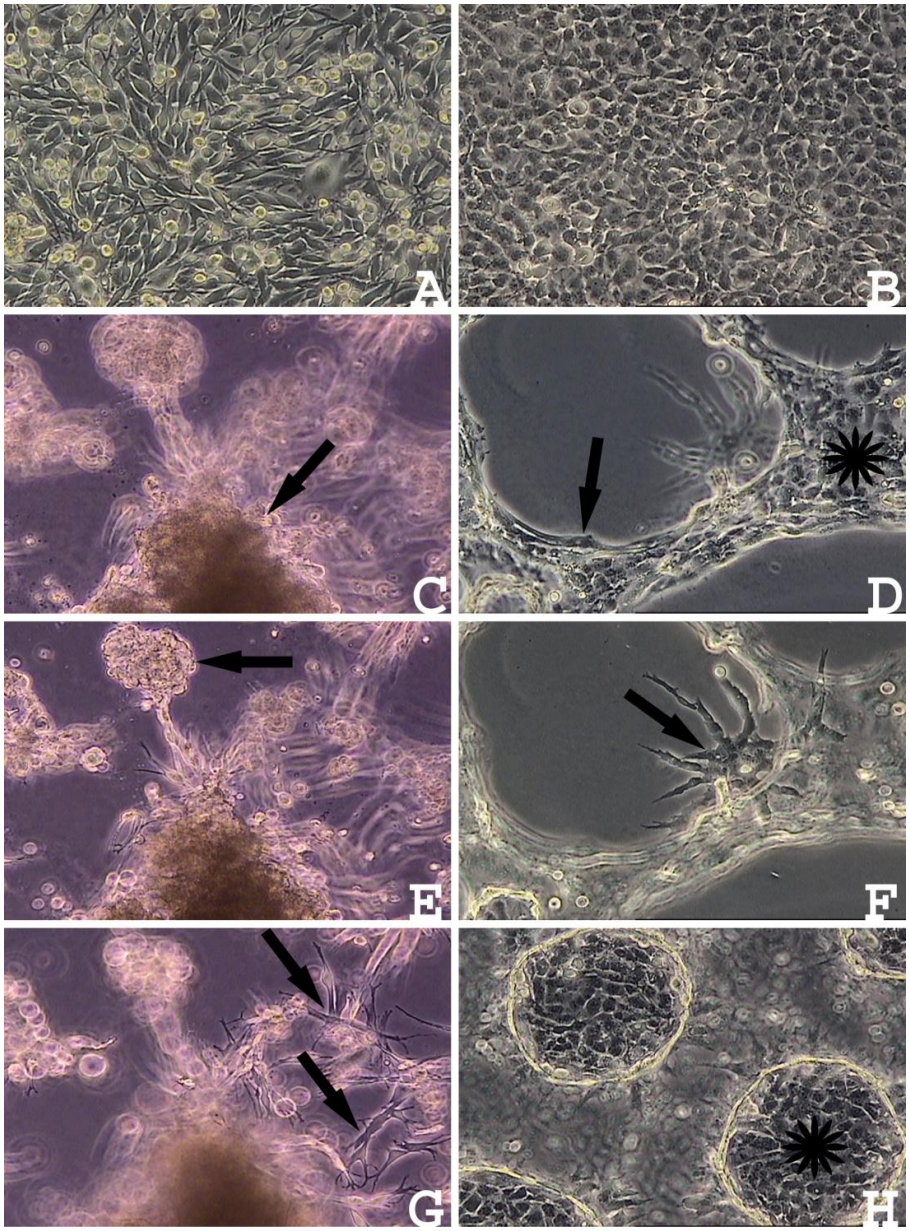

Figure 7. Morphology of OCM1 and C918 uveal melanoma cells grown in either 2D or 3D cultures. OCM1 cells grown in 2D monolayers for 5 days (A). Five-day-old 3D OCM1 culture. Arrow indicates surface aggregate of cells (C). Same 3D OCM1 culture with focus deeper on multicellular spheroid (arrow) within Matrigel (E). Same 3D OCM1 culture with focus even deeper on individual tumor cells (arrows) invading Matrigel (G). C918 cells grown in 2D monolayers for 5 days (B). Three-day-old 3D C918 culture with focus on Matrigel surface. Arrow indicates vasculogenic mimicry forming cells and asterix marks tumor cells growing in monolayer on Matrigel surface (D). Same 3D C918 culture with focus on tumor cells (arrow) invading the Matrigel matrix (F). Six-day-old 3D C918 culture with focus on tumor cells growing in monolayer under the Matrigel matrix (H).

These observations confirm and extend earlier observations related to the morphology of uveal melanoma cultures [64] and indicate that OCM1 and C918 uvealmelanoma cells form several morphologically distinct cell populations under 3D culture conditions.

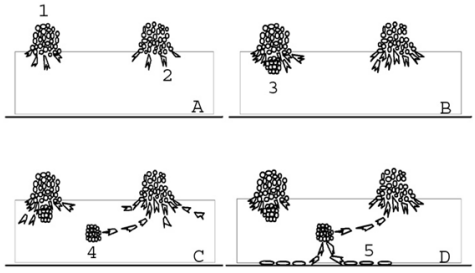

Figure 8. Schematic illustration of the morphology of 2-day-old (A), 3-day-old (B), 4-day-old (C), and 5-day-old (D) 3D OCM1 uveal melanoma cultures.

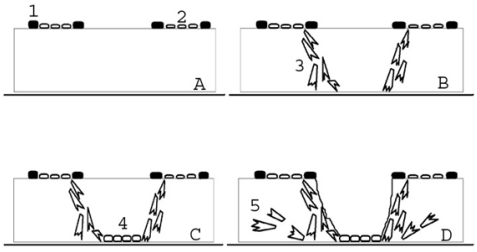

Figure 9. Schematic illustration of the morphology of 2-day-old (A), 3-day-old (B), 4-day-old (C), and 5-day-old (D) 3D C918 uveal melanoma cultures.

4.2.2 Rapid destruction of 2D and a delayed and incomplete destruction of 3D uveal melanoma cultures by wt HSV-1 and HSV-1 K26GFP

2D and 3D cultures of OCM1 and C918 cells were inoculated with wt HSV-1 strain KOS or HSV-1 strain K26GFP by placing virus solutions on the surface of the cultures. HSV-1 K26GFP exhibits fluorescence on replication [63]. Cultures were followed for evidence of cytopathic effects and virus replication (GFP expression/fluorescence) by an inverted fluorescence microscope.

We found that 2D cultures were completely destroyed by both HSV-1 strains within a few days (Tab. 3) with no evidence of surviving cells by Trypan blue staining. In contrast, virus inoculated 3D cultures showed delayed and incomplete destruction (Tab. 3). Importantly, a portion of both OCM1 and C918 cells seemed to survive HSV-1 KOS and HSV-1 K26GFP infection in 3D cultures for up to 4 weeks. Cell populations with increased resistance included C918 cells that formed vasculogenic mimicry patterns on the Matrigel surface, OCM1 cells that formed multicellular spheroids within the Matrigel matrix, and both C918 and OCM1 cells that invaded Matrigel individually.

Cell line	Culture condition	HSV-1 strain	Day of 95% destruction
OCM1	2D	KOS	4
	3D	KOS	8
	2D	K26GFP	4
	3D	K26GFP	8
C918	2D	KOS	5
	3D	KOS	9
	2D	K26GFP	5
	3D	K26GFP	9

Table 3. Elapsed time from inoculation of HSV-1 KOS or HSV-1 K26GFP (at M.O.I.=0.5 PFU per cell) to at least 95% destruction of 2D and 3D OCM1 and C918 uveal melanoma cultures.

In K26GFP inoculated 2D OCM1 and C918 cultures, 20–50% of tumor cells showed GFP expression by 1 day post infection (p.i.), and after 3 days p.i., it was very difficult to find any cells without fluorescence consistent with the complete viral replication-mediated destruction of these cultures by 4–5 days (Fig. 10A, B; Fig. 12A, B). In contrast, 3D cultures of both OCM1 and C918 showed a significant number of GFP-negative cells throughout the 4-week observation period (Fig. 10C–H; Fig. 11A–F; Fig. 12C–H; Fig. 13A–F).

In 3D cultures of OCM1, cells forming aggregates on the Matrigel surface showed widespread fluorescence (virus replication) by 1 day p.i., and after 4 days p.i., it was very difficult to find any cells without fluorescence in these structures consistent with the complete virus-mediated destruction of these surface cell aggregates by K26GFP by 8 days p.i. (Fig. 10C, D). Individual OCM1 cells growing into the Matrigel matrix showed variable fluorescence and some apparently viable and GFP-negative cells were consistently present during the 4-week observation period. Cells forming multicellular spheroids inside the matrix and cells forming spheroids at the bottom, matrix immersed portion of surface aggregates showed marked resistance to HSV-1 replication (Fig. 10C–H; Fig. 11A, B). Although occasional spheroids showed widespread fluorescence by 4 days p.i., others contained only a few GFP-positive cells and many remained completely devoid of GFP expression for days to weeks. GFP-negative spheroids contained viable cells as radial outgrowth of individual cells into the Matrigel matrix was observed from many of these structures as the cultures were aging (Fig. 11A, C, E). Interestingly, this outgrowth was often associated with the appearance of fluorescence in outgrowing cells and in cells within the spheroids (Fig. 11D, F), whereas in

other cases, both spheroids and outgrowing cells remained GFP negative (Fig. 11B). Cells growing under the matrix in monolayers were susceptible to HSV-1 and showed widespread fluorescence.

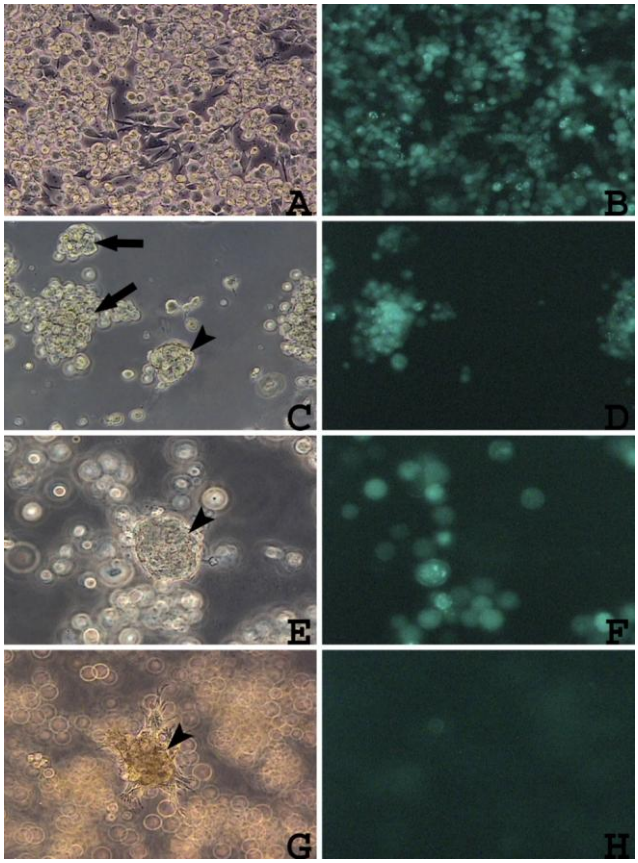

Figure 10: Morphology and GFP expression in HSV-1 K26GFP inoculated OCM1 uveal melanoma 2D and 3D cultures. 2D OCM1 culture 1 day after virus inoculation; morphology (A) and GFP expression (B). 3D OCM1 cultures 1 day after virus inoculation; morphology (C) and GFP expression (D). Arrows in panel (C) indicate tumor cell aggregates on the Matrigel surface that are GFP positive in panel D and arrowhead in panel C indicates a multicellular spheroid within the Matrigel matrix that is GFP negative in panel D. 3D OCM1 cultures 3 days after virus inoculation; morphology (E) and GFP expression (F). Arrowhead in panel E indicates a multicellular spheroid within the Matrigel matrix that is GFP negative in panel F. 3D OCM1 cultures 12 days after virus inoculation; morphology (G) and GFP expression (H). Arrowhead in panel G indicates a multicellular spheroid within the Matrigel matrix showing outgrowth of individual tumor cells at the periphery that is GFP negative in panel H.

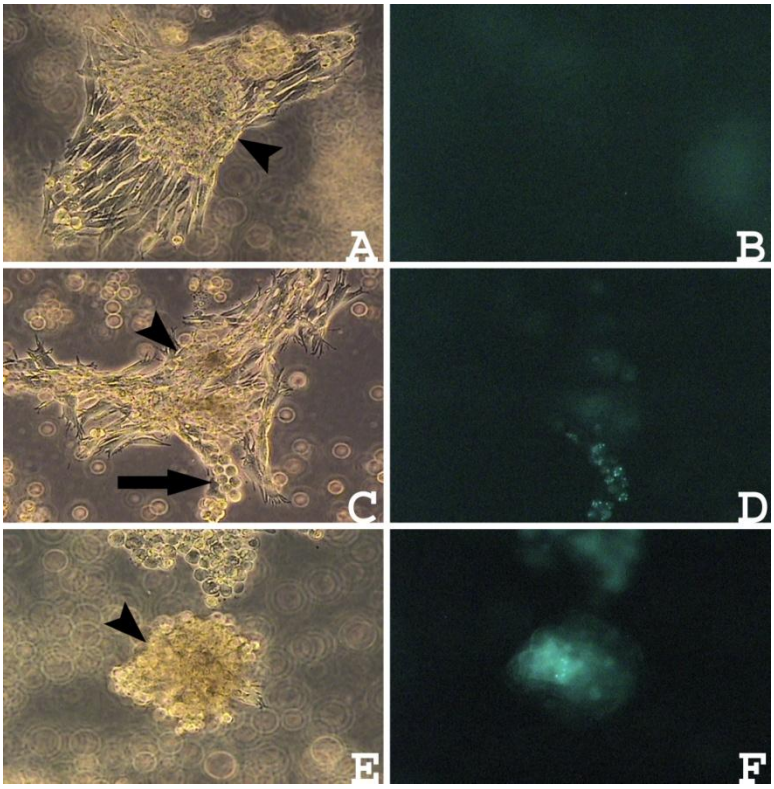

Figure 11: Morphology and GFP expression in HSV-1 K26GFP inoculated 3D OCM1 uveal melanoma cultures 12 days after virus inoculation. Arrowhead in panel (A) indicates a multicellular spheroid within the Matrigel matrix that shows outgrowth of individual tumor cells at its periphery that are GFP negative in panel (B). Arrowhead in panel (C) indicates a multicellular spheroid within the Matrigel matrix showing outgrowth of individual tumor cells. Some of the outgrowing tumor cells show GFP expression in panel (D). Arrowhead in panel (E) indicates a multicellular spheroid within the Matrigel matrix with outgrowth of individual tumor cells at the periphery with cells within the core of the spheroid showing GFP expression in panel (F).

In 3D cultures of C918 cells, cells growing on the matrix surface in a single layer showed widespread fluorescence (virus replication) as early as 1 day p.i. consistent with the complete destruction of this cell population by K26GFP by 9 days p.i. (Fig. 12C, D). In contrast, cells forming vasculogenic mimicry patterns on the Matrigel surface showed increased resistance to HSV-1 (Fig. 12E, F) and GFP-negative cells could be observed in these structures throughout the 4-week observation period. Similarly, cells invading the matrix individually showed increased resistance to HSV-1 and this cell population also included many GFP-negative cells throughout the 4-week observation period (Fig. 12G–H; 13A-F). Tumor cells growing in monolayers under the Matrigel showed widespread fluorescence and susceptibility to HSV-1 (Figure 12E, F).

These observations clearly identify certain uveal melanoma populations with increased resistance against HSV-1 in the 3D environment. Consequent experiments were designed to identify the mechanism(s) responsible for the observed resistance of tumor cells against HSV-1 in 3D cultures.

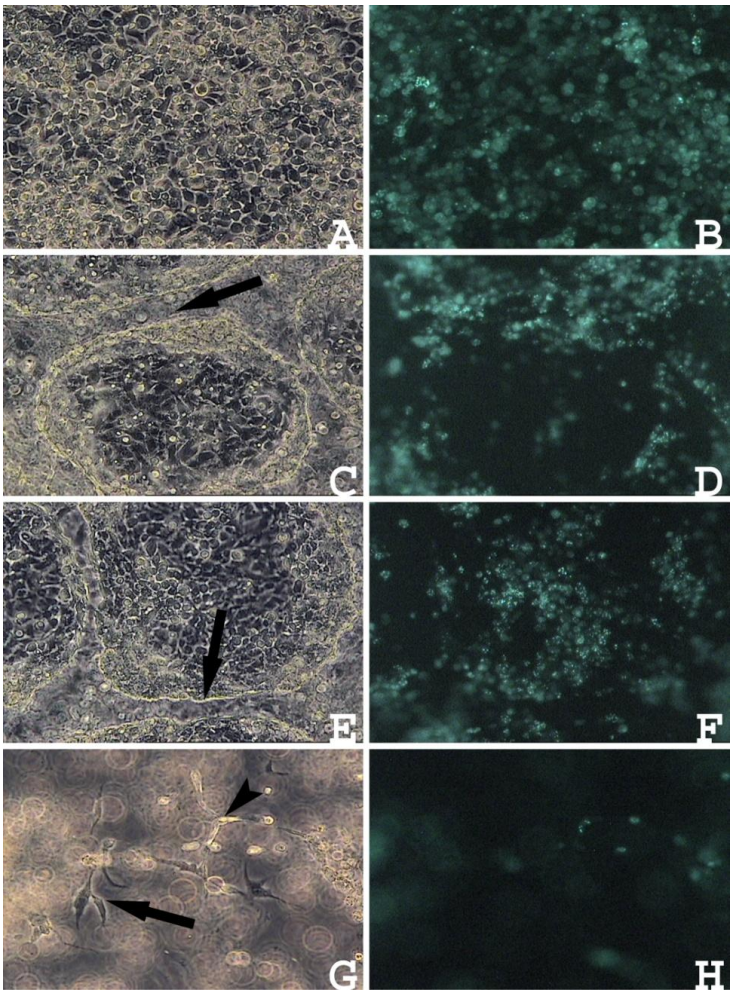

Figure 12. Morphology and GFP expression in HSV-1 K26GFP inoculated C918 uveal melanoma cells grown in 2D and 3D cultures. 2D C918 monolayer culture 3 days after virus inoculation; morphology (A) and GFP expression (B). 3D C918 culture 3 days after virus inoculation; morphology (C) and GFP expression (D). Arrow in panel (C) indicates tumor cells growing in monolayer on the Matrigel surface that express GFP in panel (D). 3D C918 culture 3 days after virus inoculation; morphology (E) and GFP expression (F). Arrow in panel (E) indicates tumor cells forming vasculogenic mimicry pattern on the Matrigel surface that only partially expresses GFP in panel (F). 3D C918 culture 3 days after virus inoculation; morphology (G) and GFP expression (H). Arrow in panel (G) indicates a tumor cell invading Matrigel that does not express GFP in panel (H). Arrowhead in panel (G) indicates a tumor cell invading Matrigel that expresses GFP in panel (H).

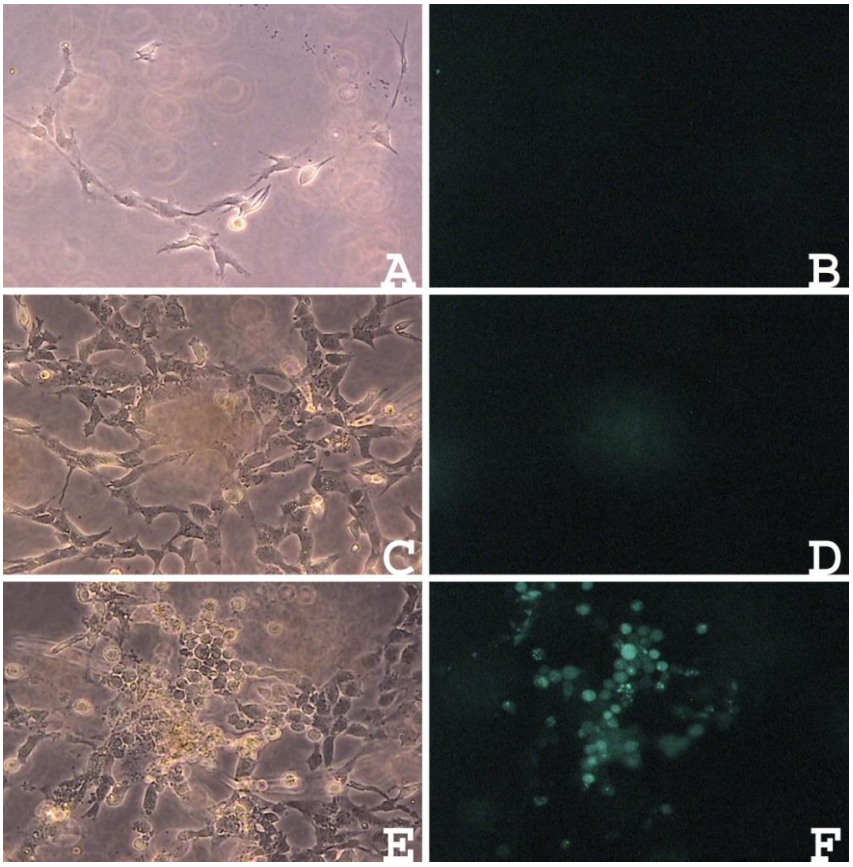

Figure 13. Morphology (A, C, E) and GFP expression (B, D, F) of cells invading the Matrigel matrix in HSV-1 K26GFP inoculated 3D C918 uveal melanoma cultures 12 days after virus inoculation. Note the lack of GFP expression in panels (B, D) and the variable expression of GFP by tumor cells in panel (F).

4.2.3 Matrigel impairs HSV-1 spread

To determine whether inhibition of HSV-1 spread through Matrigel was a mechanism responsible for the absence of virus replication (GFP expression) in some tumor cells in 3D cultures, monolayers of OCM1 and C918 cells were covered with an approximately 1mm thick layer of Matrigel and then HSV-1 K26GFP was placed on the Matrigel surface. As controls, monolayers of OCM1 and C918 cells without a Matrigel cover were also inoculated with the same amount of virus. Virus inoculated uveal monolayers with no Matrigel cover showed widespread GFP expression by 18–24 h p.i. and were completely destroyed within a few days. In contrast, cells covered with Matrigel and inoculated with HSV-1 K26GFP showed continued viability and growth during a 2-week observation period with no evidence of GFP expression. These findings indicate that Matrigel inhibits HSV-1 spread.

4.2.4 ECM mediates inhibition of HSV-1 replication after virus entry into tumor cells

To determine whether inhibition of viral replication after virus entry into tumor cells is a mechanism responsible for the absence of virus replication (GFP expression) in some tumor cells in 3D cultures, uveal melanoma cells were first inoculated with HSV-1 K26GFP under 2D conditions (allowing for unimpeded entry of virus into cells) and were then cultured under either 2D or 3D conditions.

After the plating of earlier mock-infected OCM1 and C918 cells on tissue culture dishes, tumor cells established monolayers (2D cultures) that showed normal growth and no evidence of GFP expression. Growing of earlier mock-infected OCM1 and C918 cells under 3D conditions in Matrigel was initially associated with single cells suspended in matrix. After the first day, growth of OCM1 cells was associated with the development of tumor cell spheroids, many of which later showed outgrowth of individual cells into the matrix. Growth of mock-infected C918 cells was associated with the establishment of extensive network of tumor cells invading the matrix. No GFP expression was detected in the mock-infected 3D cultures of OCM1 and C918 cells.

After the plating of earlier HSV-1 K26GFP inoculated OCM1 and C918 cells on tissue culture dishes, tumor cells established monolayers (2D cultures) that were completely destroyed by virus replication within a few days. At 18 h p.i., 29.53 ± 15.01% of OCM1 cells and 40.33 ± 15.17% of C918 cells showed fluorescence (evidence of HSV-1 replication) (Tab. 4). Nearly all OCM1 cells were GFP positive by 72 h and nearly all C918 cells were GFP positive by 96 h. These findings are consistent with replication of input virus in infected cells at 18 h p.i. and virus spread to all cells in the following days.

Culturing of earlier HSV-1 K26GFP inoculated OCM1 and C918 cells in 3D was initially associated with single cells suspended in matrix. More than half of the cells showed morphologic changes during the first day of the establishment of the 3D cultures including rounding and a minority of cells showed morphological features of apoptosis. At 18 h p.i., the numbers of OCM1 and C918 cells in the virus-infected 3D cultures were 12.5 and 8.5% lower than those in their mock-infected 3D counterparts. At 18 h p.i., 2.80 ± 2.75% of OCM1 cells and 2.22 ± 3.05% of C918 cells showed fluorescence (Tab. 4) in the HSV-1-infected 3D cultures. The number of GFP-expressing cells did not increase the following days. Thus, at 18 h p.i., a significantly smaller percentage of cells showed evidence of virus replication in 3D cultures than what was expected on the basis of the amount of input virus. These observations

indicate that the ECM can mediate the inhibition of HSV-1 replication after virus entry into tumor cells.

Cell line	Inoculation in 2D	Consequent culture	Percent of cells GFP + [a]
OCM1	Mock	2D	0
	HSV-1 K26GFP	2D	29.53 ± 15.01
	Mock	3D	0
	HSV-1 K26GFP	3D	2.8 ± 2.75
C918	Mock	2D	0
	HSV-1 K26GFP	2D	40.33 ± 15.17
	Mock	3D	0
	HSV-1 K26GFP	3D	2.22 ± 3.05

Table 4. GFP expression in OCM1 and C918 uveal melanoma cells inoculated with 0.5 PFU per cell of HSV-1 K26GFP or mock infected with PBS under 2D conditions for 1 h and then cultured for 17 h either under 2D or 3D conditions. [a]Percentage of GFP-expressing cells was determined by counting the number of GFP-expressing and GFP-negative cells in 16 high power microscopic fields for each studied type of treatment.

In HSV-1-infected 3D cultures, the majority of cells remained GFP negative throughout a 4-week observation period (data not shown). Interestingly, the outgrowth of individual OCM1 cells into the Matrigel matrix from spheroids that have been GFP negative for days to weeks was occasionally associated with the appearance of GFP expression in outgrowing cells and in cells within the spheroids similarly to the process shown in Fig. 11C-F. As Matrigel does not allow HSV-1 spread, these observations suggest that HSV-1 established a quiescent infection in some tumor cells within multicellular spheroids and that this quiescent infection could revert to productive viral infection when the tumor growth pattern changed.

5. DISCUSSION

A general biological characteristic of herpes viruses is their ability to sustain lifelong infection of the host despite an operable immune response. The complex mechanism behind this process is called latency and can be defined as an infection in which the viral genome exists in a non-replicating form in an infected cell from which the virus can periodically reactivate. Occasional re-activation and shedding of the virus then allows the infection of new hosts and maintains high levels of viral infection, and seropositivity, within the population [65]. Recurrent lesions develop during the life of an infected individual, generally at epithelial sites such as lips (herpes labialis), oral cavity (herpetic stomatitis), the eye (herpetic keratitis), orofacial complex (herpes facialis) and skin. Additionally, epidemiological data suggest that HSV-1 is one of the environmental risk factors for Alzheimer's disease which disease characterized by progressive neuron loss, brain atrophy, and cognitive impairment [66, 67]. Furthermore many properties – including latency – instates HSV-1 especially appropriate for using it as a vector to treat inherited genetic diseases affecting the nervous system, such as ataxias, chronical diseases of the central nervous system, such as Parkinson´s disease or mediate selective oncolysis of malignant brain tumors ("virus therapy") [68].

In our first model system we used quantitative morphometric analyses to test whether latent HSV-1 infection affects mean neuron diameter, neuronal nucleus diameter, neuron density, and neuron number in the TG of mice. For these studies, we used TG tissues obtained from BALB/c mice 1, 12, and 31 weeks after corneal inoculation of HSV-1 at 5 weeks of age. These tissues were previously demonstrated to harbor productive HSV-1 infection at 1 week and latent HSV-1 infection at 12 and 31 weeks after virus inoculation (57). These results provide strong evidence that latent HSV-1 infection is associated with chronic progressive deficits in mean neuron diameter, neuronal nucleus diameter, neuron density, and neuron number in the murine TG. This work provides a link between HSV latency and progressive neural damage and establishes an experimental platform to explore mechanisms of HSV induced chronic neurological disease. We show here using careful morphometric analyses that in healthy adult mice, mean neuron diameter, mean neuron nucleus diameter, TG volume, and mean number of neurons per TG gradually increase between 6 and 37 weeks of age. The detection of increasing neuron diameter, neuronal nucleus diameter, and TG volume is not surprising and consistent with normal growth of these mice. Our findings of increasing neuron numbers in the TG of mock-infected mice are similar to those made in several reports of gradually increasing numbers of mature neurons in the sensory ganglia of healthy adult rats

[15, 16, 69-73]. In rats, both ongoing neurogenesis and maturation of undifferentiated or partially differentiated post-mitotic cells have been proposed as possible mechanisms for the observed increase in the number of mature neurons in adult animals [15, 16, 69-74]. A similar situation may be operant in mice.

Numerous previous studies indicate that corneal inoculation of immunocompetent mice with HSV-1 is followed by virus replication in the TG for about two weeks, which in turn is followed by the establishment of life-long HSV-1 latency in the TG [47, 75]. Consistent with these reports and our previous analyses of the TG tissues used in this study [76], we detected productive HSV-1 infection in the TG at 1 week after virus inoculation and evidence of latent HSV-1 infection in the TG at 12 and 31 weeks after virus inoculation. In the TG of mice euthanized 1 week after corneal HSV-1 inoculation, mean neuron diameter and mean neuronal nucleus diameter increased, while neuron density and mean neuron number per TG decreased relative to age-matched mock-infected controls. These findings are not surprising as these ganglia harbor productive HSV-1 infection, and HSV-1 replication is associated with cytopathic effects that include cellular swelling and nuclear enlargement [77, 78]. Furthermore, neuronal death in the TG of mice during the first few weeks of infection is well documented [75, 77, 79], which would account for the decrease in neuron number.

The key finding of our study is that in the TG of mice 12 and 31 weeks after HSV-1 inoculation (at 17 and 36 weeks of age), mean neuron diameter, neuronal nucleus diameter, neuron density, and mean neuron number per TG were significantly less than those in age matched mock-infected control TG. Interestingly, the deficits in neuron diameter, neuronal nucleus diameter, neuron density, and neuron number in latently infected TG were more substantial at 36 weeks than at 17 weeks of age. It is possible that diminished neuron size and number at 12 weeks after corneal virus inoculation is attributable to neuron destruction and delayed neuron growth caused by productive HSV-1 infection during the first weeks of infection. However, as only latent HSV-1 infection was detected in TG neurons at 12 and 31 weeks after corneal virus inoculation, the progressive reductions in neuron size and number between these intervals are unlikely to occur as a consequence of virus replication during the first few weeks of infection.

Mean neuron diameter, mean neuronal nucleus diameter, and mean neuron number per TG increased in absolute numbers between 17 and 36 weeks in latently infected mice. However, these increases were substantially less than those in mock-infected controls. Furthermore, the increases detected were less than expected for resumption of normal TG growth at these times. Resumption of normal TG growth would be expected to be associated

with stable or decreasing deficits in neuron size, density, and number in latently infected TG between 12 and 31 weeks after virus inoculation (between 16 and 36 weeks of age) relative to age-matched controls. However, these relative deficits all increased during latency. These findings indicate that latent HSV-1 infection is associated with chronic progressive deficits in neuron size, density, and number in the nervous system of an immunocompetent host.

Mechanisms by which latent HSV-1 infection leads to chronic progressive alterations in neuron size, density, and number in the nervous system are not clear from our study. As spontaneous HSV-1 reactivation occurs in latently infected mice [47, 79], albeit rarely, it is possible that reactivation events contribute to changes in neuronal size and number. Detection of extremely rare HSV-1 protein-expressing cells in a minority of TG at 12 and 31 weeks after HSV-1 inoculation is consistent with virus reactivation. However, potential causes of progressive neuronal injury are not restricted to HSV-1 reactivation events, as latent infection and the associated persistent inflammatory response also can cause neuronal dysfunction and tissue injury [58, 59, 76, 80]. Latent HSV-1 infection in the murine TG is associated with low-level expression of replication-cycle HSV-1 genes in the absence of infectious virus production [55]. Marginal HSV-1 protein expression associated with these incomplete reactivation attempts may induce neuronal injury. Persistent inflammation during HSV-1 latency in the murine TG also may cause neuronal injury, possibly mediated by cytokines and oxidative stress [58, 59, 76]. Indeed, the extent of neuronal injury during latent infection in our current study seemed to correlate with the extent of inflammation in the TG. These viral and inflammatory processes may injure mature neurons or interfere with ongoing neurogenesis and neuronal maturation in the TG.

While mice surviving the acute phase of experimental HSV infection do not show signs and symptoms of encephalitis, numerous studies documented chronic behavioral and neurological deficits and chronic pain in these animals [53, 54, 56, 57, 81-83]. In the current study, mice were observed daily for signs and symptoms of encephalitis, but detailed neurological and behavioral studies were not performed. Future experiments will need to determine whether HSV-1 latent infection-associated progressive pathologic changes documented here cause progressive neurological or behavioral deficits in mice. These studies will provide an excellent experimental platform to dissect mechanisms of HSV-induced chronic neurological disease. A role for genetic susceptibility of latent HSV-induced chronic neuronal injury should be a focus of future studies using this experimental system as genetic susceptibility has been repeatedly proposed to be important for the pathogenesis of HSV-induced chronic neurological disease in humans [21, 84-90]. These studies may lead to major

new insights into mechanisms by which latent viral infections contribute to the pathogenesis of chronic neurological and neuropsychiatric diseases and foster development of virus-specific intervention strategies.

In our second model system we used 2D and 3D cultures of uveal melanoma cells and were designed to find answers to the following questions related to HSV-1 oncolytic therapy: (i) Can 3D tumor cell cultures be used to identify morphologically distinct tumor cell populations that have increased resistance to HSV-1? (ii) Can 3D tumor cell cultures be used to learn about mechanisms of ECM mediated tumor cell resistance to HSV-1 oncolytic therapy?

We show for the first time that 3D tumor cell cultures can be used to identify morphologically distinct tumor cell populations with increased resistance to HSV-1. Specifically, we show that tumor cells forming vasculogenic mimicry patterns and multicellular spheroids and cells that invade the ECM individually have increased resistance to HSV-1. Furthermore, we show that mechanisms of tumor resistance against HSV-1 in the 3D environment include impaired virus spread in the ECM and ECM-mediated inhibition of viral replication after viral entry into tumor cells. Observations reported here also suggest that HSV-1 can establish quiescent infection in some tumor cells present in multicellular spheroids and that this can revert to productive viral infection on outgrowth of individual tumor cells into the Matrigel matrix.

It is well established that 3D tumor cell cultures are useful for preclinical evaluation of the cytotoxic effect of anticancer agents, and multiple cell types within individual tumors have differential sensitivities to drugs and radiation both in vivo and in 3D cultures [46, 48, 49, 91]. However, so far very few studies have used 3D tumor cell cultures in the context of viral oncolytic therapy. These studies have indicated that tumor cells grown in 3D cultures are also more resistant to viral, including HSV-1 and adenovirus-mediated oncolytic therapy, than cells grown in 2D culture [51, 52]. Observations reported here confirm and extend the finding of these studies and identify morphologically distinct tumor cell populations present in 3D cultures that have increased resistance to viral oncolytic therapy. These observations are likely of clinical relevance as, for instance, vasculogenic mimicry patterns are present in a wide variety of malignancies and their detection in several tumor types is associated with adverse outcome [92, 93].

Factors limiting the effectiveness of HSV-1 oncolytic therapy remain poorly understood in part because related studies have been limited to expensive and time-consuming experimental animal models. Theoretical considerations and experimental observations made

thus far indicate that mechanisms of tumor resistance to HSV-1 therapy include ECM-mediated impairment of intratumoral virus spread, impaired viral entry into tumor cells because of decreased expression of HSV-1 entry receptors, inhibition of viral replication after viral entry into tumor cells, and virus clearance by the host immune system [32-34, 38, 39, 41, 94, 95]. In this study, we found that at least two of these potential mechanisms of virus resistance — impaired virus spread in the ECM and inhibition of viral replication after viral entry into tumor cells — are also relevant to 3D tumor cell cultures.

HSV-1 oncolysis can be improved by degradation of fibrillar collagen in tumors indicating that the ECM has an important function in determining treatment efficacy [94]. This study indicates that laminin-rich ECM, Matrigel inhibits HSV-1 spread. These findings are consistent with the earlier reported inhibition of HSV-1 spread by epithelial basement membrane *in vivo* and by Matrigel *in vitro* [96]. It is important to note that HSV-1 could clearly infect and replicate in some uveal melanoma cells that have invaded the Matrigel matrix in this study. These observations indicate that HSV-1 can spread through Matrigel if tumor cells infiltrating the ECM are present. Whether HSV-1 can spread from cell to cell within the Matrigel matrix through intercellular contacts or through spaces in Matrigel created by growing tumor cells remains unclear at this point.

This study also indicates that inhibition of viral replication at a stage beyond viral entry is an important mechanism by which the ECM can modulate viral replication in tumors. It is well known that adhesion of cancer cells to the ECM mediates drug and radiation resistance [46, 97, 98]. The connection of tumor cells to ECM proteins such as collagen and laminin through cell adhesion molecules, in particular integrin receptors, is associated with tumor cell survival and drug resistance through the activation of a variety of signaling pathways. It is unclear at this point to what extent, if any, mechanisms of drug and radiation resistance in 3D tumor cell cultures are overlapping with mechanisms of virus resistance. It is possible that ECM-mediated signaling affects the expression of cellular transcription factors that can regulate the expression of viral genes in a manner that is not favorable for the progression of the viral replication cycle after HSV-1 entry.

Interestingly, observations made in this study suggest that HSV-1 establishes quiescent infection in some tumor cells in 3D cultures. When OCM1 and C918 cells were inoculated with HSV-1 under 2D conditions and were then cultured within Matrigel, only a small minority of tumor cells that have taken up HSV-1 showed evidence of virus replication (GFP expression). As discussed earlier, these findings indicated that the viral replication cycle was inhibited at a post-entry step in the majority of infected tumor cells. Consequent growth of

virus inoculated OCM1 cells in 3D cultures was associated with the establishment of multicellular tumor cell spheroids. Many OCM1 cells forming multicellular spheroids remained GFP negative throughout a 4-week observation period. However, the outgrowth of individual OCM1 cells into the Matrigel matrix from spheroids that have been GFP negative for days to weeks was often associated with the appearance of GFP expression in outgrowing cells and in cells within the spheroids. As Matrigel inhibits virus spread, reappearance of GFP expression in multicellular spheroids was very suggestive of virus reactivation from quiescence in earlier HSV-1 inoculated cells. It is well known that HSV-1 can establish quiescent infection in cultured non-neuronal cells if the progression of the viral replication cycle is blocked shortly after virus entry [75, 99]. However, establishment of quiescent infection in tumor cells induced by the ECM environment and reactivation of viral replication on changing tumor growth pattern have not yet been reported. It will be of practical significance to determine whether similar processes also occur in vivo during HSV-1 oncolytic therapy. Our observations reported here provide novel information about virus resistance of distinct tumor cell subpopulations in 3D tumor cell cultures and about mechanisms of ECM-mediated virus resistance of tumor cells. It is clear that additional studies will be required to fully understand the mechanisms by which the ECM mediates increased HSV-1 resistance of tumor cells in 3D cultures and to assess the clinical relevance of information collected in these cultures. However, our observations suggest that the experimental platform provided by 3D tumor cultures will be invaluable for studies aimed at the improvement and preclinical evaluation of viral oncolytic agents similarly to its usefulness in the case of chemotherapeutic agents and radiation therapy.

In summary, HSV-1 is an important human pathogen responsible for significant morbidity and mortality. To better understand the difficult and compound pathways cooperating with the pathogenesis of this virus the use of tissue and cell cultures and animal models are important, but thus far many issues regarding both pathogenesis and effective therapy are unclear. Intensive research concerning HSV-1 vectors is ongoing which can be used to express potential therapeutic genes or accomplish effective oncolysis of malignant tumors. It is clear from this discussion that there are plenty of mentioned topics requiring further exploration with focus on latency to broaden our current knowledge and thereby providing an improved patient care.

6. SUMMARY

In our work, we investigated two aspects of HSV-1 latency using *in vivo* and *in vitro* model systems. In the first part of our work, we examined some pathologic consequences of latent HSV-1 infection in mice and in the second part of our work we examined melanoma resistance to HSV-1-mediated oncolysis using two uveal melanoma cell lines.

Primary infection with HSV-1 is rapidly controlled by immunocompetent individuals but result in the establishment of viral latency in neurons primarily in peripheral sensory ganglia. Latent HSV-1 infection of the trigeminal ganglia becomes increasingly prevalent in humans with age and affects a majority of adults. Infection with HSV-1 has been epidemiologically linked to several common chronic neuropsychiatric and neurodegenerative diseases. Experimental HSV-1 infection of mice can lead to chronic behavioral and neurological deficits and chronic pain. While neuron injury and loss are well-documented consequences of the acute phase of infection, the pathologic consequences of latent HSV-1 infection are poorly understood. The objective of this study was to determine whether latent HSV-1 infection can cause neuronal injury in mice. Trigeminal ganglia derived from adult BALB/c mice 1, 12 and 31 weeks after corneal HSV-1 inoculation were analyzed for evidence of productive or latent HSV-1 infection, inflammation and changes in neuron size, density and number. Latent HSV-1 infection between 12 and 31 weeks after corneal virus inoculation was associated with inflammation and progressive deficits in mean neuron diameter, neuronal nucleus diameter, neuron density and neuron number in the TG relative to mock-infected controls. The extent of neuronal injury during latent infection correlated with the extent of inflammation. Our observations demonstrate that latent HSV-1 infection is associated with progressive neuronal pathology and may lead to a better understanding of the role of HSV-1 infections in chronic neurological diseases.

To better understand melanoma resistance to herpes simplex virus type-1 (HSV-1)-mediated oncolysis, traditional two-dimensional (2D) monolayer cultures and extracellular matrix containing (ECM) three-dimensional (3D) cultures of OCM1 and C918 uveal melanoma cells were infected with an HSV-1 strain that expresses the green fluorescent protein (GFP) marker during replication. Although 2D cultures were completely destroyed within a few days of HSV-1 inoculation, viable GFP-negative tumor cells remained detectable in 3D cultures for several weeks. Tumor cells with increased resistance to HSV-1 included cells that formed vasculogenic mimicry patterns and multicellular spheroids and cells that invaded Matrigel individually. Mechanisms of tumor resistance against HSV-1 in the 3D

environment included impaired virus spread in the ECM and ECM-mediated inhibition of viral replication after viral entry into tumor cells. Our observations also suggested that HSV-1 established latent infection in some tumor cells present in multicellular spheroids and that this could revert to productive viral infection when the tumor growth pattern changed. These findings indicate that 3D tumor cell cultures can be used to identify distinct tumor cell populations with latent HSV-1 infection and to explore mechanisms of ECM-mediated tumor resistance to oncolytic virotherapy.

7. ÖSSZEFOGLALÁS

Munkánk során két szempontból vizsgáltuk a humán herpesz szimplex-1 (HSV-1) által létrehozott látens (lappangó, rejtett) fertőzést; *in vivo* és *in vitro* modell rendszerekben.

A *Herpesviridae* család nagy és változatos csoportot alkot, a csoport tagjai a főemlősöktől a halakig bezáróan okoznak betegségeket. Biológiai tulajdonságaik alapján a *Herpesviridae* családot további három alcsaládra lehet osztani; *Alphaherpesvirinae, Betaherpesvirinae* és *Gammaherpesvirinae*. Az orvosi szempontból jelentős HSV-1 és HSV-2 az *Alphaherpesvirinae* alcsaládba tartozik. Közös jellemzőik, hogy viszonylag rövid reprodukciós ciklusra képesek, gyorsan terjednek sejttenyészetben, hatékonyan elpusztítják a fertőzött sejteket és képesek létrehozni látens fertőzést elsősorban, de nem kizárólag, az érző idegdúcokban. A herpeszfertőzés a sérült bőr vagy nyálkahártya hámsejtjeiben megy végbe, az elsődleges fertőzés gyakran a korai gyermekkorban történik. A vírus a hámsejtekben szaporodik, a fertőzés gyakran tünetmentes, de előfordulhat, hogy hólyagok jelennek meg a nyálkahártyán, melyek végül fekélyekké alakulnak a fertőzés területén. Az elsődleges fertőzést követően, mely a hámsejtek pusztulásával jár, a vírus az érzőideg-végződésekbe jut, majd az idegnyúlványokon keresztül a gerincvelő hátsó gyöki ganglionjaiban telepszik meg, ahol lítikus (a sejt pusztulásához vezető) vagy látens (élethosszig tartó lappangás) virális génexpresszió következik be.

A látens fertőzés alatt az idegdúcban kevés a kimutatható virális fehérje, a virális genomról történő átírás korlátozódik a látencia-asszociált transzkriptumokra (LATs). Nem ismert, hogy a látens HSV-1 fertőzés maga, vagy az ismételt reaktivációs események és az ehhez kapcsolódó gyulladásos válasz áll-e az idegdúcok károsodása mögött. A trigeminális ganglionokban található látens HSV-1 fertőzés a kor előrehaladtával egyre elterjedtebb és érinti a felnőttek többségét. A HSV-1 fertőzés járványtanilag kapcsolható számos idült neuropszichiátriai és neurodegeneratív betegséghez. Kísérleti körülmények között a HSV-1 fertőzés egerekben vezethet idült viselkedési és idegrendszeri károsodáshoz, illetve krónikus fájdalomhoz. Míg az idegsejtek károsodása jól dokumentált következménye a fertőzés heveny szakaszának, a látens fertőzés patológiás következményei kevésbé ismertek. Kutatásunk célja annak megállapítása volt, hogy a látens HSV-1 fertőzés okozhat-e idegsejt károsodást az egerek trigeminus idegdúcaiban. Felnőtt BALB/c egerekből származó trigeminális idegdúcokat vizsgáltunk 1, 12 és 31 héttel a szaruhartyán keresztüli HSV-1 fertőzést követően. Vizsgáltuk a fertőzés produktív vagy látens jellegét, illetve azt, hogy milyen változások történtek a neuronok méretét, sűrűségét és számát illetően. A látens HSV-1

fertőzés során, 12 és 31 héttel a szaruhártya vírusfertőzését követően fokozódó csökkenést tapasztatnunk az idegsejtek átmérőjében, az idegsejtek sűrűségében illetve az idegsejtek számában a kontroll idegdúcokhoz képest. Megfigyeléseink azt mutatják, hogy látens HSV-1 fertőzéshez progresszív idegsejt károsodás társul, ez hozzásegíthet a HSV-1 fertőzések krónikus neurológiai betegségekben betöltött szerepének jobb megértéséhez.

A HSV-1 ezen felül egy ígéretes jelölt a vírus közvetített onkolitikus (daganat pusztító) terápia területén. Az onkolitikus HSV-1 terápia függ a vírus szaporodásától a daganatsejtekben, illetve fokozza a szervezet vírusellenes - és ez által daganatellenes - immunválaszát. Annak ellenére, hogy jelentős előrelépések történtek, a vírus közvetített onkolitikus terápia a mai napig kihívásokkal néz szembe. Bár kísérleti körülmények között, hagyományos egyrétegű, kétdimenziós daganatsejt-tenyészeteket használva hatékonyan lehet HSV-1 vírusokkal sejttenyeszeteket megsemmisíteni, elő szervezetben a tumor sejtek elpusztítása gyakran nem teljes. Ezen jelenség okai a mai napig nem tisztazottak. Azonban számos megfigyelés azt sugallja, hogy a potenciális problémák közé tartozik többek között az extracelluláris mátrix gátló hatása a daganatsejtek közötti vírusterjedésre, illetve a virális receptorok csökkent kifejeződése a különböző daganatsejt populációkban. Munkánk második részben a HSV-1 által közvetített onkolízist vizsgáltuk két melanoma (rosszindulatú festéksejtes daganat) sejtvonal (OCM1 és C918) tanulmányozásával. Hogy bővebb betekintést nyerjünk a melanoma sejtek HSV-1 által közvetített onkolízissel szembeni ellenállásának folyamatába, egyrétegű/kétdimenziós és extracelluláris mátrixot tartalmazó háromdimenziós sejttenyészeteket fertőztünk meg egy módosított HSV-1 vírus törzzsel, mely replikációja során zöld fluoreszcens fehérjét fejez ki. Bár a kétdimenziós sejttenyészetek a HSV-1 fertőzés után néhány napon belül teljesen elpusztultak, a háromdimenziós sejtkultúrákban életképes és GFP-negatív tumor sejtek maradtak megfigyelhetőek a HSV-1 fertőzést követően. Azon tumor sejtek, melyek fokozott ellenállást tanúsítottak a HSV-1 fertőzéssel szemben, jellegzetes növekedési formákat mutattak, úgynevezett vasculogenezist utánzó növekedési mintázatot követtek, illetve több sejtből álló gömböcskéket (spheroidok) formáltak. Háromdimenziós környezetben a tumor sejtek túlélését a következő mechanizmusok segíthetik elő: a vírus terjedésének csökkenése az extracelluláris mátrixban, illetve az extracelluláris mátrix által kiváltott vírusszaporodás gátlása. Megfigyeléseink azt mutatják, hogy a HSV-1 látens fertőzést hozott létre néhány spheroidban és ez a látens fertőzés produktív formát öltött, mikor a daganatsejtek növekedési mintázata megváltozott. Eredmények azt mutatják, hogy a háromdimenziós tumorsejt-tenyészetek jól használhatók különböző, látens HSV-1 fertőzést tartalmazó tumorsejt-populáció azonosítására, illetve

annak további vizsgálatára, úgymint az extracelluláris matrix milyen mechanizmusokkal befolyásolja az onkolitikus vírus terápia hatékonyságát.

8. REFERENCES

[1] Field's Virology, Sixth edition ed., Lippincott Williams & Willkins, 2013.

[2] L. Collier, J. Oxford, Human Virology, Third edition ed., Oxford University Press, 2006.

[3] A. Bosque, V. Planelles, Induction of HIV-1 latency and reactivation in primary memory CD4+ T cells, Blood, 113 (2009) 58-65.

[4] M. Ranzani, S. Annunziato, D.J. Adams, E. Montini, Cancer gene discovery: exploiting insertional mutagenesis, Molecular cancer research : MCR, 11 (2013) 1141-1158.

[5] B. Roizman, L.E. Carmichael, F. Deinhardt, G. de-The, A.J. Nahmias, W. Plowright, F. Rapp, P. Sheldrick, M. Takahashi, K. Wolf, Herpesviridae. Definition, provisional nomenclature, and taxonomy. The Herpesvirus Study Group, the International Committee on Taxonomy of Viruses, Intervirology, 16 (1981) 201-217.

[6] D. Shukla, P.G. Spear, Herpesviruses and heparan sulfate: an intimate relationship in aid of viral entry, J Clin Invest, 108 (2001) 503-510.

[7] K. Grunewald, P. Desai, D.C. Winkler, J.B. Heymann, D.M. Belnap, W. Baumeister, A.C. Steven, Three-dimensional structure of herpes simplex virus from cryo-electron tomography, Science, 302 (2003) 1396-1398.

[8] T.J. Liesegang, Biology and molecular aspects of herpes simplex and varicella-zoster virus infections, Ophthalmology, 99 (1992) 781-799.

[9] B. Roizmann, R.C. Desrosiers, B. Fleckenstein, C. Lopez, A.C. Minson, M.J. Studdert, The family Herpesviridae: an update. The Herpesvirus Study Group of the International Committee on Taxonomy of Viruses, Archives of virology, 123 (1992) 425-449.

[10] J.P. Quinn, R.G. Dalziel, A.A. Nash, Herpes virus latency in sensory ganglia--a comparison with endogenous neuronal gene expression, Progress in neurobiology, 60 (2000) 167-179.

[11] L. Corey, P.G. Spear, Infections with herpes simplex viruses (2), N Engl J Med, 314 (1986) 749-757.

[12] D.A. Scott, W.A. Coulter, P.A. Biagioni, H.O. O'Neill, P.J. Lamey, Detection of herpes simplex virus type 1 shedding in the oral cavity by polymerase chain reaction and enzyme-linked immunosorbent assay at the prodromal stage of recrudescent herpes labialis, Journal of oral pathology & medicine : official publication of the International Association of Oral Pathologists and the American Academy of Oral Pathology, 26 (1997) 305-309.

[13] P.G. Arduino, S.R. Porter, Herpes Simplex Virus Type 1 infection: overview on relevant clinico-pathological features, Journal of oral pathology & medicine : official publication of the International Association of Oral Pathologists and the American Academy of Oral Pathology, 37 (2008) 107-121.

[14] B.W.J. Mahy, M.H.V. Van Regenmortel, Encyclopedia of Virology, Third edition ed., Elsevier, 2008.

[15] M. Devor, R. Govrin-Lippmann, Neurogenesis in adult rat dorsal root ganglia: on counting and the count, Somatosensory & motor research, 8 (1991) 9-12.

[16] M. Devor, R. Govrin-Lippmann, I. Frank, P. Raber, Proliferation of primary sensory neurons in adult rat dorsal root ganglion and the kinetics of retrograde cell loss after sciatic nerve section, Somatosensory research, 3 (1985) 139-167.

[17] P.G. Kennedy, A. Chaudhuri, Herpes simplex encephalitis, Journal of neurology, neurosurgery, and psychiatry, 73 (2002) 237-238.

[18] A. Sauerbrei, U. Eichhorn, G. Hottenrott, P. Wutzler, Virological diagnosis of herpes simplex encephalitis, Journal of clinical virology : the official publication of the Pan American Society for Clinical Virology, 17 (2000) 31-36.

[19] J.R. Baringer, P. Pisani, Herpes simplex virus genomes in human nervous system tissue analyzed by polymerase chain reaction, Annals of neurology, 36 (1994) 823-829.

[20] N.W. Fraser, W.C. Lawrence, Z. Wroblewska, D.H. Gilden, H. Koprowski, Herpes simplex type 1 DNA in human brain tissue, Proc Natl Acad Sci U S A, 78 (1981) 6461-6465.

[21] R.F. Itzhaki, W.R. Lin, D. Shang, G.K. Wilcock, B. Faragher, G.A. Jamieson, Herpes simplex virus type 1 in brain and risk of Alzheimer's disease, Lancet, 349 (1997) 241-244.

[22] W. Liedtke, B. Opalka, C.W. Zimmermann, E. Lignitz, Age distribution of latent herpes simplex virus 1 and varicella-zoster virus genome in human nervous tissue, Journal of the neurological sciences, 116 (1993) 6-11.

[23] J.R. Baringer, P. Swoveland, Recovery of herpes-simplex virus from human trigeminal ganglions, N Engl J Med, 288 (1973) 648-650.

[24] K.D. Croen, J.M. Ostrove, L.J. Dragovic, S.E. Straus, Patterns of gene expression and sites of latency in human nerve ganglia are different for varicella-zoster and herpes simplex viruses, Proc Natl Acad Sci U S A, 85 (1988) 9773-9777.

[25] I. Steiner, J.G. Spivack, D.R. O'Boyle, 2nd, E. Lavi, N.W. Fraser, Latent herpes simplex virus type 1 transcription in human trigeminal ganglia, J Virol, 62 (1988) 3493-3496.

[26] J.G. Stevens, L. Haarr, D.D. Porter, M.L. Cook, E.K. Wagner, Prominence of the herpes simplex virus latency-associated transcript in trigeminal ganglia from seropositive humans, The Journal of infectious diseases, 158 (1988) 117-123.

[27] P.R. Krause, K.D. Croen, S.E. Straus, J.M. Ostrove, Detection and preliminary characterization of herpes simplex virus type 1 transcripts in latently infected human trigeminal ganglia, J Virol, 62 (1988) 4819-4823.

[28] D. Theil, T. Derfuss, I. Paripovic, S. Herberger, E. Meinl, O. Schueler, M. Strupp, V. Arbusow, T. Brandt, Latent herpesvirus infection in human trigeminal ganglia causes chronic immune response, Am J Pathol, 163 (2003) 2179-2184.

[29] Z.S. Guo, S.H. Thorne, D.L. Bartlett, Oncolytic virotherapy: molecular targets in tumor-selective replication and carrier cell-mediated delivery of oncolytic viruses, Biochimica et biophysica acta, 1785 (2008) 217-231.

[30] T.C. Liu, D. Kirn, Gene therapy progress and prospects cancer: oncolytic viruses, Gene therapy, 15 (2008) 877-884.

[31] D.S. Latchman, Herpes simplex virus-based vectors for the treatment of cancer and neurodegenerative disease, Current opinion in molecular therapeutics, 7 (2005) 415-418.

[32] Y. Shen, J. Nemunaitis, Herpes simplex virus 1 (HSV-1) for cancer treatment, Cancer gene therapy, 13 (2006) 975-992.

[33] S. Varghese, S.D. Rabkin, Oncolytic herpes simplex virus vectors for cancer virotherapy, Cancer gene therapy, 9 (2002) 967-978.

[34] E.A. Chiocca, The host response to cancer virotherapy, Current opinion in molecular therapeutics, 10 (2008) 38-45.

[35] F. Benencia, M.C. Courreges, N.W. Fraser, G. Coukos, Herpes virus oncolytic therapy reverses tumor immune dysfunction and facilitates tumor antigen presentation, Cancer biology & therapy, 7 (2008) 1194-1205.

[36] H. Fukuhara, T. Todo, Oncolytic herpes simplex virus type 1 and host immune responses, Current cancer drug targets, 7 (2007) 149-155.

[37] C.G. Miller, N.W. Fraser, Requirement of an integrated immune response for successful neuroattenuated HSV-1 therapy in an intracranial metastatic melanoma model, Molecular therapy : the journal of the American Society of Gene Therapy, 7 (2003) 741-747.

[38] G. Guzman, S. Oh, D. Shukla, H.H. Engelhard, T. Valyi-Nagy, Expression of entry receptor nectin-1 of herpes simplex virus 1 and/or herpes simplex virus 2 in normal and neoplastic human nervous system tissues, Acta virologica, 50 (2006) 59-66.

[39] G. Guzman, S. Oh, D. Shukla, T. Valyi-Nagy, Nectin-1 expression in the normal and neoplastic human uterine cervix, Archives of pathology & laboratory medicine, 130 (2006) 1193-1195.

[40] D. Kolodkin-Gal, G. Zamir, Y. Edden, E. Pikarsky, A. Pikarsky, H. Haim, Y.S. Haviv, A. Panet, Herpes simplex virus type 1 preferentially targets human colon carcinoma: role of extracellular matrix, J Virol, 82 (2008) 999-1010.

[41] M.A. Rueger, A. Winkeler, H. Miletic, C. Kaestle, R. Richter, G. Schneider, R. Hilker, M.T. Heneka, R.I. Ernestus, J.A. Hampl, C. Fraefel, A.H. Jacobs, Variability in infectivity of primary cell cultures of human brain tumors with HSV-1 amplicon vectors, Gene therapy, 12 (2005) 588-596.

[42] A. Abbott, Cell culture: biology's new dimension, Nature, 424 (2003) 870-872.

[43] M.J. Friedrich, Studying cancer in 3 dimensions: 3-D models foster new insights into tumorigenesis, Jama, 290 (2003) 1977-1979.

[44] S. Ghosh, G.C. Spagnoli, I. Martin, S. Ploegert, P. Demougin, M. Heberer, A. Reschner, Three-dimensional culture of melanoma cells profoundly affects gene expression profile: a high density oligonucleotide array study, Journal of cellular physiology, 204 (2005) 522-531.

[45] K.S. Smalley, M. Lioni, M. Herlyn, Life isn't flat: taking cancer biology to the next dimension, In vitro cellular & developmental biology. Animal, 42 (2006) 242-247.

[46] R. Schmidmaier, P. Baumann, ANTI-ADHESION evolves to a promising therapeutic concept in oncology, Current medicinal chemistry, 15 (2008) 978-990.

[47] E.K. Wagner, D.C. Bloom, Experimental investigation of herpes simplex virus latency, Clinical microbiology reviews, 10 (1997) 419-443.

[48] F. Xu, K.J. Burg, Three-dimensional polymeric systems for cancer cell studies, Cytotechnology, 54 (2007) 135-143.

[49] T. Jacks, R.A. Weinberg, Taking the study of cancer cell survival to a new dimension, Cell, 111 (2002) 923-925.

[50] C.O. Yun, Overcoming the extracellular matrix barrier to improve intratumoral spread and therapeutic potential of oncolytic virotherapy, Current opinion in molecular therapeutics, 10 (2008) 356-361.

[51] N. Shimony, R. Gorodetsky, G. Marx, D. Gal, R. Rivkin, A. Ben-Ari, A. Landsman, Y.S. Haviv, Fibrin microbeads (FMB) as a 3D platform for kidney gene and cell therapy, Kidney international, 69 (2006) 625-633.

[52] K. Valyi-Nagy, R. Folberg, T. Valyi-Nagy, A.J. Maniotis, Role of tumor invasiveness, the extracellular matrix, and chromatin sequestration in the susceptibility of uveal melanoma to herpes simplex virus type 1, Experimental eye research, 84 (2007) 991-1000.

[53] A.G. Armien, S. Hu, M.R. Little, N. Robinson, J.R. Lokensgard, W.C. Low, M.C. Cheeran, Chronic cortical and subcortical pathology with associated neurological deficits ensuing experimental herpes encephalitis, Brain pathology, 20 (2010) 738-750.

[54] L.S. Crnic, L.I. Pizer, Behavioral effects of neonatal herpes simplex type 1 infection of mice, Neurotoxicology and teratology, 10 (1988) 381-386.

[55] L.T. Feldman, A.R. Ellison, C.C. Voytek, L. Yang, P. Krause, T.P. Margolis, Spontaneous molecular reactivation of herpes simplex virus type 1 latency in mice, Proc Natl Acad Sci U S A, 99 (2002) 978-983.

[56] R. Mahalingam, M.C. Wellish, A.N. Dueland, R.J. Cohrs, D.H. Gilden, Localization of herpes simplex virus and varicella zoster virus DNA in human ganglia, Annals of neurology, 31 (1992) 444-448.

[57] J.H. McLean, M.T. Shipley, D.I. Bernstein, D. Corbett, Selective lesions of neural pathways following viral inoculation of the olfactory bulb, Experimental neurology, 122 (1993) 209-222.

[58] D. Milatovic, Y. Zhang, S.J. Olson, K.S. Montine, L.J. Roberts, 2nd, J.D. Morrow, T.J. Montine, T.S. Dermody, T. Valyi-Nagy, Herpes simplex virus type 1 encephalitis is associated with elevated levels of F2-isoprostanes and F4-neuroprostanes, Journal of neurovirology, 8 (2002) 295-305.

[59] T. Valyi-Nagy, T.S. Dermody, Role of oxidative damage in the pathogenesis of viral infections of the nervous system, Histology and histopathology, 20 (2005) 957-967.

[60] S.M. Brown, D.A. Ritchie, J.H. Subak-Sharpe, Genetic studies with herpes simplex virus type 1. The isolation of temperature-sensitive mutants, their arrangement into complementation groups and recombination analysis leading to a linkage map, J Gen Virol, 18 (1973) 329-346.

[61] T. Valyi-Nagy, S.L. Deshmane, J.G. Spivack, I. Steiner, C.I. Ace, C.M. Preston, N.W. Fraser, Investigation of herpes simplex virus type 1 (HSV-1) gene expression and DNA synthesis during the establishment of latent infection by an HSV-1 mutant, in1814, that does not replicate in mouse trigeminal ganglia, J Gen Virol, 72 (Pt 3) (1991) 641-649.

[62] T. Tandrup, Unbiased estimates of number and size of rat dorsal root ganglion cells in studies of structure and cell survival, J Neurocytol, 33 (2004) 173-192.

[63] P. Desai, S. Person, Incorporation of the green fluorescent protein into the herpes simplex virus type 1 capsid, J Virol, 72 (1998) 7563-7568.

[64] A.J. Maniotis, R. Folberg, A. Hess, E.A. Seftor, L.M. Gardner, J. Pe'er, J.M. Trent, P.S. Meltzer, M.J. Hendrix, Vascular channel formation by human melanoma cells in vivo and in vitro: vasculogenic mimicry, Am J Pathol, 155 (1999) 739-752.

[65] A. Gil, A. Gonzalez, R. Dal-Re, P. Ortega, V. Dominguez, Prevalence of antibodies against varicella zoster, herpes simplex (types 1 and 2), hepatitis B and hepatitis A viruses among Spanish adolescents, The Journal of infection, 36 (1998) 53-56.

[66] R. Piacentini, G. De Chiara, D.D. Li Puma, C. Ripoli, M.E. Marcocci, E. Garaci, A.T. Palamara, C. Grassi, HSV-1 and Alzheimer's disease: more than a hypothesis, Frontiers in pharmacology, 5 (2014) 97.

[67] G. De Chiara, M.E. Marcocci, R. Sgarbanti, L. Civitelli, C. Ripoli, R. Piacentini, E. Garaci, C. Grassi, A.T. Palamara, Infectious agents and neurodegeneration, Molecular neurobiology, 46 (2012) 614-638.

[68] A. Jacobs, X.O. Breakefield, C. Fraefel, HSV-1-based vectors for gene therapy of neurological diseases and brain tumors: part I. HSV-1 structure, replication and pathogenesis, Neoplasia, 1 (1999) 387-401.

[69] T. Cecchini, R. Cuppini, S. Ciaroni, P. Barili, R. De Matteis, P. Del Grande, Changes in the number of primary sensory neurons in normal and vitamin-E-deficient rats during aging, Somatosensory & motor research, 12 (1995) 317-327.

[70] S. Ciaroni, T. Cecchini, R. Cuppini, P. Ferri, P. Ambrogini, C. Bruno, P. Del Grande, Are there proliferating neuronal precursors in adult rat dorsal root ganglia?, Neuroscience letters, 281 (2000) 69-71.

[71] M. Devor, R. Govrin-Lippmann, Neurogenesis in adult rat dorsal root ganglia, Neuroscience letters, 61 (1985) 189-194.

[72] A. Lagares, H.Y. Li, X.F. Zhou, C. Avendano, Primary sensory neuron addition in the adult rat trigeminal ganglion: evidence for neural crest glio-neuronal precursor maturation, The Journal of neuroscience : the official journal of the Society for Neuroscience, 27 (2007) 7939-7953.

[73] G.J. Popken, P.B. Farel, Sensory neuron number in neonatal and adult rats estimated by means of stereologic and profile-based methods, The Journal of comparative neurology, 386 (1997) 8-15.

[74] P.B. Farel, Late differentiation contributes to the apparent increase in sensory neuron number in juvenile rat, Brain research. Developmental brain research, 144 (2003) 91-98.

[75] C.M. Preston, Repression of viral transcription during herpes simplex virus latency, J Gen Virol, 81 (2000) 1-19.

[76] T. Valyi-Nagy, S.J. Olson, K. Valyi-Nagy, T.J. Montine, T.S. Dermody, Herpes simplex virus type 1 latency in the murine nervous system is associated with oxidative damage to neurons, Virology, 278 (2000) 309-321.

[77] B. Roizman, R.J. Whitley, The nine ages of herpes simplex virus, Herpes : the journal of the IHMF, 8 (2001) 23-27.

[78] M. Simpson-Holley, R.C. Colgrove, G. Nalepa, J.W. Harper, D.M. Knipe, Identification and functional evaluation of cellular and viral factors involved in the alteration of nuclear architecture during herpes simplex virus 1 infection, J Virol, 79 (2005) 12840-12851.

[79] R. Whitley, Herpes simplex viruses., in: K.D.M. Fields B N, Howley P M (Ed.) Fields Virology, Philadelphia : Lippincott Williams & Wilkins, 2001, pp. 2461-2509.

[80] M.F. Kramer, W.J. Cook, F.P. Roth, J. Zhu, H. Holman, D.M. Knipe, D.M. Coen, Latent herpes simplex virus infection of sensory neurons alters neuronal gene expression, J Virol, 77 (2003) 9533-9541.

[81] A. Sasaki, T. Mabuchi, K. Serizawa, I. Takasaki, T. Andoh, K. Shiraki, S. Ito, Y. Kuraishi, Different roles of nitric oxide synthase-1 and -2 between herpetic and postherpetic allodynia in mice, Neuroscience, 150 (2007) 459-466.

[82] M. Sato-Takeda, I. Takasaki, K. Takeda, A. Sasaki, T. Andoh, H. Nojima, K. Shiraki, Y. Kuraishi, K. Hanaoka, K. Tokunaga, T. Yabe, Major histocompatibility complex haplotype is associated with postherpetic pain in mice, Anesthesiology, 104 (2006) 1063-1069.

[83] I. Takasaki, H. Nojima, K. Shiraki, Y. Sugimoto, A. Ichikawa, F. Ushikubi, S. Narumiya, Y. Kuraishi, Involvement of cyclooxygenase-2 and EP3 prostaglandin receptor in acute herpetic but not postherpetic pain in mice, Neuropharmacology, 49 (2005) 283-292.

[84] S.L. Buka, T.D. Cannon, E.F. Torrey, R.H. Yolken, D. Collaborative Study Group on the Perinatal Origins of Severe Psychiatric, Maternal exposure to herpes simplex virus and risk of psychosis among adult offspring, Biological psychiatry, 63 (2008) 809-815.

[85] S.L. Buka, M.T. Tsuang, E.F. Torrey, M.A. Klebanoff, D. Bernstein, R.H. Yolken, Maternal infections and subsequent psychosis among offspring, Archives of general psychiatry, 58 (2001) 1032-1037.

[86] F.B. Dickerson, J.J. Boronow, C. Stallings, A.E. Origoni, S. Cole, B. Krivogorsky, R.H. Yolken, Infection with herpes simplex virus type 1 is associated with cognitive deficits in bipolar disorder, Biological psychiatry, 55 (2004) 588-593.

[87] D. Krause, J. Matz, E. Weidinger, J. Wagner, A. Wildenauer, M. Obermeier, M. Riedel, N. Muller, The association of infectious agents and schizophrenia, The world journal of biological psychiatry : the official journal of the World Federation of Societies of Biological Psychiatry, 11 (2010) 739-743.

[88] M. Mora, L. Quintero, R. Cardenas, H. Suarez-Roca, M. Zavala, N. Montiel, [Association between HSV-2 infection and serum anti-rat brain antibodies in patients with autism], Investigacion clinica, 50 (2009) 315-326.

[89] D.J. Schretlen, T.D. Vannorsdall, J.M. Winicki, Y. Mushtaq, T. Hikida, A. Sawa, R.H. Yolken, F.B. Dickerson, N.G. Cascella, Neuroanatomic and cognitive abnormalities related to herpes simplex virus type 1 in schizophrenia, Schizophrenia research, 118 (2010) 224-231.

[90] R. Yolken, Viruses and schizophrenia: a focus on herpes simplex virus, Herpes : the journal of the IHMF, 11 Suppl 2 (2004) 83A-88A.

[91] R.A. Vescio, C.H. Redfern, T.J. Nelson, S. Ugoretz, P.H. Stern, R.M. Hoffman, In vivo-like drug responses of human tumors growing in three-dimensional gel-supported primary culture, Proc Natl Acad Sci U S A, 84 (1987) 5029-5033.

[92] R. Folberg, M.J. Hendrix, A.J. Maniotis, Vasculogenic mimicry and tumor angiogenesis, Am J Pathol, 156 (2000) 361-381.

[93] R. Folberg, A.J. Maniotis, Vasculogenic mimicry, APMIS : acta pathologica, microbiologica, et immunologica Scandinavica, 112 (2004) 508-525.

[94] T.D. McKee, P. Grandi, W. Mok, G. Alexandrakis, N. Insin, J.P. Zimmer, M.G. Bawendi, Y. Boucher, X.O. Breakefield, R.K. Jain, Degradation of fibrillar collagen in a human melanoma xenograft improves the efficacy of an oncolytic herpes simplex virus vector, Cancer research, 66 (2006) 2509-2513.

[95] Z. Yu, P.S. Adusumilli, D.P. Eisenberg, E. Darr, R.A. Ghossein, S. Li, S. Liu, B. Singh, J.P. Shah, Y. Fong, R.J. Wong, Nectin-1 expression by squamous cell carcinoma is a predictor of herpes oncolytic sensitivity, Molecular therapy : the journal of the American Society of Gene Therapy, 15 (2007) 103-113.

[96] B.S. Weeks, R.S. Ramchandran, J.J. Hopkins, H.M. Friedman, Herpes simplex virus type-1 and -2 pathogenesis is restricted by the epidermal basement membrane, Archives of virology, 145 (2000) 385-396.

[97] V.M. Weaver, S. Lelievre, J.N. Lakins, M.A. Chrenek, J.C. Jones, F. Giancotti, Z. Werb, M.J. Bissell, beta4 integrin-dependent formation of polarized three-dimensional architecture confers resistance to apoptosis in normal and malignant mammary epithelium, Cancer cell, 2 (2002) 205-216.

[98] V.M. Weaver, O.W. Petersen, F. Wang, C.A. Larabell, P. Briand, C. Damsky, M.J. Bissell, Reversion of the malignant phenotype of human breast cells in three-dimensional culture and in vivo by integrin blocking antibodies, J Cell Biol, 137 (1997) 231-245.

[99] S.D. Valyi-Nagy T, Engelhard HH, Kavouras J,, S. P, Latency strategies of alphaherpesviruses: herpes simplex virus and varicella-zoster virus latency in neurons., 1st ed., Springer: New York, 2007.

Acknowledgements

I would like to thank Dr. Valéria Endrész, Ph.D for her support and professional supervision.
I wish to thank the Rosztoczy Foundation and Tibor Valyi-Nagy, MD, PhD for providing me the excellent opportunity to work at the Department of Pathology at University of Illinois at Chicago.
My special thanks to my wife for her support and continuous encouragement.

Appendix

I.

Brain Pathology ISSN 1015-6305

RESEARCH ARTICLE

Chronic Progressive Deficits in Neuron Size, Density and Number in the Trigeminal Ganglia of Mice Latently Infected with Herpes Simplex Virus

Sandor Dosa[1,7]; Karla Castellanos[1]; Sarolta Bacsa[2,8]; Eva Gagyi[1]; S. Krisztian Kovacs[1,7]; Klara Valyi-Nagy[1]; Deepak Shukla[2,3]; Terence S. Dermody[4,5,6]; Tibor Valyi-Nagy[1]

Departments of [1] Pathology, [2] Ophthalmology and Visual Sciences and [3] Microbiology and Immunology, University of Illinois at Chicago, College of Medicine, Chicago, Ill.
Departments of [4] Pediatrics and [5] Microbiology and Immunology and [6] Elizabeth B. Lamb Center for Pediatric Research, Vanderbilt University School of Medicine, Nashville, Tenn.
Departments of [7] Pathology and [8] Dermatology and Allergology, University of Szeged, Hungary.

Keywords
herpes simplex virus, latency, nervous system, neurodegeneration, trigeminal ganglia.

Corresponding author:
Tibor Valyi-Nagy, MD, PhD, Department of Pathology, College of Medicine, University of Illinois at Chicago, Room 130, 840 South Wood Street, M/C 847, Chicago, IL 60612; Phone: 312-996-1772 (E-mail: *tiborv@uic.edu*)

Received 5 January 2011; accepted 16 February 2011.

doi:10.1111/j.1750-3639.2011.00485.x

Abstract

Numerous epidemiological studies have proposed a link between herpes simplex virus (HSV) infection and several common chronic neuropsychiatric and neurodegenerative diseases. Experimental HSV infection of mice can lead to chronic behavioral and neurological deficits and chronic pain. While neuron injury and loss are well-documented consequences of the acute phase of infection, the pathologic consequences of latent HSV infection are poorly understood. To determine whether latent HSV infection can cause neuronal injury in mice, trigeminal ganglia (TG) derived from adult BALB/c mice 1, 12 and 31 weeks after corneal HSV type 1 (HSV-1) inoculation were analyzed for evidence of productive or latent HSV-1 infection, inflammation and changes in neuron size, density and number. We found that latent HSV-1 infection between 12 and 31 weeks after corneal virus inoculation was associated with inflammation and progressive deficits in mean neuron diameter, neuronal nucleus diameter, neuron density and neuron number in the TG relative to mock-infected controls. The extent of neuronal injury during latent infection correlated with the extent of inflammation. These studies demonstrate that latent HSV infection is associated with progressive neuronal pathology and may lead to a better understanding of the role of HSV infections in chronic neurological diseases.

INTRODUCTION

Primary infections with herpes simplex viruses HSV-1 and HSV-2 are rapidly controlled by immunocompetent individuals but result in the establishment of viral latency in neurons primarily in peripheral sensory ganglia (60). Latent HSV-1 infection of the trigeminal ganglia (TG) becomes increasingly prevalent in humans with age and affects a majority of adults (2, 3, 36). This latent ganglionic infection may serve as the source of virus for recurrent infections of epithelial surfaces including the cornea and also for infections of the central nervous system (CNS) (60). HSV DNA is detectable at a relatively high frequency in various sites of the adult human CNS including the brainstem, olfactory bulbs and temporal lobe (2, 19, 23, 31), although it is not clear whether virus can reactivate in the CNS.

Interestingly, infections with HSV have been epidemiologically linked to some of the most common chronic neuropsychiatric and neurodegenerative diseases in humans including Alzheimer's disease, autism and schizophrenia (5, 6, 16, 23, 28, 38, 45, 47, 61). As HSV replication is usually not detectable in the nervous system of persons affected by these disorders, it has been proposed that latent HSV infection or periodic HSV reactivation events contribute to disease pathogenesis (5, 6, 16, 23, 28, 38, 45, 47, 61).

The pathological consequences of HSV-1 latency and reactivation in the human nervous system are not well understood. During latent HSV infection in the TG, there is little detectable viral protein and infectious virus production (3, 19). HSV transcripts during latency are restricted to neurons, with *in situ* hybridization signals strongest over nuclei (12, 49, 50). Abundant transcription from the viral genome appears to be restricted to the latency-associated transcripts (LATs) that map to repeat sequences flanking the unique long region (12, 29, 49, 50). Interestingly, HSV latency in human TG is associated with chronic inflammation (53). It is not known whether latent HSV-1 infection or repeated reactivation events in the human TG cause significant peripheral nervous system injury including neuronal loss.

As many aspects of HSV-1 pathogenesis can not be efficiently studied in humans, experimental animal models of HSV-1 latency

have been widely used (41, 42, 59). One of these models involves corneal inoculation of mice with HSV-1 with the consequent establishment of latent infection in the TG. Many aspects of this model are similar to the pathogenesis of HSV-1 latency in humans (59). HSV-1 inoculation leads to viral replication in the cornea, followed by spread of virus via neural pathways to the TG and CNS, where virus may replicate and cause ganglionitis and encephalitis. Animals surviving the acute phase of infection do not display signs or symptoms of encephalitis, and infectious virus is not detectable in the nervous system by approximately 2 weeks following corneal inoculation. However, virus is not cleared from infected animals, as HSV establishes latency in neurons of the TG. HSV-1 latent infection in murine TG neurons shows features similar to those seen in humans. In latently infected mice, viral genomic DNA is present in neuronal nuclei, abundant viral gene expression is limited to the LATs and viral proteins or infectious virus are not detectable. HSV may reactivate spontaneously in the nervous system of latently infected mice. However, these reactivation events are much less frequent than those in humans. Reactivation also can be experimentally induced in mice by a variety of stressful stimuli (41, 42, 59).

While mice surviving the acute phase of experimental HSV infection do not show signs and symptoms of encephalitis, numerous studies documented chronic behavioral and neurological deficits and chronic pain in these animals (1, 11, 34, 35, 43, 44, 51). While neuron injury and loss are well documented, consequences of the acute phase of infection (20, 22, 39, 54), the pathologic consequences of latent HSV infection are poorly understood.

HSV-1 latency in the murine TG is associated with chronic inflammation and immune activation. Mononuclear inflammatory cells including $CD4^+$ T cells, $CD8^+$ T cells and macrophages persist in latently infected TG, and several cytokines including interferon-γ and tumor necrosis factor-α as well as nitric oxide are present at elevated levels in these tissues (7, 9, 21, 24, 26, 32, 33, 46, 57). Infiltrating lymphocytes may function in the maintenance of HSV-1 latency by suppressing viral replication by non-cytolytic mechanisms (25).

It has been suggested that HSV-1 latent infection or latency-associated chronic inflammatory changes cause tissue injury and resultant TG dysfunction. In mice, HSV latency is associated with modest but consistently detectable oxidative damage including oxidative marks to nucleic acid, protein and lipid in both neurons and non-neuronal cells in the TG (37, 55, 57). The pathophysiological changes associated with latent infection also are associated with alterations in gene expression (27).

In this study, we used quantitative morphometric analyses to test whether latent HSV-1 infection affects mean neuron diameter, neuronal nucleus diameter, neuron density and neuron number in the TG of mice. For these studies, we used TG tissues obtained from BALB/c mice 1, 12 and 31 weeks after corneal inoculation of HSV-1 at 5 weeks of age. These tissues were previously demonstrated to harbor productive HSV-1 infection at 1 week and latent HSV-1 infection at 12 and 31 weeks after virus inoculation (57). The results provide strong evidence that latent HSV-1 infection is associated with chronic progressive deficits in mean neuron diameter, neuronal nucleus diameter, neuron density and neuron number in the murine TG. This work provides a link between HSV latency and progressive neural damage and establishes an experimental platform to explore mechanisms of HSV-induced chronic neurological disease.

MATERIALS AND METHODS

Virus stocks

HSV-1 strain 17+(4) was propagated and titered by plaque assay using baby hamster kidney (BHK) 21 clone 13 cells.

Inoculation of mice

Five (four to six)-week-old female BALB/c mice (Harlan, Indianapolis, IN) were inoculated with 1×10^5 plaque-forming units (PFU) of HSV-1 17+ per eye after corneal scarification using Metofen anesthesia as previously described (57). Control mice were inoculated with an equivalent volume of sterile tissue culture medium using the same technique (mock infection). Mice were followed daily for signs and symptoms of disease. Groups of mice consisting of five or six randomly chosen HSV-1-infected and mock-infected mice per treatment were euthanized at 1, 12 and 31 weeks after inoculation (at 5, 17 and 35 weeks of age), and TG were aseptically removed. TG were excised by cutting the trigeminal root at its entrance into the brainstem, the mandibular branch at least 1 mm distally to the ganglion and the maxillary branch at the level of the orbital fissure. Tissues were fixed in paraformaldehyde–lysine–periodate fixate and embedded in paraffin. Before the final embedding step, TG were randomly rotated along their longitudinal axis, embedded in paraffin and sectioned. Multiple sections encompassing the complete thickness of the tissue blocks were processed for hematoxylin and eosin staining for histologic evaluation, immunohistochemistry, *in situ* hybridization and morphometric studies. Animal husbandry and experimental procedures were performed in accordance with NIH Public Health Service policy and approved by the Vanderbilt University School of Medicine Institutional Animal Care and Use Committee.

Immunohistochemistry for the detection of HSV-1 proteins

Multiple 6-μm-thick tissue sections derived from representative portions of the paraffin-embedded TG tissues were deparaffinized with xylene and dehydrated through a series of graded ethanols. HSV-1 antigens were detected using a 1:1000 dilution of a polyclonal anti-HSV-1 antiserum raised in a rabbit (DAKO, Carpinteria, CA) as previously described (58).

In situ hybridization for HSV-1-LAT gene expression

In situ hybridization was performed using a nick-translated ^{35}S-labeled DNA probe specific for HSV-1 LAT (Bst2±Bst2 fragment) and 6-μm-thick tissue sections according to previously described techniques (56).

Determination of mean neuron diameter, neuron nucleus diameter, neuron density, TG volume and neuron number per TG

For the determination of mean neuron diameter and mean neuron nucleus diameter, multiple 6-μm-thick tissue sections derived from

representative portions of the paraffin-embedded TG tissues were stained with hematoxylin, scanned at 200× magnification using the ImageScope® System (Aperio Technologies, Inc., Vista, CA) and analyzed with the aid of Aperio image analysis software. The largest diameter and the largest nuclear diameter of 100 randomly chosen neurons in each TG were measured manually by an observer blinded to the nature and time of inoculation. For each time point and treatment group, measurements were made for 7 to 12 TG sections derived from five to six mice yielding 700 to 1200 measurements per group. Mean neuron diameter and neuronal nucleus diameter and standard deviations were calculated for each treatment type (HSV-1-inoculated or mock-inoculated) and each time point (1, 12 and 31 weeks after inoculation).

For neuronal cell density measurements, multiple 20-μm-thick sections derived from representative portions of the paraffin-embedded TG tissues were cut and stained with hematoxylin and viewed using a 60× objective on an Olympus BH-2 microscope (Olympus Optical Co. Ltd, Tokyo, Japan) (magnification: 600×). For each time point and treatment group (infected or mock), five TG (randomly selected left or right) from five mice were examined using at least three sections of each TG. Neurons were identified by morphology based on the detection of nucleoli and Nissl substance (52). Neuronal cell density determinations were made with the aid of image analysis software (ImageJ, Research Service Branch, National Institute of Mental Health, Bethesda, MD, USA), digital video camera (Sony, Park Ridge, NJ, USA) and a computer system according to a published stereological optical dissector method (52). The dimensions of the dissector used were 50 × 50 μm in the *x*- and the *y*-axis. The guard area (the top and bottom of the histological section in which neurons were not counted to avoid errors) was 5 μm; the optimal dissector's height was 15 μm. Nuclei were used as counting units. Neuronal density, that is the number of neurons per unit volume of TG (neurons per volume, n_v), was determined with an optical dissector method using Tandrup's review concerning dorsal root ganglion as a guiding principle (52). The total value of n_v for a TG was then determined from:

$$n_v = \frac{\Sigma Q^-}{p \Sigma a_{(\text{frame})} h}$$

where ΣQ^- is the sum of the dissector neurons in the total dissector volumes, $a_{(\text{frame})}$ is the area of the counting frame, h is the height of the optical dissector and p is the number a points per dissector. Neuron density was determined for each examined TG separately, and mean neuron density and standard deviation per treatment group was then calculated.

The volume of TG was calculated using image analysis software (ImageJ) and digital video camera (Sony) to draw manually the contour of each analyzed TG section at a magnification of 5× and to measure automatically its area in mm^2. One of every 10 sections derived from the whole thickness of the TG was analyzed. The total volume of ganglia was calculated by multiplying the surface area by the thickness of the section and by the number of sections included in the interval between the analyzed sections and summarizing the calculated volumes for the whole TG. Mean TG volume and standard deviation for each treatment group (HSV-1-inoculated or mock-inoculated and 1, 12 and 31 weeks after inoculation) was then calculated.

The number of neurons per TG was calculated based on neuron density and TG volume as follows: $N = n_v \times V$, where N corresponds to neuron number per TG, n_v stands for neuron density and V for TG volume. Calculation was performed separately for five TG in each treatment group. Mean neuron number per TG and standard deviation for each treatment group (HSV-1-inoculated or mock-inoculated and 1, 12 and 31 weeks after inoculation) was then calculated.

Data analysis

Statistical analyses were performed with the STATISTICA software (version 8.0, Tulsa, OK) for windows. Normality was tested using the Kolmogorov–Smirnov test. All variables were normally distributed. Homogeneity of variance was determined using *F*-test and Levene's test and was considered violated when this test yielded $P < 0.05$. All variances were homogeneous; data were assessed using independent samples *T*-test and repeated measures analysis of variance (ANOVA) followed by Scheffe's *post hoc* test. Differences between the means were considered statistically significant if $P < 0.05$. The results are expressed as mean ± standard deviation (SD) values.

RESULTS

Characterization of TG tissues derived from mice at 1, 12 and 31 weeks following corneal HSV-1 inoculation

To obtain TG tissues at various stages of HSV-1 infection, mice were inoculated on the cornea with either HSV-1 or sterile tissue culture medium. Observations about consequent clinical symptoms and the detection of productive vs. latent HSV-1 infection in the TG were reported previously (57). A minority of HSV-1-infected mice demonstrated signs of encephalitis (agitation or paralysis), and 13% of the animals died within 3 weeks of infection. Animals surviving beyond 3 weeks of virus inoculation demonstrated no signs of encephalitis and developed normally. Groups of five to six randomly chosen HSV-1-infected and mock-infected mice were euthanized at 1, 12 and 31 weeks after inoculation. TG were aseptically removed from euthanized animals, and tissues were processed for immunohistochemical staining for HSV-1 antigen and *in situ* hybridization for LAT expression to document acute or latent HSV-1 infection and to evaluate for histopathologic evidence of inflammation (Figures 1–3). No HSV-1 protein expression was detected in the TG of mock-infected mice at any time point (Figure 1A,C,E). In five animals euthanized 1 week after HSV-1 inoculation, HSV-1 proteins were detected in all 10 TG by immunostaining (Figure 1B), consistent with replication of HSV-1. HSV-1 proteins were detected in numerous cells that by morphological criteria were neurons and non-neuronal cells. In TG derived from animals euthanized at 12 and 31 weeks after corneal HSV-1 inoculation, HSV-1 protein expression was not detected in the TG derived from four out of five mice tested (Figure 1D,F). One TG section at each time point demonstrated very rare non-neuronal cells that stained for HSV-1 proteins (data not shown). Abundant LAT RNA expression was detected by *in situ* hybridization in TG tissues of HSV-1-infected mice euthanized at 12 and 31 weeks after virus inoculation (Figure 2B). Sections of TG stained with hematoxylin and eosin at 1, 12 and 31 weeks after HSV-1 inoculation revealed chronic inflammatory changes

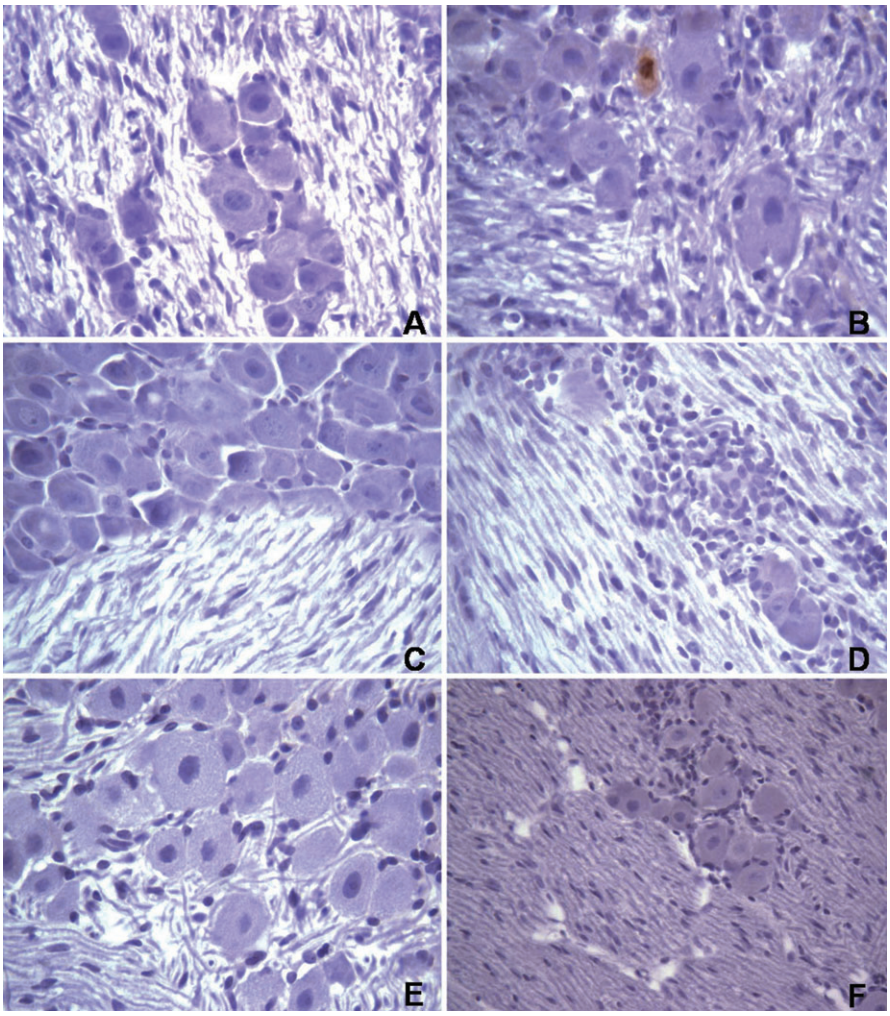

Figure 1. *HSV-1 protein expression in murine trigeminal ganglion (TG) tissues following corneal inoculation of HSV-1 or sterile medium (mock-infection) as detected by immunohistochemistry.* Brown staining indicates HSV-1 proteins. HSV-1 protein expression was not detected in TG derived from mock-infected mice at 1 (**A**), 12 (**C**) or 31 (**E**) weeks after mock inoculation. HSV-1 protein expression in a neuron in a TG derived from a mouse 1 week after corneal HSV-1 inoculation (**B**). HSV-1 protein expression was not detected in TG derived from mice 12 (**D**) or 31 (**F**) weeks after corneal HSV-1 inoculation. Magnification = 400×.

(Figure 3B, D, F). Inflammation was not detected in the TG of mock-infected animals (Figure 3A, C, E). These findings indicate that mice examined at 1 week after virus inoculation were productively infected with HSV-1, whereas those examined at 12 and 31 weeks after inoculation were latently infected with the virus. Marginal HSV-1 expression in one mouse each at 12 and 31 weeks after virus inoculation is consistent with rare focal HSV-1 reactivation. In addition, both acute and latent HSV-1 infection in the murine TG was associated with inflammation.

Mean neuron diameter, mean neuronal nucleus diameter and the number of neurons increase in the TG of mock-infected BALB/c mice

Mean neuron diameter and mean neuronal nucleus diameter gradually increased in the TG of control mice between 1 and 31 weeks after mock infection (between 6 and 36 weeks of age) (Table 1). Specifically, mean neuron diameters at 6, 17 and 36 weeks of age were 22.74 ± 5.2 μm ($n = 700$), 22.98 ± 4.9 μm ($n = 700$) and

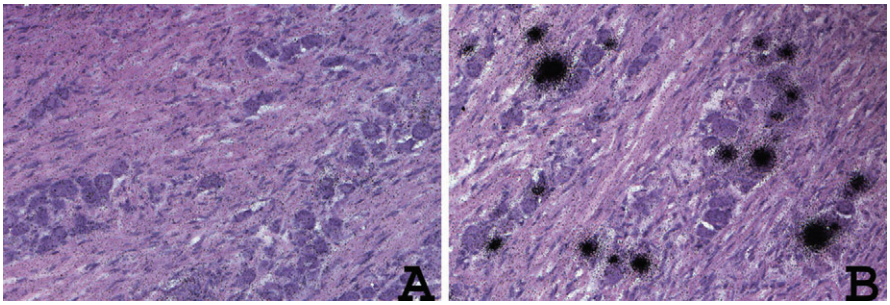

Figure 2. *Detection of HSV-1 LAT in the trigeminal ganglia (TG) of mice by* in situ *hybridization.* Accumulation of dark grains indicates LAT accumulation. **A.** There was no evidence of LAT expression in TG derived from a mouse 31 weeks after corneal mock inoculation. **B.** Numerous LAT-positive cells in TG tissue derived from a mouse 31 weeks after corneal HSV-1 inoculation. Magnification = 200×.

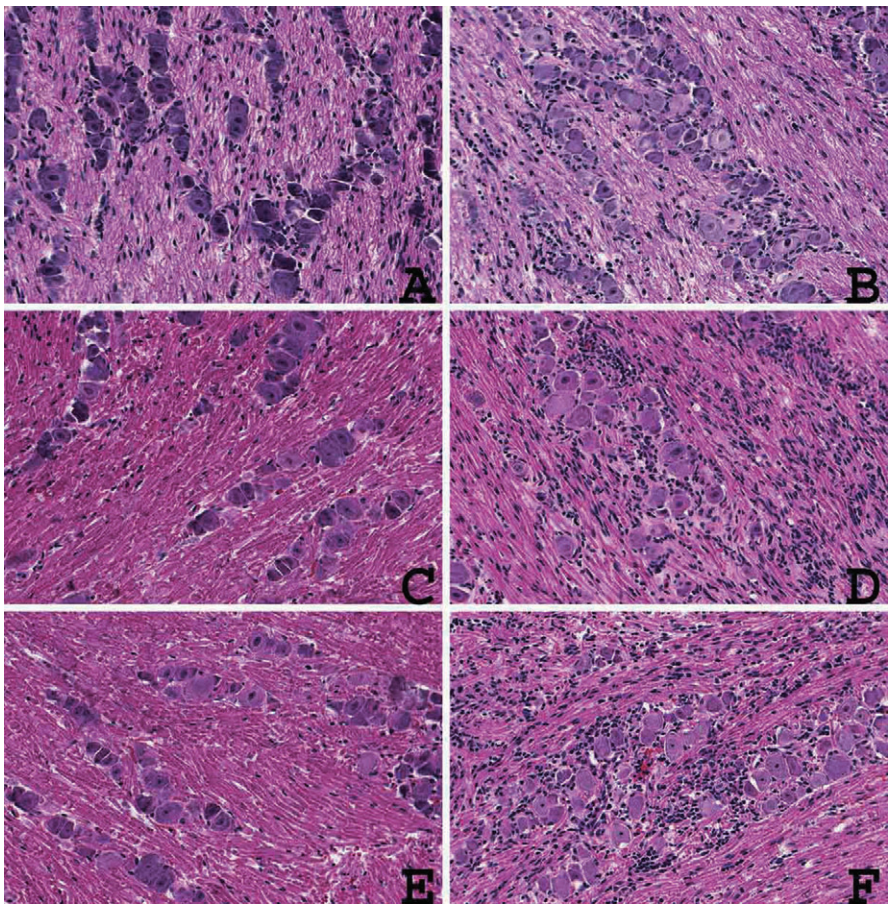

Figure 3. *Inflammation in murine trigeminal ganglion (TG) tissues following corneal inoculation of HSV-1.* No evidence of inflammation in hematoxylin and eosin–stained sections of trigeminal ganglia (TG) derived from mice at 1 (**A**), 12 (**C**) or 31 (**E**) weeks after corneal mock inoculation. Chronic inflammation in hematoxylin and eosin–stained sections of trigeminal ganglia (TG) derived from mice at 1 (**B**), 12 (**D**) and 31 (**F**) weeks after corneal HSV-1 inoculation. Magnification = 100×.

25.16 ± 5.0 μm ($n = 900$), respectively. Mean neuronal nucleus diameters at 6, 17 and 36 weeks of age were 9.15 ± 2.2 μm ($n = 700$), 9.27 ± 1.8 μm ($n = 700$) and 10.33 ± 2.0 μm ($n = 900$), respectively. Increases in mean neuron diameter and neuronal nucleus diameter did not differ statistically between 6 and 17 weeks ($P = 0.3782$ and 0.2794, respectively), but these differences were statistically significant at 6 and 36 weeks and 17 and 36 weeks ($P < 0.0001$). These findings are consistent with growth of TG neurons during the observation interval.

Neuron density in the TG decreased, while TG volume increased in mock-infected mice during the period of observation. The combination of these changes resulted in a gradual increase in the mean number of neurons per TG between 6 and 36 weeks of age (Table 1, Figures 4–6). Neuron density was $5.64 \pm 0.2 \times 10^{-5}$ neurons per μm^3 at 6 weeks of age ($n = 5$) and decreased to $4.59 \pm 0.2 \times 10^{-5}$ neurons per μm^3 by 17 weeks ($n = 5$, $P = 0.000191$). Neuron density was $4.51 \pm 0.1 \times 10^{-5}$ neurons per μm^3 at 36 weeks of age ($n = 5$), which was not significantly less than that at 16 weeks ($P = 0.99$) but significantly less than that at 6 weeks of age ($P = 0.000082$). Mean TG volume was 0.33 ± 0.03 mm^3 at 6 weeks of age ($n = 5$), 0.53 ± 0.04 mm^3 at 17 weeks ($n = 5$) and 0.89 ± 0.04 mm^3 at 36 weeks of age ($n = 5$) (Table 1, Fig. 5). These increases were statistically significant (6–16 weeks: $P = 0.000006$; 17–36 weeks: $P = 0.000005$; 6– 36 weeks: $P = 0.0000001$). The mean number of neurons per TG was 18 600 ± 1000 ($n = 5$), 24 250 ± 1800 ($n = 5$) and 40 900 ± 3100 ($n = 5$) at 6, 17 and 36 weeks of age, respectively (Table 1, Fig. 6). These increases were statistically significant (6–16 weeks: $P = 0.00054$; 17–36 weeks: $P = 0.000013$; 6–36 weeks: $P = 0.000001$). Thus, TG volume and neuron number per TG increase, while neuron density decreases in the TG of mice between 6 and 36 weeks of age.

Productive HSV-1 infection in the TG of mice is associated with increased mean neuron diameter and neuronal nucleus diameter and decreased neuron density

In the TG of mice euthanized 1 week after corneal HSV-1 inoculation, mean neuron diameter and mean neuronal nucleus diameter were greater than that detected in TG derived from mice 1 week after mock infection (Table 1). Specifically, mean neuron diameter 1 week after HSV-1 inoculation was 23.94 ± 5.2 μm ($n = 1200$) vs. 22.74 ± 5.2 μm ($n = 700$) in age-matched mock-infected controls (Table 1, $P = 0.0001$), a 5.27% increase (Table 2). Mean neuronal nucleus diameter 1 week after HSV-1 inoculation was 9.58 ± 2.0 μm ($n = 1200$) vs. 9.15 ± 2.2 μm ($n = 700$) detected in controls (Table 1, $P = 0.0001$), a 4.7% increase (Table 2). These changes in mean neuron diameter and neuronal nucleus diameter are consistent with the cytopathic effects associated with HSV-1 replication in a subset of the ganglionic neurons. Indeed, analysis of TG sections derived from mice 1 week following virus inoculation and immunostained for HSV-1 proteins indicated that mean

Table 1. Expression of HSV-1 protein and LAT, inflammation and changes in neuron diameter, neuron nucleus diameter, neuron density, trigeminal ganglion (TG) volume and neuron number in the TG of BALB/c mice following corneal inoculation of either HSV-1 or sterile medium (mock-inoculation) at 5 weeks of age.

Age (weeks)	Inoculation	HSV-1 protein	HSV-1 LAT	Inflammation	Neuron diameter (μm ± SD)	Neuron nucleus diameter (μm ± SD)	Neuron density (per μm^3 ± SD‡)	TG volume (mm^3 ± SD)	Neuron number/TG (thousands ± SD)
6	Mock	–	–	–	22.74 ± 5.2	9.15 ± 2.2	5.64 ± 0.2	0.33 ± 0.03	18.6 ± 1.0
17	Mock	–	–	–	22.98 ± 4.9	9.27 ± 1.8	4.59 ± 0.2	0.53 ± 0.04	24.25 ± 1.8
36	Mock	–	–	–	25.16 ± 5.0	10.33 ± 2.0	4.51 ± 0.1	0.89 ± 0.04	40.95 ± 3.1
6	HSV-1	+	+	+	23.94 ± 5.2	9.58 ± 2.0	5.15 ± 0.1	0.33 ± 0.03	17.0 ± 1.4
17	HSV-1	–†	+	+	22.25 ± 4.6	9.07 ± 1.8	4.18 ± 0.2	0.53 ± 0.03	21.28 ± 2.2
36	HSV-1	–†	+	+	23.55 ± 5.4	9.76 ± 2.0	3.91 ± 0.2	0.86 ± 0.04	33.62 ± 1.6

†1 out of 10 TG studied demonstrated weak HSV-1 protein expression in a few cells.
‡Results are multiplied by 10^{-5}.
HSV-1 protein = herpes simplex virus-1 protein expression as detected by immunohistochemistry; HSV-1 LAT = herpes simplex virus-1 latency associated transcript expression as detected by *in situ* hybridization; SD = standard deviation; TG = trigeminal ganglion; *N* = total number of neurons.

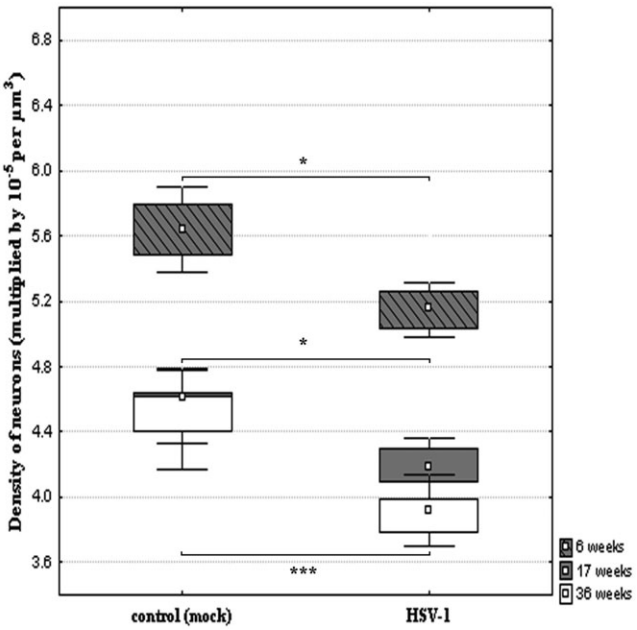

Figure 4. *Median and range of neuron density per trigeminal ganglion (TG) in mice euthanized 1, 12 and 31 weeks after corneal inoculation of HSV-1 or sterile medium (mock) at 6, 17 and 36 weeks of age.* TG number (*n*) was 5 for all time points and treatment groups. Rectangles represent 25% to 75% quartiles. $*P < 0.05$; $**P < 0.001$; $***P < 0.0001$.

neuron diameter and neuronal nucleus diameter were significantly greater in HSV-1 protein expressing neurons than in HSV-1 antigen–negative neurons ($P < 0.001$). Specifically, mean neuron diameter and neuronal nucleus diameter measurements were 31.10 ± 6.36 μm ($n = 27$) and 14.22 ± 2.32 μm ($n = 12$), respectively, in HSV-1 antigen–positive neurons, while mean neuron diameter and neuronal nucleus diameter were measured at 25.93 ± 4.32 μm ($n = 50$) and 11.66 ± 1.5 μm ($n = 50$), respectively, in HSV-1 antigen–negative neurons.

Mean neuron density was 8.69% less ($5.15 \pm 0.1 \times 10^{-5}$ neurons per μm^3, $n = 5$) in TG derived from HSV-1-inoculated mice than in mock-infected controls ($5.64 \pm 0.2 \times 10^{-5}$ neurons per μm^3, $n = 5$) 1 week after inoculation (Tables 1 and 2, Figure 4, $P = 0.002646$). Mean TG volume was similar [0.33 ± 0.3 mm^3 ($n = 5$) vs. 0.33 ± 0.3 mm^3 ($n = 5$)] in HSV-1- and mock-infected mice at 1 week after inoculation (Table 1, Figure 5). The mean number of neurons per TG was 17 000 ± 1400 ($n = 5$) in virus-infected vs. 18 600 ± 1000 ($n = 5$) in mock-infected TG (Table 1, Figure 6), an 8.61% decrease (Table 2). This decrease in neuron number per TG did not reach statistical significance ($P = 0.082395$). Collectively, these findings are consistent with neuron destruction by productive HSV-1 infection in the TG.

Latent HSV-1 infection in the TG of mice is associated with decreased mean neuron diameter, neuronal nucleus diameter and neuron density and number

In the TG of mice euthanized 12 weeks after corneal HSV-1 inoculation (at 17 weeks of age), mean neuron diameter, mean neuronal

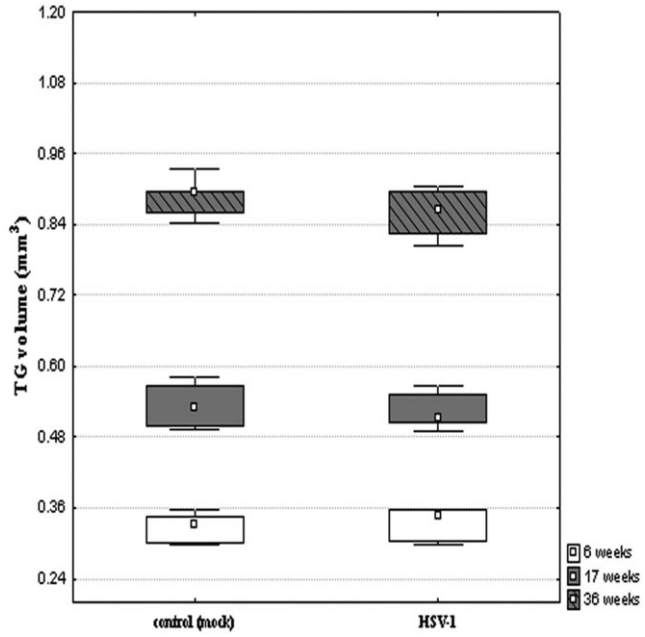

Figure 5. *Median and range of trigeminal ganglion (TG) volume in mice euthanized 1, 12 and 31 weeks after corneal inoculation of HSV-1 or sterile medium (mock) at 6, 17 and 36 weeks of age.* TG number (*n*) was 5 for all time points and treatment groups. Rectangles represent 25% to 75% quartiles. **P* < 0.05; ***P* < 0.001; ****P* < 0.0001.

nucleus diameter, neuron density and mean neuron number per TG were all significantly less than those in age-matched mock-infected control mice (Tables 1 and 2, Figures 4 and 6). Specifically, mean neuron diameter at 12 weeks after HSV-1 inoculation was

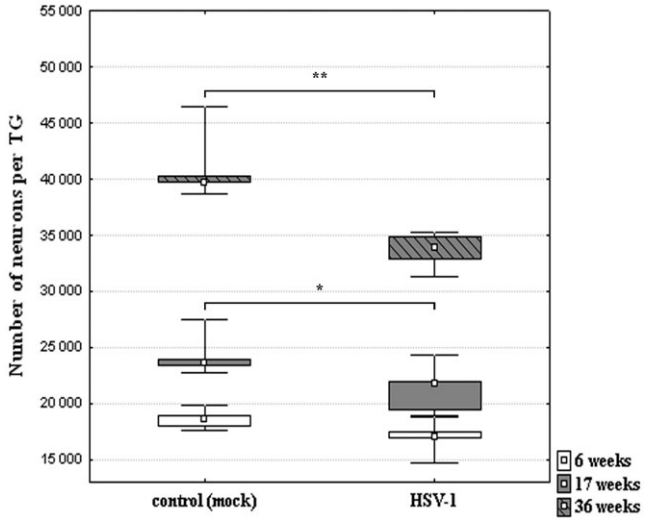

Figure 6. *Median and range of neuron number per trigeminal ganglion (TG) in mice euthanized 1, 12 and 31 weeks after corneal inoculation of HSV-1 or sterile medium (mock) at 6, 17 and 36 weeks of age.* TG number (*n*) was 5 for all time points and treatment groups. Rectangles represent 25% to 75% quartiles. **P* < 0.05; ***P* < 0.01.

Table 2. Percentage change in mean neuron diameter, mean neuronal nucleus diameter, neuron density and mean neuron number per TG in HSV-1-infected mice relative to age-matched mock-infected mice.

Age	6 weeks	17 weeks	36 weeks
Neuron diameter (infected/control)	+5.27%	–3.17%	–6.4%
Neuron nucleus diameter (infected/control)	+4.7%	–2.15%	–5.5%
Neuron density (infected/control)	–8.69%	–8.94%	–13.3%
Neuron number per TG (infected/control)	–8.61%	–12.25%	–17.9%

TG = trigeminal ganglion.

22.25 ± 4.6 μm ($n = 1000$) vs. 22.98 ± 4.9 μm ($n = 700$) detected in age-matched mock-infected controls (Table 1, $P = 0.0023$), a 3.17% decrease (Table 2). Mean neuronal nucleus diameter at 12 weeks after HSV-1 inoculation was 9.07 ± 1.8 μm ($P = 1000$) vs. 9.27 ± 1.8 μm ($P = 700$) in controls (Table 1, $P = 0.0249$), a 2.15% reduction (Table 2). Neuron density was 8.94% less ($4.18 \pm 0.2 \times 10^{-5}$ neurons per μm^3, $n = 5$) in TG derived from HSV-1-infected mice in comparison with those from mock-infected mice ($4.59 \pm 0.2 \times 10^{-5}$ neurons per μm^3, $n = 5$) at 12 weeks after inoculation (Table 1, Figure 4, $P = 0.00458$). Mean TG volume did not differ significantly (0.53 ± 0.03 vs. 0.53 ± 0.04 mm^3, $n = 5$ for each) in HSV-1- and mock-infected mice at 12 weeks after inoculation (Table 1, Figure 5). However, the mean number of neurons per TG was significantly less in HSV-1-infected mice than in mock-infected mice at 12 weeks after inoculation (Table 1, Figure 6). Specifically, the total number of neurons was 21 280 ± 2200 ($n = 5$) in virus-infected vs. 24 250 ± 1800 ($n = 5$) in mock-infected TG (Table 1, Figures 6, $P = 0.04718$), a 12.25% decrease (Table 2). Thus, neuron size and number are decreased in the TG of mice 12 weeks after HSV-1 corneal inoculation.

In the TG of mice euthanized 31 weeks after corneal HSV-1 inoculation (at 36 weeks of age), mean neuron diameter, mean neuronal nucleus diameter, neuron density and mean neuron number per TG were all significantly less than those detected in age-matched mock-infected control mice (Table 1, Figures 4 and 6). Specifically, mean neuron diameter at 31 weeks after HSV-1 inoculation was 23.55 ± 5.4 μm ($n = 1000$) vs. 25.16 ± 5.0 μm ($n = 900$) in age-matched mock-infected controls (Table 1, $P = 0.0001$), a 6.4% decrease (Table 2). Mean neuronal nucleus diameter at 31 weeks after HSV-1 inoculation was 9.76 ± 2.0 μm ($n = 1000$) vs. 10.33 ± 2.0 μm ($n = 900$) in controls (Table 1, $P = 0.0001$), a 5.5% reduction (Table 2). Neuron density was 13.3% less ($3.91 \pm 0.2 \times 10^{-5}$ neurons per μm^3, $n = 5$) in TG derived from HSV-1-infected mice in comparison with those from mock-infected mice ($4.51 \pm 0.1 \times 10^{-5}$ neurons per μm^3, $n = 5$) at 31 weeks after inoculation (Table 1, Figure 4, $P = 0.000054$). Mean TG volume did not differ significantly (0.86 ± 0.04, $n = 5$ vs. 0.89 ± 0.04 mm^3, $n = 5$) in HSV-1- and mock-infected mice at 31 weeks after inoculation (Table 1, Figure 5). However, like the TG from mice at 12 weeks after HSV-1 inoculation, the number of neurons per TG was significantly less in HSV-1-infected mice than in mock-infected mice at 31 weeks after inoculation (Table 1, Figure 6). Specifically, the total number of neurons was

33 620 ± 1600 ($n = 5$) in virus-infected vs. 40 950 ± 3100 ($n = 5$) in mock-infected TG (Table 1, $P = 0.0016$), a 17.9% relative decrease (Table 1, Figure 6).

Deficits in mean neuron diameter, neuron nucleus diameter, neuron density and neuron number per TG relative to age-matched mock-infected controls were all more substantial at 31 weeks than at 12 weeks after corneal virus inoculation (Table 2). As only latent HSV-1 infection was detected in TG neurons at 12 and 31 weeks after corneal virus inoculation, the progressive deficits in neuron size, density and number between these times are consistent with chronic progressive neural injury during latent HSV-1 infection.

Decreased mean neuron diameter and neuronal nucleus diameter correlate with the extent of inflammation in the TG of mice latently infected with HSV-1

To investigate the role of LAT expression and inflammation in the detected changes of neuron morphology during latent infection, the number of LAT expressing cells, mean neuron diameter, mean neuronal nucleus diameter and the extent of inflammation were determined in TG sections of four latently infected mice (Table 3). As grains associated with LAT detection by *in situ* hybridization did not allow precise morphometric analysis, the following approach was used. The number of LAT expressing cells was counted in one TG section derived from each mice, and mean neuron diameter, mean neuronal nucleus diameter and the extent of inflammation was determined in a neighboring hematoxylin-stained TG section. The extent of inflammation was expressed as the percentage of TG section area demonstrating inflammation. The extent of neuronal injury during latent infection seemed to correlate with the extent of inflammation but not with the number of LAT-expressing neurons (Table 3). Specifically, mean neuron diameter and mean neuronal nucleus diameter were the smallest in the most inflamed TG and were the greatest in the least inflamed TG. Intermediate mean neuron diameter and nucleus diameter values were detected in two ganglia harboring intermediate levels of inflammation. These findings suggest that decreased mean neuron diameter and neuronal nucleus diameter correlate with the extent of inflammation in the TG of mice latently infected with HSV-1.

Table 3. Number of HSV-1 LAT+ cells per section, mean neuron diameter, mean neuronal nucleus diameter and extent of inflammation in TG sections derived from four mice euthanized 31 weeks after corneal HSV-1 inoculation at 36 weeks of age.

	Number of LAT+ cells	Mean cell diameter (μm) ± SD	Mean nucleus diameter (μm) ± SD	Inflammation (%)
TG #1	55	24.171 ± 6.24	9.608 ± 2.23	10.2
TG #2	161	23.65 ± 4.49	9.645 ± 1.74	8.6
TG #3	198	21.409 ± 4.69	9.085 ± 1.65	79
TG #4	29	22.497 ± 5.33	9.441 ± 1.58	21

HSV-1 LAT = herpes simplex virus-1 latency-associated transcript expression as detected by *in situ* hybridization; SD = standard deviation; Inflammation (%) = percent area of TG section demonstrating inflammation.

DISCUSSION

We show here using careful morphometric analyses that in healthy adult mice, mean neuron diameter, mean neuron nucleus diameter, TG volume and mean number of neurons per TG gradually increase between 6 and 37 weeks of age. The detection of increasing neuron diameter, neuronal nucleus diameter and TG volume is not surprising and consistent with normal growth of these mice. Our findings of increasing neuron numbers in the TG of mock-infected mice are similar to those made in several reports of gradually increasing numbers of mature neurons in the sensory ganglia of healthy adult rats (8, 10, 13–15, 30, 40). In rats, both ongoing neurogenesis and maturation of undifferentiated or partially differentiated post-mitotic cells have been proposed as possible mechanisms for the observed increase in the number of mature neurons in adult animals (8, 10, 13–15, 17, 30, 40). A similar situation may be operant in mice.

Numerous previous studies indicate that corneal inoculation of immunocompetent mice with HSV-1 is followed by virus replication in the TG for about 2 weeks, which in turn is followed by the establishment of life-long HSV-1 latency in the TG (41, 59). Consistent with these reports and our previous analyses of the TG tissues used in this study (57), we detected productive HSV-1 infection in the TG at 1 week after virus inoculation and evidence of latent HSV-1 infection in the TG at 12 and 31 weeks after virus inoculation. In the TG of mice euthanized 1 week after corneal HSV-1 inoculation, mean neuron diameter and mean neuronal nucleus diameter increased, while neuron density and mean neuron number per TG decreased relative to age-matched mock-infected controls (Tables 1 and 2). These findings are not surprising as these ganglia harbor productive HSV-1 infection, and HSV-1 replication is associated with cytopathic effects that include cellular swelling and nuclear enlargement (42, 48). Furthermore, neuronal death in the TG of mice during the first few weeks of infection is well documented (41, 42, 60), which would account for the decrease in neuron number.

The key finding of our study is that in the TG of mice 12 and 31 weeks after HSV-1 inoculation (at 17 and 36 weeks of age), mean neuron diameter, neuronal nucleus diameter, neuron density and mean neuron number per TG were significantly less than those in age-matched mock-infected control TG. Interestingly, the deficits in neuron diameter, neuronal nucleus diameter, neuron density and neuron number in latently infected TG were more substantial at 36 weeks than at 17 weeks of age (Table 2). It is possible that diminished neuron size and number at 12 weeks after corneal virus inoculation is attributable to neuron destruction and delayed neuron growth caused by productive HSV-1 infection during the first weeks of infection. However, as only latent HSV-1 infection was detected in TG neurons at 12 and 31 weeks after corneal virus inoculation, the progressive reductions in neuron size and number between these intervals are unlikely to occur as a consequence of virus replication during the first few weeks of infection.

Mean neuron diameter, mean neuronal nucleus diameter and mean neuron number per TG increased in absolute numbers between 17 and 36 weeks in latently infected mice (Table 1). However, these increases were substantially less than those in mock-infected controls. Furthermore, the increases detected were less than expected for resumption of normal TG growth at these times. Resumption of normal TG growth would be expected to be

associated with stable or decreasing deficits in neuron size, density and number in latently infected TG between 12 and 31 weeks after virus inoculation (between 16 and 36 weeks of age) relative to age-matched controls. However, these relative deficits all increased during latency (Table 2). These findings indicate that latent HSV-1 infection is associated with chronic progressive deficits in neuron size, density and number in the nervous system of an immunocompetent host.

Mechanisms by which latent HSV-1 infection leads to chronic progressive alterations in neuron size, density and number in the nervous system are not clear from our study. As spontaneous HSV-1 reactivation occurs in latently infected mice (59, 60), albeit rarely, it is possible that reactivation events contribute to changes in neuronal size and number. Detection of extremely rare HSV-1 protein-expressing cells in a minority of TG at 12 and 31 weeks after HSV-1 inoculation is consistent with virus reactivation. However, potential causes of progressive neuronal injury are not restricted to HSV-1 reactivation events, as latent infection and the associated persistent inflammatory response also can cause neuronal dysfunction and tissue injury (27, 37, 55, 57). Latent HSV-1 infection in the murine TG is associated with low-level expression of replication-cycle HSV-1 genes in the absence of infectious virus production (18). Marginal HSV-1 protein expression associated with these incomplete reactivation attempts may induce neuronal injury. Persistent inflammation during HSV-1 latency in the murine TG also may cause neuronal injury, possibly mediated by cytokines and oxidative stress (37, 55, 57). Indeed, the extent of neuronal injury during latent infection in our current study seemed to correlate with the extent of inflammation in the TG (Table 3). These viral and inflammatory processes may injure mature neurons or interfere with ongoing neurogenesis and neuronal maturation in the TG.

While mice surviving the acute phase of experimental HSV infection do not show signs and symptoms of encephalitis, numerous studies documented chronic behavioral and neurological deficits and chronic pain in these animals (1, 11, 34, 35, 43, 44, 51). In the current study, mice were observed daily for signs and symptoms of encephalitis, but detailed neurological and behavioral studies were not performed. Future experiments will need to determine whether HSV-1 latent infection-associated progressive pathologic changes documented here cause progressive neurological or behavioral deficits in mice. These studies will provide an excellent experimental platform to dissect mechanisms of HSV-induced chronic neurological disease. A role for genetic susceptibility of latent HSV-induced chronic neuronal injury should be a focus of future studies using this experimental system as genetic susceptibility has been repeatedly proposed to be important for the pathogenesis of HSV-induced chronic neurological disease in humans (5, 6, 16, 23, 28, 38, 45, 47, 61). These studies may lead to major new insights into mechanisms by which latent viral infections contribute to the pathogenesis of chronic neurological and neuropsychiatric diseases and foster development of virus-specific intervention strategies.

ACKNOWLEDGMENTS

These studies were supported by fellowship grants to SD, SB, EG and SKK by the Rosztoczy Foundation and Public Health Services award R37 AI38296 from the National Institute of Allergy and Infectious Diseases to TSD. Additional funding was provided by the Elizabeth B. Lamb Center for Pediatric Research.

REFERENCES

1. Armien AG, Hu S, Little MR, Robinson N, Lokensgard JR, Low WC, Cheeran MC (2010) Chronic cortical and subcortical pathology with associated neurological deficits ensuing experimental herpes encephalitis. *Brain Pathol* **20**:738–750.
2. Baringer JR, Pisani P (1994) Herpes simplex virus genomes in human nervous system tissue analyzed by polymerase chain reaction. *Ann Neurol* **36**:823–829.
3. Baringer JR, Swoveland P (1973) Recovery of herpes-simplex virus from human trigeminal ganglions. *N Engl J Med* **288**:648–650.
4. Brown SM, Ritchie DA, Subak-Sharpe JH (1973) Genetic studies with herpes simplex virus type 1. The isolation of temperature-sensitive mutants, their arrangement into complementation groups and recombination analysis leading to a linkage map. *J General Virol* **18**:329–346.
5. Buka SL, Cannon TD, Torrey EF, Yolken RH (2008) Maternal exposure to herpes simplex virus and risk of psychosis among adult offspring. *Biol Psych* **63**:809–815.
6. Buka SL, Tsuang MT, Torrey EF, Klebanoff MA, Bernstein D, Yolken RH (2001) Maternal infections and subsequent psychosis among offspring. *Arch Gen Psychiatry* **58**:1032–1037.
7. Cantin EM, Hinton DR, Chen J, Openshaw H (1995) Gamma interferon expression during acute and latent nervous system infection by herpes simplex virus type 1. *J Virol* **69**:4898–4905.
8. Cecchini T, Cuppini R, Ciaroni S, Barili P, De Matteis R, Del Grande P (1995) Changes in the number of primary sensory neurons in normal and vitamin-E-deficient rats during aging. *Somatosens Mot Res* **12**:317–327.
9. Chen SH, Garber DA, Schaffer PA, Knipe DM, Coen DM (2000) Persistent elevated expression of cytokine transcripts in ganglia latently infected with herpes simplex virus in the absence of ganglionic replication or reactivation. *Virology* **278**:207–216.
10. Ciaroni S, Cecchini T, Cuppini R, Ferri P, Ambrogini P, Bruno C, Del Grande P (2000) Are there proliferating neuronal precursors in adult rat dorsal root ganglia? *Neurosci Lett* **281**:69–71.
11. Crnic LS, Pizer LI (1988) Behavioral effects of neonatal herpes simplex type 1 infection of mice. *Neurotoxicol Teratol* **10**:381–386.
12. Croen KD, Ostrove JM, Dragovic LJ, Straus SE (1988) Patterns of gene expression and sites of latency in human nerve ganglia are different for varicella-zoster and herpes simplex viruses. *Proc Natl Acad Sci USA* **85**:9773–9777.
13. Devor M, Govrin-Lippmann R (1985) Neurogenesis in adult rat dorsal root ganglia. *Neurosci Lett* **61**:189–194.
14. Devor M, Govrin-Lippmann R (1991) Neurogenesis in adult rat dorsal root ganglia: on counting and the count. *Somatosens Mot Res* **8**:9–12.
15. Devor M, Govrin-Lippmann R, Frank I, Raber P (1985) Proliferation of primary sensory neurons in adult rat dorsal root ganglion and the kinetics of retrograde cell loss after sciatic nerve section. *Somatosens Res* **3**:139–167.
16. Dickerson FB, Boronow JJ, Stallings C, Origoni AE, Cole S, Krivogorsky B, Yolken RH (2004) Infection with herpes simplex virus type 1 is associated with cognitive deficits in bipolar disorder. *Biol Psych* **55**:588–593.
17. Farel PB (2003) Late differentiation contributes to the apparent increase in sensory neuron number in juvenile rat. *Brain Res* **144**:91–98.
18. Feldman LT, Ellison AR, Voytek CC, Yang L, Krause P, Margolis TP (2002) Spontaneous molecular reactivation of herpes simplex virus type 1 latency in mice. *Proc Natl Acad Sci USA* **99**:978–983.

19. Fraser NW, Lawrence WC, Wroblewska Z, Gilden DH, Koprowski H (1981) Herpes simplex type 1 DNA in human brain tissue. *Proc Natl Acad Sci USA* **78**:6461–6465.
20. Geiger KD, Nash TC, Sawyer S, Krahl T, Patstone G, Reed JC *et al* (1997) Interferon-gamma protects against herpes simplex virus type 1-mediated neuronal death. *Virology* **238**:189–197.
21. Halford WP, Gebhardt BM, Carr DJ (1996) Persistent cytokine expression in trigeminal ganglion latently infected with herpes simplex virus type 1. *J Immunol* **157**:3542–3549.
22. Henken DB, Goldstein ME, Martin JR (1993) Herpes simplex virus type-2 infection by a footpad route results in neuronal death in mouse spinal ganglia. *J Neurol Sci* **115**:177–183.
23. Itzhaki RF, Lin WR, Shang D, Wilcock GK, Faragher B, Jamieson GA (1997) Herpes simplex virus type 1 in brain and risk of Alzheimer's disease. *Lancet* **349**:241–244.
24. Khanna KM, Bonneau RH, Kinchington PR, Hendricks RL (2003) Herpes simplex virus-specific memory $CD8^+$ T cells are selectively activated and retained in latently infected sensory ganglia. *Immunity* **18**:593–603.
25. Knickelbein JE, Khanna KM, Yee MB, Baty CJ, Kinchington PR, Hendricks RL (2008) Noncytotoxic lytic granule-mediated $CD8^+$ T cell inhibition of HSV-1 reactivation from neuronal latency. *Science* **322**:268–271.
26. Koprowski H, Zheng YM, Heber-Katz E, Fraser N, Rorke L, Fu ZF *et al* (1993) *In vivo* expression of inducible nitric oxide synthase in experimentally induced neurologic diseases. *Proc Natl Acad Sci USA* **90**:3024–3027.
27. Kramer MF, Cook WJ, Roth FP, Zhu J, Holman H, Knipe DM, Coen DM (2003) Latent herpes simplex virus infection of sensory neurons alters neuronal gene expression. *J Virol* **77**:9533–9541.
28. Krause D, Matz J, Weidinger E, Wagner J, Wildenauer A, Obermeier M *et al* (2010) The association of infectious agents and schizophrenia. *World J Biol Psychiatry* **11**:739–743.
29. Krause PR, Croen KD, Straus SE, Ostrove JM (1988) Detection and preliminary characterization of herpes simplex virus type 1 transcripts in latently infected human trigeminal ganglia. *J Virol* **62**:4819–4823.
30. Lagares A, Li HY, Zhou XF, Avendano C (2007) Primary sensory neuron addition in the adult rat trigeminal ganglion: evidence for neural crest glio-neuronal precursor maturation. *J Neurosci* **27**:7939–7953.
31. Liedtke W, Opalka B, Zimmermann CW, Lignitz E (1993) Age distribution of latent herpes simplex virus 1 and varicella-zoster virus genome in human nervous tissue. *J Neurol Sci* **116**:6–11.
32. Liu T, Khanna KM, Chen X, Fink DJ, Hendricks RL (2000) CD8(+) T cells can block herpes simplex virus type 1 (HSV-1) reactivation from latency in sensory neurons. *J Exp Med* **191**:1459–1466.
33. Liu T, Tang Q, Hendricks RL (1996) Inflammatory infiltration of the trigeminal ganglion after herpes simplex virus type 1 corneal infection. *J Virol* **70**:264–271.
34. McFarland DJ, Hotchin J (1983) Host genetics and the behavioral sequelae to herpes encephalitis in mice. *Physiol Behav* **30**:881–884.
35. McLean JH, Shipley MT, Bernstein DI, Corbett D (1993) Selective lesions of neural pathways following viral inoculation of the olfactory bulb. *Exp Neurol* **122**:209–222.
36. Mahalingam R, Wellish MC, Dueland AN, Cohrs RJ, Gilden DH (1992) Localization of herpes simplex virus and varicella zoster virus DNA in human ganglia. *Ann Neurol* **31**:444–448.
37. Milatovic D, Zhang Y, Olson SJ, Montine KS, Roberts LJ 2nd, Morrow JD *et al* (2002) Herpes simplex virus type 1 encephalitis is associated with elevated levels of F2-isoprostanes and F4-neuroprostanes. *J Neurovirol* **8**:295–305.
38. Mora M, Quintero L, Cardenas R, Suarez-Roca H, Zavala M, Montiel N (2009) [Association between HSV-2 infection and serum anti-rat brain antibodies in patients with autism]. *Invest Clin* **50**:315–326.
39. Perng GC, Jones C, Ciacci-Zanella J, Stone M, Henderson G, Yukht A *et al* (2000) Virus-induced neuronal apoptosis blocked by the herpes simplex virus latency-associated transcript. *Science* **287**:1500–1503.
40. Popken GJ, Farel PB (1997) Sensory neuron number in neonatal and adult rats estimated by means of stereologic and profile-based methods. *J Compar Neurol* **386**:8–15.
41. Preston CM (2000) Repression of viral transcription during herpes simplex virus latency. *J General Virol* **81**:1–19.
42. Roizman BKD (2001) Herpes simplex viruses and their replication. In: *Fields Virology*, 4th edn. PM KDaH (ed.), pp. 2399–2459. Lippincott Williams and Wilkins: Philadelphia.
43. Sasaki A, Mabuchi T, Serizawa K, Takasaki I, Andoh T, Shiraki K *et al* (2007) Different roles of nitric oxide synthase-1 and -2 between herpetic and postherpetic allodynia in mice. *Neuroscience* **150**:459–466.
44. Sato-Takeda M, Takasaki I, Takeda K, Sasaki A, Andoh T, Nojima H *et al* (2006) Major histocompatibility complex haplotype is associated with postherpetic pain in mice. *Anesthesiology* **104**:1063–1069.
45. Schretlen DJ, Vannorsdall TD, Winicki JM, Mushtaq Y, Hikida T, Sawa A, Cascella NG (2010) Neuroanatomic and cognitive abnormalities related to herpes simplex virus type 1 in schizophrenia. *Schizophr Res* **118**:224–231.
46. Shimeld C, Whiteland JL, Nicholls SM, Grinfeld E, Easty DL, Gao H, Hill TJ (1995) Immune cell infiltration and persistence in the mouse trigeminal ganglion after infection of the cornea with herpes simplex virus type 1. *J Neuroimmunol* **61**:7–16.
47. Shirts BH, Kim JJ, Reich S, Dickerson FB, Yolken RH, Devlin B, Nimgaonkar VL (2007) Polymorphisms in MICB are associated with human herpes virus seropositivity and schizophrenia risk. *Schizophr Res* **94**:342–353.
48. Simpson-Holley M, Colgrove RC, Nalepa G, Harper JW, Knipe DM (2005) Identification and functional evaluation of cellular and viral factors involved in the alteration of nuclear architecture during herpes simplex virus 1 infection. *J Virol* **79**:12840–12851.
49. Steiner I, Spivack JG, O'Boyle DR 2nd, Lavi E, Fraser NW (1988) Latent herpes simplex virus type 1 transcription in human trigeminal ganglia. *J Virol* **62**:3493–3496.
50. Stevens JG, Haarr L, Porter DD, Cook ML, Wagner EK (1988) Prominence of the herpes simplex virus latency-associated transcript in trigeminal ganglia from seropositive humans. *J Infect Dis* **158**:117–123.
51. Takasaki I, Nojima H, Shiraki K, Sugimoto Y, Ichikawa A, Ushikubi F *et al* (2005) Involvement of cyclooxygenase-2 and EP3 prostaglandin receptor in acute herpetic but not postherpetic pain in mice. *Neuropharmacology* **49**:283–292.
52. Tandrup T (2004) Unbiased estimates of number and size of rat dorsal root ganglion cells in studies of structure and cell survival. *J Neurocytol* **33**:173–192.
53. Theil D, Derfuss T, Paripovic I, Herberger S, Meinl E, Schueler O *et al* (2003) Latent herpesvirus infection in human trigeminal ganglia causes chronic immune response. *Am J Pathol* **163**:2179–2184.
54. Thompson RL, Sawtell NM (2001) Herpes simplex virus type 1 latency-associated transcript gene promotes neuronal survival. *J Virol* **75**:6660–6675.
55. Valyi-Nagy T, Dermody TS (2005) Role of oxidative damage in the pathogenesis of viral infections of the nervous system. *Histology Histopathology* **20**:957–967.
56. Valyi-Nagy T, Gesser RM, Raengsakulrach B, Deshmane SL, Randazzo BP, Dillner AJ, Fraser NW (1994) A thymidine kinase-negative HSV-1 strain establishes a persistent infection in SCID mice that features uncontrolled peripheral replication but only marginal nervous system involvement. *Virology* **199**:484–490.

57. Valyi-Nagy T, Olson SJ, Valyi-Nagy K, Montine TJ, Dermody TS (2000) Herpes simplex virus type 1 latency in the murine nervous system is associated with oxidative damage to neurons. *Virology* **278**:309–321.
58. Valyi-Nagy T, Sheth V, Clement C, Tiwari V, Scanlan P, Kavouras JH *et al* (2004) Herpes simplex virus entry receptor nectin-1 is widely expressed in the murine eye. *Curr Eye Res* **29**:303–309.
59. Wagner EK, Bloom DC (1997) Experimental investigation of herpes simplex virus latency. *Clin Microbiol Rev* **10**:419–443.
60. Whitley R (2001) Herpes simplex viruses. In: *Fields Virology*, 4th edn. PM KDaH (ed.), pp. 2461–2509. Lippincott Williams and Wilkins: Philadelphia.
61. Yolken R (2004) Viruses and schizophrenia: a focus on herpes simplex virus. *Herpes* **11**(Suppl. 2):83A–88A.

II.

Cancer Gene Therapy (2010) 17, 223–234
 0929-1903/10 $32.00
www.nature.com/cgt

ORIGINAL ARTICLE

Identification of virus resistant tumor cell subpopulations in three-dimensional uveal melanoma cultures

K Valyi-Nagy[1], S Dosa[1], SK Kovacs[1], S Bacsa[2], A Voros[1], D Shukla[2,3], R Folberg[1] and T Valyi-Nagy[1]

[1]*Department of Pathology, University of Illinois at Chicago, College of Medicine, Chicago, IL, USA;* [2]*Department of Ophthalmology, University of Illinois at Chicago, College of Medicine, Chicago, IL, USA and* [3]*Department of Microbiology and Immunology, University of Illinois at Chicago, College of Medicine, Chicago, IL, USA*

To better understand melanoma resistance to herpes simplex virus type 1 (HSV-1)-mediated oncolysis, traditional two-dimensional (2D) cultures and extracellular matrix (ECM) containing three-dimensional (3D) cultures of OCM1 and C918 uveal melanoma cells were infected with an HSV-1 strain that expresses the green fluorescent protein (GFP) marker during replication. Although 2D cultures were completely destroyed within a few days of HSV-1 inoculation, viable GFP-negative tumor cells remained detectable in 3D cultures for several weeks. Tumor cells with increased resistance to HSV-1 included cells that formed vasculogenic mimicry patterns and multicellular spheroids and cells that invaded Matrigel individually. Mechanisms of tumor resistance against HSV-1 in the 3D environment included impaired virus spread in the ECM and ECM-mediated inhibition of viral replication after viral entry into tumor cells. Observations also suggested that HSV-1 established quiescent infection in some tumor cells present in multicellular spheroids and that this could revert to productive viral infection when the tumor growth pattern changed. These findings indicate that 3D tumor cell cultures can be used to identify distinct tumor cell populations with increased resistance to HSV-1 and to explore mechanisms of ECM-mediated tumor resistance to oncolytic virotherapy.
Cancer Gene Therapy (2010) **17,** 223–234; doi:10.1038/cgt.2009.73; published online 6 November 2009

Keywords: extracellular matrix; vasculogenic mimicry; herpes simplex virus; oncolytic therapy; quiescence; Matrigel

Introduction

Virus, including herpes simplex virus type 1 (HSV-1)-mediated oncolytic therapy, is a promising novel modality of tumor therapy with potential usefulness against a wide variety of malignancies.[1–6] Oncolytic HSV-1 therapy is dependent on virus replication in tumor cells and is augmented by host antiviral and infection-induced anti-tumor immune responses.[7–11] In spite of significant progress, oncolytic virotherapy faces significant challenges. Although traditional two-dimensional (2D) monolayer cultures of many types of tumor cells are efficiently destroyed by a variety of HSV-1 vectors *in vitro*, tumor destruction is often incomplete *in vivo*.[1,7] Factors limiting the effectiveness of HSV-1 oncolytic therapy *in vivo* remain incompletely understood. However, observations indicate that potential problems include the impairment of intratumoral virus spread by the extracellular matrix (ECM), decreased expression of viral entry receptors by different tumor cell populations, activation of intracellular tumor defenses to viral infection, and quick virus clearance by the host immune system.[7,12–19] It is clear that many aspects of the complex virus–host interactions that determine the effectiveness of HSV-1 oncolytic therapy are difficult to impossible to study in traditional 2D tissue culture systems.

The behavior of cells *in vivo* is controlled by their interactions with neighboring cells and with the ECM.[20–23] Cancer cells grown in three-dimensional (3D) cultures in a polymeric ECM closely mimic the biology of tumor development *in vivo* and numerous studies indicate that 3D cultures are superior to traditional 2D monolayer cultures for studies of key cellular behaviors such as differentiation, proliferation, invasion, and apoptosis.[23–29] Cancer cells grown in 3D culture are more resistant to chemotherapeutic agents and radiation than cells in 2D culture and 3D tumor cell cultures are useful for preclinical evaluation of the cytotoxic effect of anticancer agents.[25,27,30] It is well established that multiple cell types within individual tumors have differential sensitivities to drugs and radiation both *in vivo* and in 3D cultures.[25,27,30,31]

Correspondence: Dr T Valyi-Nagy, Department of Pathology, University of Illinois at Chicago, 840 South Wood Street, Room 130 CSN, M/C 847, Chicago, IL 60612, USA.
E-mail: tiborv@uic.edu
Received 1 March 2009; revised 1 June 2009; accepted 11 July 2009; published online 6 November 2009

Although 3D cultures provide an excellent experimental system to study mechanisms of tumor cell resistance to drugs and radiation, very few studies have used 3D tumor cell cultures in the context of viral oncolytic therapy.[19,32,33] Earlier work in our laboratory indicated that 3D cultures of uveal melanoma cells show increased resistance to HSV-1 relative to 2D cultures.[33] Specifically, destruction of 95% of tumor cells occurred several days later in 3D cultures than in 2D cultures after HSV-1 inoculation. These findings suggested that HSV-1 inoculation of 3D uveal melanoma cultures could provide a useful model to study mechanisms of ECM-mediated tumor resistance to HSV-1 oncolytic therapy.

The ECM environment is a critically important determinant of the morphology and gene expression profile of uveal melanomas *in vivo* and of uveal melanoma cultures *in vitro*.[34–39] Highly invasive uveal melanoma cells, including C918 cells, and uveal melanoma cells of low invasive potential, including OCM1 cells, all grow as monolayers in 2D cultures. In 3D cultures established with the use of laminin-rich ECM (Matrigel), highly invasive uveal melanoma cells form vasculogenic mimicry patterns. In contrast, uveal melanoma cells of low invasive potential do not form vasculogenic mimicry patterns under 3D conditions, but rather grow in tumor cell aggregates on the matrix surface and form multicellular spheroids inside the matrix. In addition to these structures, 3D cultures of uveal melanoma cells contain a variety of other morphologically distinguishable cell populations that are defined by their spatial relationship to the ECM. For instance, 3D cultures of both highly invasive uveal melanoma cells and uveal melanoma cells of low invasive potential contain individual tumor cells invading the ECM. Observations indicate that morphologically distinct tumor cell populations present in 3D cultures are of clinical relevance. For instance, vasculogenic mimicry patterns are present in a wide variety of malignancies including uveal melanomas and their detection is associated with increased mortality.[34,37]

This study has used 2D and 3D cultures of uveal melanoma cells and was designed to find answers to the following questions related to HSV-1 oncolytic therapy. (i) Can 3D tumor cell cultures be used to identify morphologically distinct tumor cell populations that have increased resistance to HSV-1? (ii) Can 3D tumor cell cultures be used to learn about mechanisms of ECM-mediated tumor cell resistance to HSV-1 oncolytic therapy?

We show here that 3D tumor cell cultures can be used to identify distinct tumor cell populations with increased resistance to HSV-1 oncolytic therapy. We report that uveal melanoma cell populations with increased resistance to HSV-1 in 3D cultures include cells forming vasculogenic mimicry patterns and multicellular spheroids and tumor cells that invade the ECM individually. Furthermore, we show that mechanisms of tumor resistance against HSV-1 in the 3D environment include impaired virus spread in the Matrigel matrix and ECM-mediated inhibition of viral replication after viral entry into tumor cells.

Materials and methods

Viruses

Wild-type (wt) HSV-1 strain KOS and recombinant HSV-1 strain K26GFP (a gift from P Desai, The Johns Hopkins University, Baltimore, MD) were amplified and quantitated as described elsewhere.[40,41] Cells infected with HSV-1 strain K26GFP exhibit punctate nuclear fluorescence at early times in the replication cycle and at later times during infection, a generalized cytoplasmic and nuclear fluorescence, including fluorescence at the cell membranes can be observed.[40] K26GFP was shown to grow wt virus as well in cell culture.[40]

Cells

Uveal melanoma cells of low (OCM1) and high (C918) invasive potential were maintained in Eagle's Minimal Essential Medium (BioWhittaker Inc., Walkersville, MD) supplemented with heat inactivated 15% fetal bovine serum (Fisher, Ontario, Canada) without the addition of exogenous ECM molecules or growth factors. These cell lines have been described in detail earlier.[38,39,42]

2D and 3D uveal melanoma cultures

Melanoma cells were grown on six-well plates in Eagle's Minimal Essential Medium medium either in the presence (3D cultures) or in the absence (2D cultures) of ECM rich in laminin (Matrigel, BD Biosciences, Bedford, MA). For 3D cultures, Matrigel was poured onto tissue culture plates to a depth of approximately 0.2 mm followed by polymerization for 1 h at 37 °C before placement of melanoma cells on the Matrigel surface. Cultures were incubated in repeatedly refreshed culture medium for up to 4 weeks and observed daily under an inverted microscope (Leica, Bannockburn, IL).

Determination of susceptibility of uveal melanoma cells to wt HSV-1 (KOS) and HSV-1 K26GFP-mediated destruction in 2D and 3D cultures

C918 and OCM1 uveal melanoma cells were grown on six-well tissue culture plates in the presence (3D cultures) or absence of Matrigel (2D cultures). After 3–4 days, when in the 3D cultures C918 cells formed prominent vasculogenic mimicry patterns and OCM-1 cells formed cell aggregates on the Matrigel surface and both cell lines showed invasion of tumor cells into the Matrigel matrix, the tissue culture medium was removed and one of the following inocula was gently placed on the surface of the cultures: (i) 0.5 ml of sterile PBS (mock infection); (ii) wt HSV-1 (strain KOS) with a calculated multiplicity of infection (MOI) of 0.5 plaque forming units (PFU) per cell diluted in PBS to a final volume of 0.5 ml; (iii) HSV-1 K26GFP with a calculated MOI of 0.5 PFU per cell diluted in PBS to a final volume of 0.5 ml. After incubation for 1 h, the original inocula were removed and fresh tissue culture medium (3 ml) was added to each well and further incubated in repeatedly refreshed culture medium for up to 4 weeks. During this 4-week period, cultures were observed daily under an inverted fluorescence microscope (Leica, Bannockburn, IL) for evidence

of viral cytopathic effects and green fluorescent protein (GFP) expression. The day when at least 95% of the melanoma cells were destroyed was noted. Cell death was confirmed by the uptake of the charged cationic dye Trypan blue (0.2%) by >95% of residual cells after incubation of cultures with Trypan blue (0.2%) for 10 min at 37 °C.

Determination of HSV-1 spread through Matrigel

C918 and OCM1 uveal melanoma cells were grown on 12-well tissue culture plates in monolayers (2D cultures). When the cultures have reached approximately 70% confluency, culture media were removed and either 0.5 ml of a 1:1 mixture of PBS and Matrigel or 0.5 ml of PBS was layered on the cells. Cultures were then incubated at 37 °C for 1 h to allow Matrigel to polymerize and form an approximately 1 mm thick layer matrix on the cells. Next, cultures were either inoculated with 0.5 ml HSV-1 K26GFP diluted in PBS to a calculated MOI of 0.5 PFU per cell or were mock infected with 0.5 ml PBS by gently layering these solutions on the cultures making sure that the Matrigel surface was not violated. After further incubation at 37 °C for 1 h, additional 2 ml of fresh tissue culture media was added to each well. Cultures were then further incubated for up to 2 weeks at 37 °C with fresh culture medium added to the cultures every 2 days. During this 2-week period, cultures were observed regularly under an inverted fluorescence microscope (Leica, Bannockburn, IL) for evidence of GFP expression.

Placement and culturing of earlier HSV-1 inoculated uveal melanoma cells in 2D or 3D environments

C918 and OCM1 uveal melanoma cells were grown on 12-well tissue culture plates in monolayers (2D cultures). When the cultures have reached approximately 70% confluency, culture media were removed and the cells were exposed at 37 °C to one of the following inocula: (i) 0.5 ml of sterile PBS (mock infection) or (ii) HSV-1 K26GFP with a calculated MOI of 0.5 PFU per cell diluted in PBS to a final volume of 0.5 ml. After incubation for 1 h, the original inocula were removed and the monolayers were washed in sterile PBS twice and 1 ml of sterile PBS was added to each well. Cells were than scraped off using sterile, disposable cell scrapers. Cell solutions were than centrifuged and cell pellets were resuspended in culture medium. Equal volumes (0.25 ml) of the cell solutions were then used to either establish new 2D cultures in 12-well tissue culture plates or 3D cultures as follows. For 3D cultures, Matrigel was poured onto tissue culture plates to a depth of approximately 0.2 mm followed by polymerization for 1 h at 37 °C Cell suspensions of HSV-1 K26GFP or mock-infected uveal melanoma cells were mixed with Matrigel 1:1 (0.25:0.25 ml) and poured on the Matrigel-coated wells. Finally, 2 ml of fresh culture medium was added. 2D and 3D cultures were then further incubated for up to 4 weeks at 37 °C with fresh culture medium added to the cultures every 2 days. During this 4-week period, cultures were observed regularly under an inverted fluorescence microscope (Leica, Bannockburn, IL) for evidence of GFP expression and the percentage of GFP-expressing cells was determined by counting the number of GFP-positive and GFP-negative cells in 16 high power microscopic fields for each studied type of treatment at selected time points.

Results

OCM1 and C918 uveal melanoma cells form several morphologically distinct cell populations under 3D culture conditions

To define in detail the growth pattern of uveal melanoma cells in 2D and 3D cultures, OCM1 and C918 cells were grown either in the presence or absence of laminin-rich ECM (Matrigel). In the absence of Matrigel (2D cultures), both OCM1 and C918 grew in monolayers (Figure 1a and b). In the presence of Matrigel, both cell lines developed 3D structures (Figures 1c–h. 2a–d, 3a–d). When OCM1 cells were placed on the Matrigel surface, the cells first formed aggregates that were loosely attached to the Matrigel surface (Figures 1c, 2a). As the cell aggregates were growing further, their attachment to the Matrigel surface became wider and firmer and single tumor cells began to invade the Matrigel matrix (Figure 2a and b). During further growth, individual tumor cells invaded the matrix deeply and some of these cells formed multicellular spheroids showing a smooth surface and consisting of cells tightly attached to each other (Figures 1e, 2c). Tumor cell aggregates on the Matrigel surface also showed similar spheroid formation at their bottom portion that completely immersed in the Matrigel matrix (Figure 2b and c). Many of the tumor cell spheroids were stable for days to weeks, whereas others showed outgrowth of individual cells into the matrix. Cells invading the matrix (Figure 1g) eventually reached the bottom of the tissue culture plate and grew under the matrix in monolayers (Figure 2d). The growth of OCM1 cells within the Matrigel matrix did not cause massive destruction of the matrix until the end of the 4-week observation period.

When C918 cells were placed on the Matrigel surface, the cells started to grow on the matrix surface in a single layer and formed circular vasculogenic mimicry patterns that surrounded round matrix surfaces free of tumor cells (Figures 1d, 3a). Next, individual tumor cells started to grow into the Matrigel at the line defined by the vasculogenic mimicry patterns (Figures 1f, 3b). Cells invading the matrix migrated to the bottom of the culture plate and formed monolayers there (Figures 1h, 3c and d). Interestingly, the formation of these bottom monolayers was restricted to areas that were under the Matrigel surfaces that were not colonized by cells and were surrounded by vasculogenic mimicry patterns (Figure 3c). Next, individual tumor cells invaded the matrix underlying cell monolayers on the Matrigel surface (Figure 3d). Tumor cell growth and matrix invasion eventually caused a loss of Matrigel in areas surrounded by vasculogenic mimicry patterns (Figure 3d).

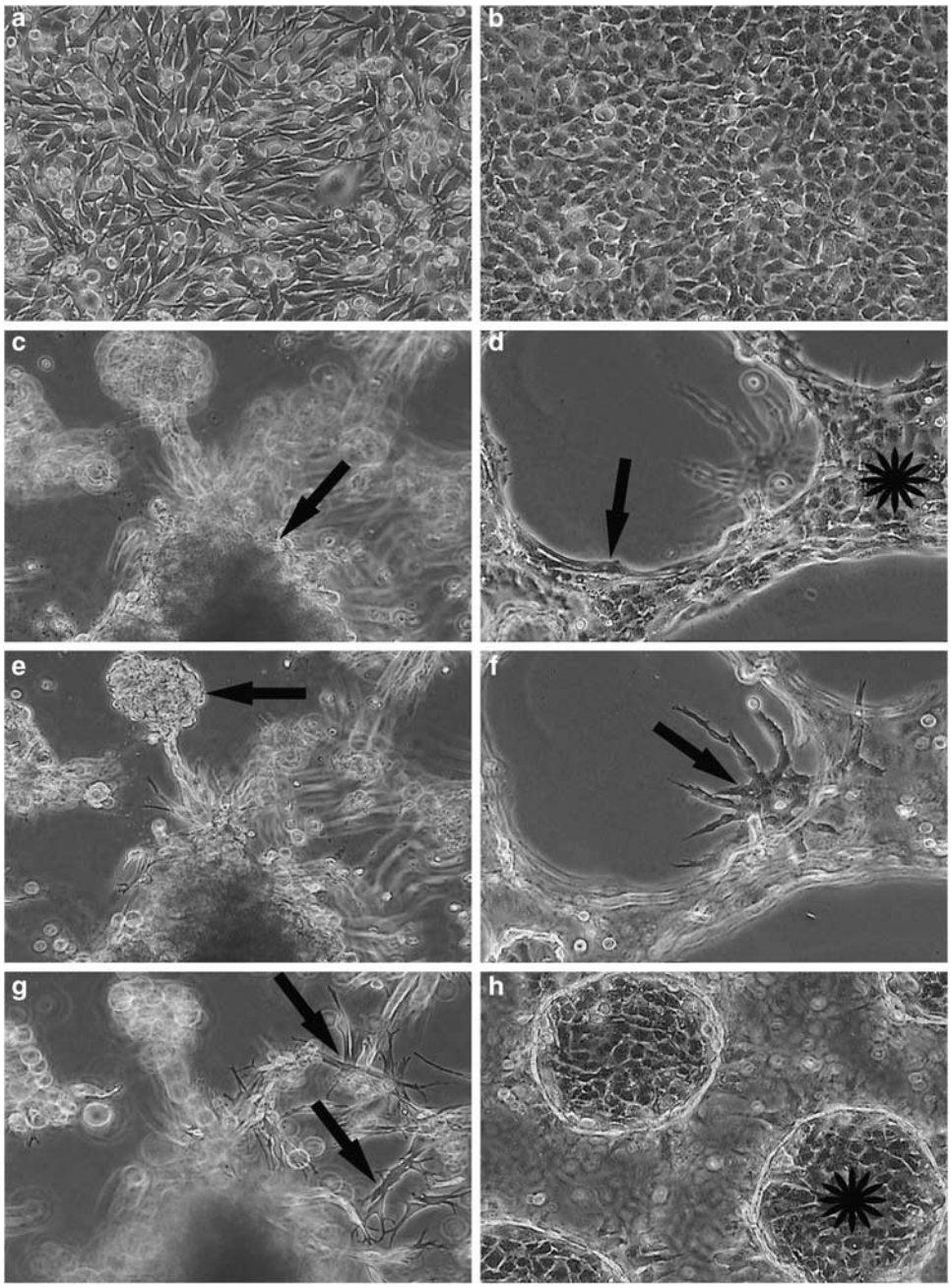

Figure 1 Morphology of OCM1 and C918 uveal melanoma cells grown in either 2D or 3D cultures. OCM1 cells grown in 2D monolayers for 5 days (**a**). Five-day-old 3D OCM1 culture. Arrow indicates surface aggregate of cells (**c**). Same 3D OCM1 culture with focus deeper on multicellular spheroid (arrow) within Matrigel (**e**). Same 3D OCM1 culture with focus even deeper on individual tumor cells (arrows) invading Matrigel (**g**). C918 cells grown in 2D monolayers for 5 days (**b**). Three-day-old 3D C918 culture with focus on Matrigel surface. Arrow indicates vasculogenic mimicry forming cells and asterix marks tumor cells growing in monolayer on Matrigel surface (**d**). Same 3D C918 culture with focus on tumor cells (arrow) invading the Matrigel matrix (**f**). Six-day-old 3D C918 culture with focus on tumor cells growing in monolayer under the Matrigel matrix (**h**).

These observations confirm and extend earlier observations related to the morphology uveal melanoma cultures[38] and indicate that OCM1 and C918 uveal melanoma cells form several morphologically distinct cell populations under 3D culture conditions.

Rapid destruction of 2D and delayed and incomplete destruction of 3D uveal melanoma cultures by wt HSV-1 and HSV-1 K26GFP

2D and 3D cultures of OCM1 and C918 cells were inoculated with wt HSV-1 strain KOS or HSV-1 strain

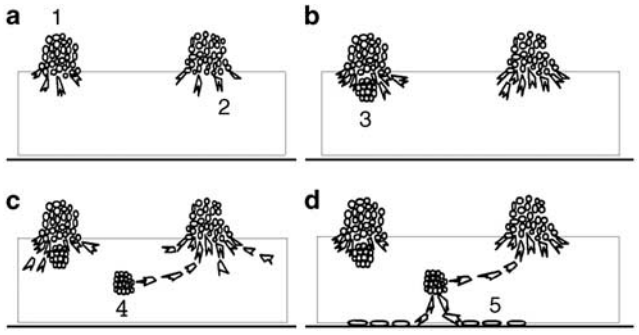

Figure 2 Schematic illustration of the morphology of 2-day-old (**a**), 3-day-old (**b**), 4-day-old (**c**), and 5-day-old (**d**) 3D OCM1 uveal melanoma cultures. 1, cells forming aggregates on Matrigel surface; 2, individual cells invading Matrigel; 3, multicellular spheroids at the bottom portion of aggregates immersed into the Matrigel; 4, tumor cell spheroid within Matrigel not associated with surface aggregates; and 5, tumor cells growing in monolayers under the Matrigel on the surface of the culture dish.

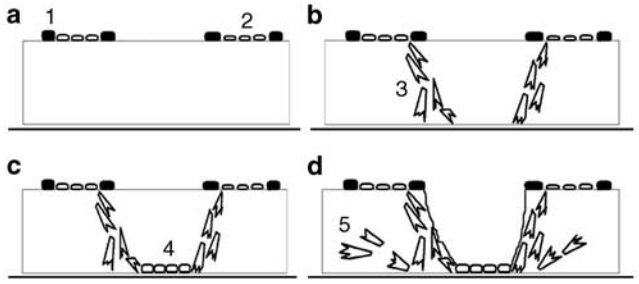

Figure 3 Schematic illustration of the morphology of 2-day-old (**a**), 3-day-old (**b**), 4-day-old (**c**), and 5-day-old (**d**) 3D C918 uveal melanoma cultures. 1 (cells marked dark), cells forming vasculogenic mimicry patterns on the Matrigel surface; 2, cells forming monolayers on the Matrigel surface; 3, individual tumor cells invading Matrigel and growing toward the bottom of the culture dish; 4, tumor cells growing in monolayers under the Matrigel in the center of vasculogenic mimicry patterns; and 5, individual tumor cells invading Matrigel underlying cell monolayers on the Matrigel surface.

K26GFP by placing virus solutions on the surface of the cultures. HSV-1 K26GFP exhibits fluorescence on replication.[40] Cultures were followed for evidence of cytopathic effects and virus replication (GFP expression/fluorescence) by an inverted fluorescence microscope.

We found that 2D cultures were completely destroyed by both HSV-1 strains within a few days (Table 1) with no evidence of surviving cells by Trypan blue staining (data not shown). In contrast, virus inoculated 3D cultures showed delayed and incomplete destruction (Table 1). Importantly, a portion of both OCM1 and C918 cells seemed to survive HSV-1 KOS and HSV-1 K26GFP infection in 3D cultures for up to 4 weeks. Cell populations with increased resistance included C918 cells that formed vasculogenic mimicry patterns on the Matrigel surface, OCM1 cells that formed multicellular spheroids within the Matrigel matrix, and both C918 and OCM1 cells that invaded Matrigel individually.

Table 1 Elapsed time from inoculation of HSV-1 KOS or HSV-1 K26GFP (at MOI = 0.5 PFU per cell) to at least 95% destruction of 2D and 3D OCM1 and C918 uveal melanoma cultures

Cell line	*Culture condition*	*HSV-1 strain*	*Day of 95% destruction*
OCM1	2D	KOS	4
	3D	KOS	8
	2D	K26GFP	4
	3D	K26GFP	8
C918	2D	KOS	5
	3D	KOS	9
	2D	K26GFP	5
	3D	K26GFP	9

In K26GFP inoculated 2D OCM1 and C918 cultures, 20–50% of tumor cells showed GFP expression by 1 day post infection (p.i.), and after 3 days p.i., it was very difficult to find any cells without fluorescence consistent with the complete viral replication-mediated destruction of these cultures by 4–5 days (Figures 4a and b, 6a and b). In contrast, 3D cultures of both OCM1 and C918 showed a significant number of GFP-negative cells throughout the 4-week observation period (Figures 4c–h, 5a–f, 6c–h, 7a–f).

In 3D cultures of OCM1, cells forming aggregates on the Matrigel surface showed widespread fluorescence (virus replication) by 1 day p.i., and after 4 days p.i., it was very difficult to find any cells without fluorescence in these structures consistent with the complete virus-mediated destruction of these surface cell aggregates by K26GFP by 8 days p.i. (Figure 4c and d). Individual OCM1 cells growing into the Matrigel matrix showed variable fluorescence and some apparently viable, and GFP-negative cells were consistently present during the 4-week observation period. Cells forming multicellular spheroids inside the matrix and cells forming spheroids at the bottom, matrix immersed portion of surface aggregates showed marked resistance to HSV-1 replication (Figures 4c–h, 5a and b). Although occasional spheroids showed widespread fluorescence by 4 days p.i., others contained only a few GFP-positive cells and many remained completely devoid of GFP expression for days to weeks. GFP-negative spheroids contained viable cells as radial outgrowth of individual cells into the Matrigel matrix was observed from many of these structures as the cultures were aging (Figure 5a,c and e). Interestingly, this outgrowth was often associated with the appearance of fluorescence in outgrowing cells and in cells within the spheroids (Figure 5d and f), whereas in other cases, both spheroids and outgrowing cells remained GFP negative (Figure 5b). Cells growing under the matrix in monolayers were susceptible to HSV-1 and showed widespread fluorescence.

In 3D cultures of C918 cells, cells growing on the matrix surface in a single layer showed widespread fluorescence (virus replication) as early as 1 day p.i. consistent with the complete destruction of this cell population by K26GFP by 9 days p.i. (Figure 6c and d). In contrast, cells forming vasculogenic mimicry

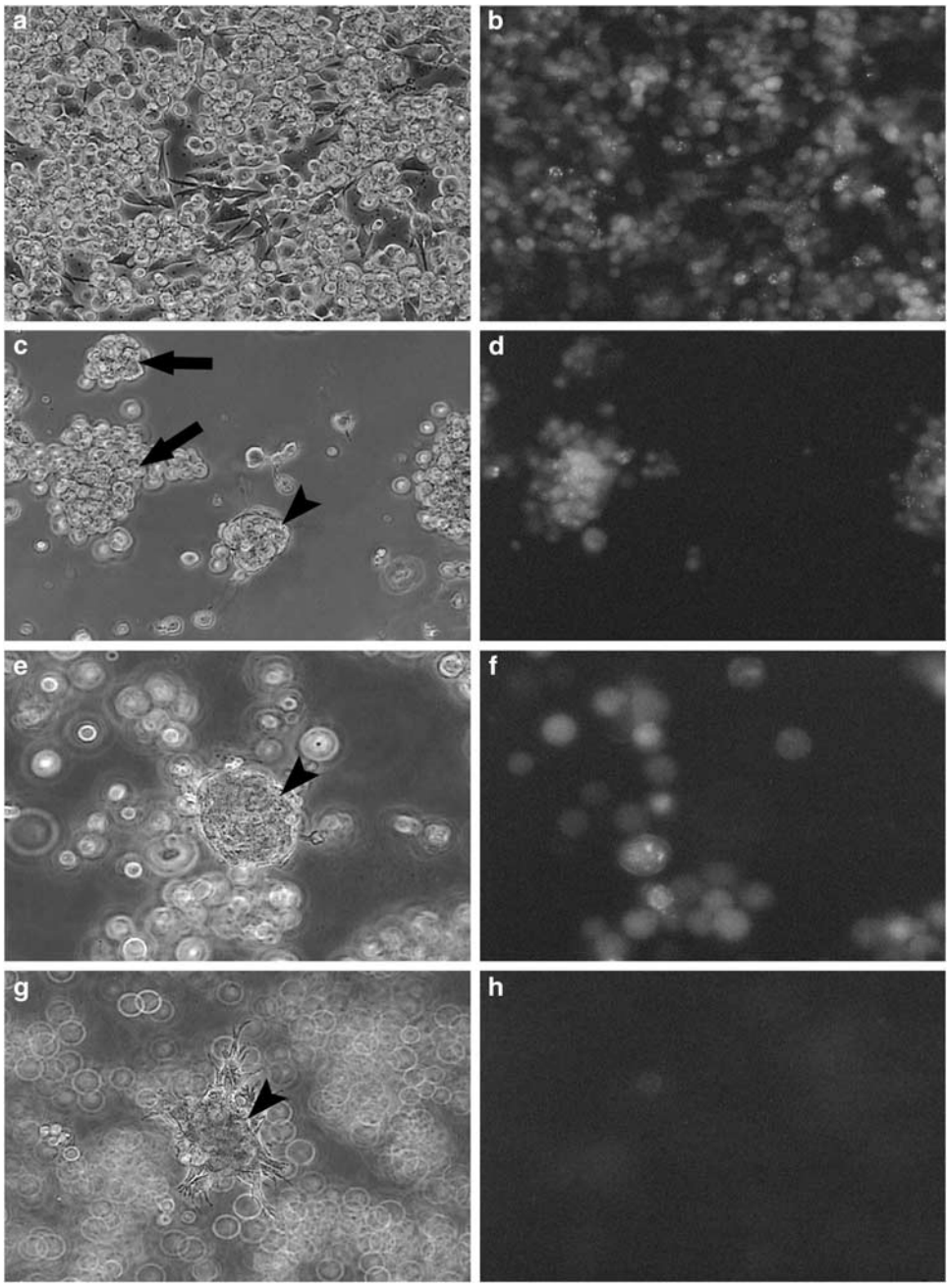

Figure 4 Morphology and GFP expression in HSV-1 K26GFP inoculated OCM1 uveal melanoma 2D and 3D cultures. 2D OCM1 culture 1 day after virus inoculation; morphology (**a**) and GFP expression (**b**). 3D OCM1 cultures 1 day after virus inoculation; morphology (**c**) and GFP expression (**d**). Arrows in panel (**c**) indicate tumor cell aggregates on the Matrigel surface that are GFP positive in panel D and arrowhead in panel C indicates a multicellular spheroid within the Matrigel matrix that is GFP negative in panel D. 3D OCM1 cultures 3 days after virus inoculation; morphology (**e**) and GFP expression (**f**). Arrowhead in panel E indicates a multicellular spheroid within the Matrigel matrix that is GFP negative in panel F. 3D OCM1 cultures 12 days after virus inoculation; morphology (**g**) and GFP expression (**h**). Arrowhead in panel G indicates a multicellular spheroid within the Matrigel matrix showing outgrowth of individual tumor cells at the periphery that is GFP negative in panel H.

patterns on the Matrigel surface showed increased resistance to HSV-1 (Figure 6e and f) and GFP-negative cells could be observed in these structures throughout the 4-week observation period. Similarly, cells invading the matrix individually showed increased resistance to HSV-1 and this cell population also included many GFP-negative cells throughout the 4-week observation period (Figures 6g–h, 7a–f). Tumor cells growing in monolayers under the Matrigel showed widespread fluorescence and susceptibility to HSV-1 (Figure 6e and f).

These observations clearly identify certain uveal melanoma populations with increased resistance against HSV-1 in the 3D environment. Consequent experiments were designed to identify the mechanism(s) responsible for the

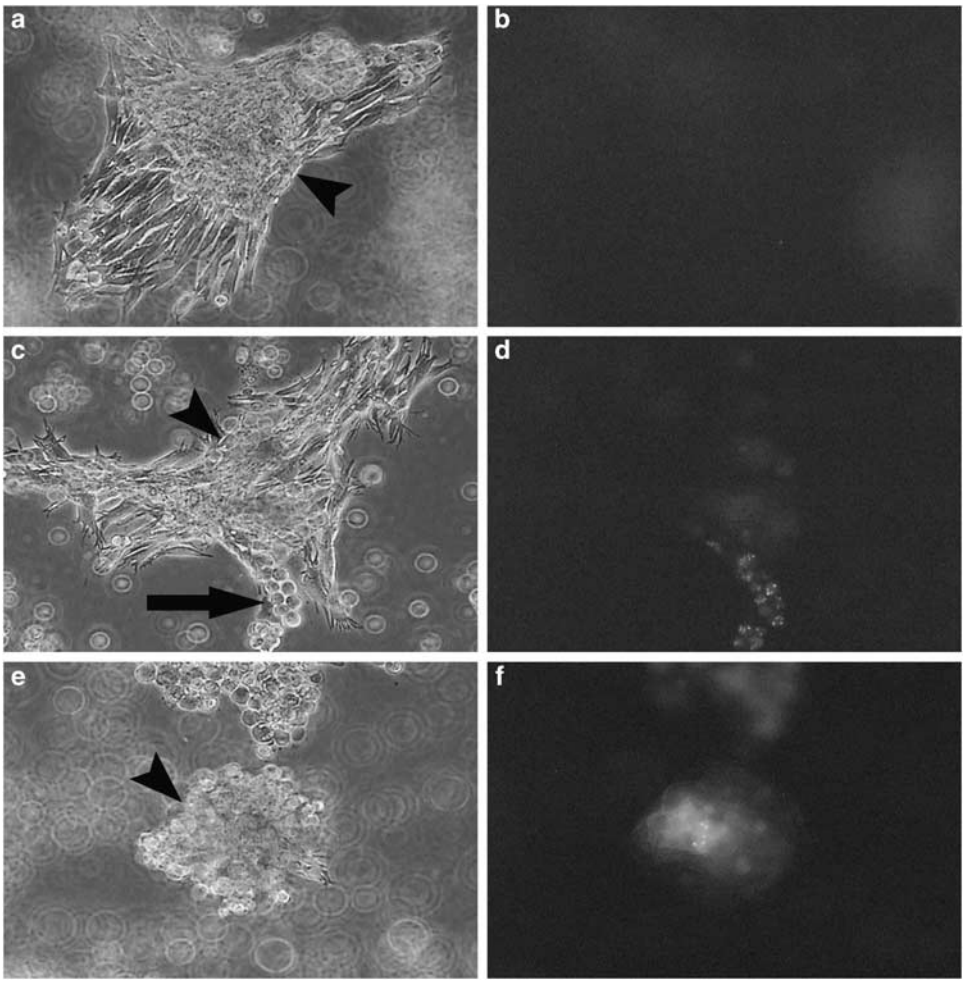

Figure 5 Morphology and GFP expression in HSV-1 K26GFP inoculated 3D OCM1 uveal melanoma cultures 12 days after virus inoculation. Arrowhead in panel (**a**) indicates a multicellular spheroid within the Matrigel matrix that shows outgrowth of individual tumor cells at its periphery that are GFP negative in panel (**b**). Arrowhead in panel (**c**) indicates a multicellular spheroid within the Matrigel matrix showing outgrowth of individual tumor cells. Some of the outgrowing tumor cells show GFP expression in panel (**d**). Arrowhead in panel (**e**) indicates a multicellular spheroid within the Matrigel matrix with outgrowth of individual tumor cells at the periphery with cells within the core of the spheroid showing GFP expression in panel (**f**).

observed resistance of tumor cells against HSV-1 in 3D cultures.

Matrigel impairs HSV-1 spread

To determine whether inhibition of HSV-1 spread through Matrigel was a mechanism responsible for the absence of virus replication (GFP expression) in some tumor cells in 3D cultures, monolayers of OCM1 and C918 cells were covered with an approximately 1 mm thick layer of Matrigel and then HSV-1 K26GFP was placed on the Matrigel surface. As controls, monolayers of OCM and C918 cells without a Matrigel cover were also inoculated with the same amount of virus. Virus inoculated uveal monolayers with no Matrigel cover showed widespread GFP expression by 18–24 h p.i. and were completely destroyed within a few days. In contrast, cells covered with Matrigel and inoculated with HSV-1 K26GFP showed continued viability and growth during a 2-week observation period with no evidence of GFP expression. These findings indicate that Matrigel inhibits HSV-1 spread.

ECM mediates inhibition of HSV-1 replication after virus entry into tumor cells

To determine whether inhibition of viral replication after virus entry into tumor cells is a mechanism responsible for the absence of virus replication (GFP expression) in some tumor cells in 3D cultures, uveal melanoma cells were first inoculated with HSV-1 K26GFP under 2D conditions (allowing for unimpeded entry of virus into cells) and were then cultured under either 2D or 3D conditions. Briefly, C918 and OCM1 uveal melanoma cells grown in monolayers were either exposed to HSV-1 K26GFP at a calculated MOI of 0.5 PFU per cell or to sterile PBS (mock infection) for 1 h. The original inocula were then removed and the inoculated cells were scraped off and were resuspended in fresh culture medium. Equal volumes of the cell solutions were then used to either establish new

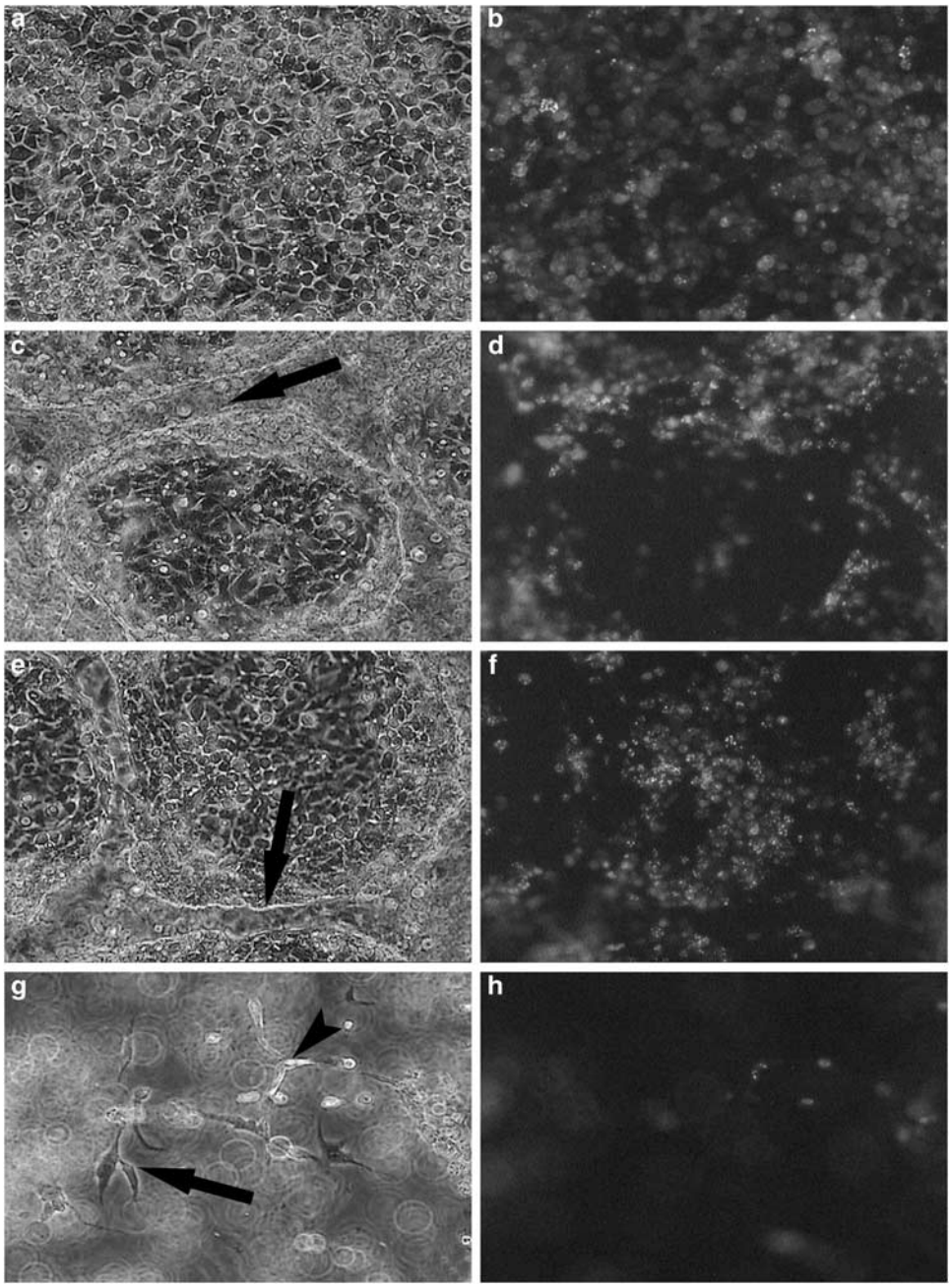

Figure 6 Morphology and GFP expression in HSV-1 K26GFP inoculated C918 uveal melanoma cells grown in 2D and 3D cultures. 2D C918 monolayer culture 3 days after virus inoculation; morphology (**a**) and GFP expression (**b**). 3D C918 culture 3 days after virus inoculation; morphology (**c**) and GFP expression (**d**). Arrow in panel (**c**) indicates tumor cells growing in monolayer on the Matrigel surface that express GFP in panel (**d**). 3D C918 culture 3 days after virus inoculation; morphology (**e**) and GFP expression (**f**). Arrow in panel (**e**) indicates tumor cells forming vasculogenic mimicry pattern on the Matrigel surface that only partially expresses GFP in panel (**f**). 3D C918 culture 3 days after virus inoculation; morphology (**g**) and GFP expression (**h**). Arrow in panel (**g**) indicates a tumor cell invading Matrigel that does not express GFP in panel (**h**). Arrowhead in panel (**g**) indicates a tumor cell invading Matrigel that expresses GFP in panel (**h**).

2D or 3D cultures. For 3D cultures, cell suspensions of HSV-1 K26GFP or mock-infected uveal melanoma cells were mixed with Matrigel 1:1 and these mixtures were poured on earlier Matrigel-coated tissue culture plates.

After the plating of earlier mock-infected OCM1 and C918 cells on tissue culture dishes, tumor cells established monolayers (2D cultures) that showed normal growth and no evidence of GFP expression. Growing of earlier mock-infected OCM1 and C918 cells under 3D conditions in Matrigel was initially associated with single cells suspended in matrix. After the first day, growth of OCM1 cells was associated with the development of tumor cell spheroids, many of which later showed outgrowth of individual cells into the matrix. Growth of mock-infected

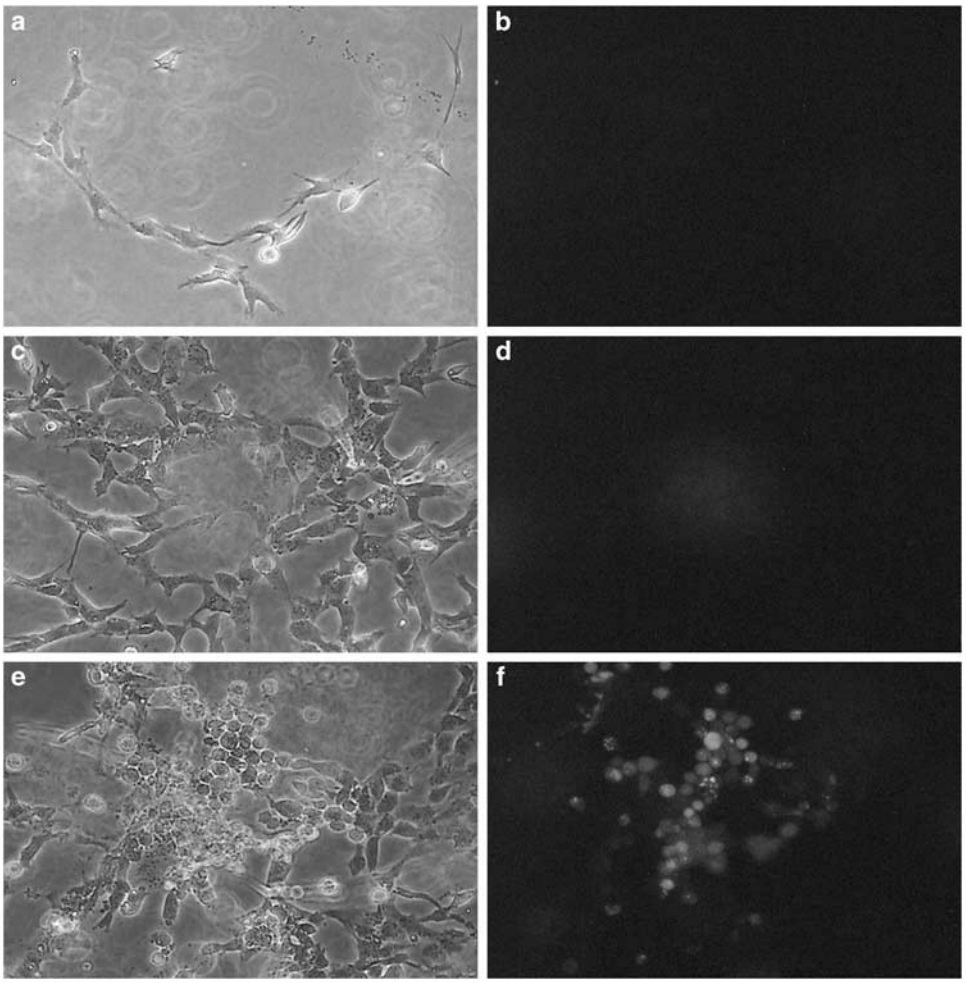

Figure 7 Morphology (**a**, **c**, **e**) and GFP expression (**b**, **d**, **f**) of cells invading the Matrigel matrix in HSV-1 K26GFP inoculated 3D C918 uveal melanoma cultures 12 days after virus inoculation. Note the lack of GFP expression in panels (**b**, **d**) and the variable expression of GFP by tumor cells in panel (**f**).

C918 cells was associated with the establishment of extensive network of tumor cells invading the matrix. No GFP expression was detected in the mock-infected 3D cultures of OCM1 and C918 cells.

After the plating of earlier HSV-1 K26GFP inoculated OCM1 and C918 cells on tissue culture dishes, tumor cells established monolayers (2D cultures) that were completely destroyed by virus replication within a few days. At 18 h p.i., 29.53 ± 15.01% of OCM1 cells and 40.33 ± 15.17% of C918 cells showed fluorescence (evidence of HSV-1 replication) (Table 2). Nearly all OCM1 cells were GFP positive by 72 h and nearly all C918 cells were GFP positive by 96 h. These findings are consistent with replication of input virus in infected cells at 18 h p.i. and virus spread to all cells in the following days.

Culturing of earlier HSV-1 K26GFP inoculated OCM1 and C918 cells in 3D was initially associated with single cells suspended in matrix. More than half of the cells showed morphologic changes during the first day of the establishment of the 3D cultures including rounding and a minority of cells showed morphological features of apoptosis. At 18 h p.i., the numbers of OCM1 and C918 cells in the virus-infected 3D cultures were 12.5 and 8.5% lower than those in their mock-infected 3D counterparts. At 18 h p.i., 2.80 ± 2.75% of OCM1 cells

Table 2 GFP expression in OCM1 and C918 uveal melanoma cells inoculated with 0.5 PFU per cell of HSV-1 K26GFP or mock infected with PBS under 2D conditions for 1 h and then cultured for 17 h either under 2D or 3D conditions

Cell line	*Inoculation in 2D*	*Consequent culture*	*Percent of cells GFP +*[a]
OCM1	mock	2D	0
	HSV-1 K26GFP	2D	29.53 ± 15.01
	mock	3D	0
	HSV-1 K26GFP	3D	2.8 ± 2.75
C918	mock	2D	0
	HSV-1 K26GFP	2D	40.33 ± 15.17
	mock	3D	0
	HSV-1 K26GFP	3D	2.22 ± 3.05

[a]Percentage of GFP-expressing cells was determined by counting the number of GFP-expressing and GFP-negative cells in 16 high power microscopic fields for each studied type of treatment.

and $2.22 \pm 3.05\%$ of C918 cells showed fluorescence (Table 2) in the HSV-1-infected 3D cultures. The number of GFP-expressing cells did not increase the following days. Thus, at 18 h p.i., a significantly smaller percentage of cells showed evidence of virus replication in 3D cultures than what was expected on the basis of the amount of input virus. These observations indicate that the ECM can mediate the inhibition of HSV-1 replication after virus entry into tumor cells.

In HSV-1-infected 3D cultures, the majority of cells remained GFP negative throughout a 4-week observation period (data not shown). Interestingly, the outgrowth of individual OCM1 cells into the Matrigel matrix from spheroids that have been GFP negative for days to weeks was occasionally associated with the appearance of GFP expression in outgrowing cells and in cells within the spheroids similarly to the process shown in Figure 5c–f. As Matrigel does not allow HSV-1 spread, these observations suggest that HSV-1 established a quiescent infection in some tumor cells within multicellular spheroids and that this quiescent infection could revert to productive viral infection when the tumor growth pattern changed.

Discussion

We show here for the first time that 3D tumor cell cultures can be used to identify morphologically distinct tumor cell populations with increased resistance to HSV-1. Specifically, we show that tumor cells forming vasculogenic mimicry patterns and multicellular spheroids and cells that invade the ECM individually have increased resistance to HSV-1. Furthermore, we show that mechanisms of tumor resistance against HSV-1 in the 3D environment include impaired virus spread in the ECM and ECM-mediated inhibition of viral replication after viral entry into tumor cells. Observations reported here also suggest that HSV-1 can establish quiescent infection in some tumor cells present in multicellular spheroids and that this can revert to productive viral infection on outgrowth of individual tumor cells into the Matrigel matrix.

It is well established that 3D tumor cell cultures are useful for preclinical evaluation of the cytotoxic effect of anticancer agents, and multiple cell types within individual tumors have differential sensitivities to drugs and radiation both *in vivo* and in 3D cultures.[25,27,30,31] However, so far very few studies have used 3D tumor cell cultures in the context of viral oncolytic therapy. These studies have indicated that tumor cells grown in 3D cultures are also more resistant to viral, including HSV-1 and adenovirus-mediated oncolytic therapy, than cells grown in 2D culture.[32,33] Observations reported here confirm and extend these studies and identify morphologically distinct tumor cell populations present in 3D cultures that have increased resistance to viral oncolytic therapy. These observations are likely of clinical relevance as, for instance, vasculogenic mimicry patterns are present in a wide variety of malignancies and their detection in several tumor types is associated both with adverse outcome.[34,37]

Factors limiting the effectiveness of HSV-1 oncolytic therapy remain poorly understood in part because related studies have been limited to expensive and time-consuming experimental animal models. Theoretical considerations and experimental observations made thus far indicate that mechanisms of tumor resistance to HSV-1 therapy include ECM-mediated impairment of intratumoral virus spread, impaired viral entry into tumor cells because of decreased expression of HSV-1 entry receptors, inhibition of viral replication after viral entry into tumor cells, and virus clearance by the host immune system.[5–7,12–15,17–18] In this study, we found that at least two of these potential mechanisms of virus resistance—impaired virus spread in the ECM and inhibition of viral replication after viral entry into tumor cells—are also relevant to 3D tumor cell cultures.

HSV-1 oncolysis can be improved by degradation of fibrillar collagen in tumors indicating that the ECM has an important function in determining treatment efficacy.[15] This study indicates that laminin-rich ECM, Matrigel inhibits HSV-1 spread. These findings are consistent with the earlier reported inhibition of HSV-1 spread by epithelial basement membrane *in vivo* and by Matrigel *in vitro*.[43] It is important to note that HSV-1 could clearly infect and replicate in some uveal melanoma cells that have invaded the Matrigel matrix in this study. These observations indicate that HSV-1 can spread through Matrigel if tumor cells infiltrating the ECM are present. Whether HSV-1 can spread from cell to cell within the Matrigel matrix through intercellular contacts or through spaces in Matrigel created by growing tumor cells remains unclear at this point.

This study also indicates that inhibition of viral replication at a stage beyond viral entry is an important mechanism by which the ECM can modulate viral replication in tumors. It is well known that adhesion of cancer cells to the ECM mediates drug and radiation resistance.[27,29,44] The connection of tumor cells to ECM proteins such as collagen and laminin through cell adhesion molecules, in particular integrin receptors, is associated with tumor cell survival and drug resistance through the activation of a variety of signaling pathways. It is unclear at this point to what extent, if any, mechanisms of drug and radiation resistance in 3D tumor cell cultures are overlapping with mechanisms of virus resistance. It is possible that ECM-mediated signaling affects the expression of cellular transcription factors that can regulate the expression of viral genes in a manner that is not favorable for the progression of the viral replication cycle after HSV-1 entry.

Interestingly, observations made in this study suggest that HSV-1 establishes quiescent infection in some tumor cells in 3D cultures. When OCM1 and C918 cells were inoculated with HSV-1 under 2D conditions and were then cultured within Matrigel, only a small minority of tumor cells that have taken up HSV-1 showed evidence of virus replication (GFP expression). As discussed earlier,

these findings indicated that the viral replication cycle was inhibited at a post-entry step in the majority of infected tumor cells. Consequent growth of virus inoculated OCM1 cells in 3D cultures was associated with the establishment of multicellular tumor cell spheroids. Many OCM1 cells forming multicellular spheroids remained GFP negative throughout a 4-week observation period. However, the outgrowth of individual OCM1 cells into the Matrigel matrix from spheroids that have been GFP negative for days to weeks was often associated with the appearance of GFP expression in outgrowing cells and in cells within the spheroids. As Matrigel inhibits virus spread, reappearance of GFP expression in multicellular spheroids was very suggestive of virus reactivation from quiescence in earlier HSV-1 inoculated cells. It is well known that HSV-1 can establish quiescent infection in cultured non-neuronal cells if the progression of the viral replication cycle is blocked shortly after virus entry.[45,46] However, establishment of quiescent infection in tumor cells induced by the ECM environment and reactivation of viral replication on changing tumor growth pattern have not been yet been reported. It will be of practical significance to determine whether similar processes also occur *in vivo* during HSV-1 oncolytic therapy.

In summary, observations reported here provide novel information about virus resistance of distinct tumor cell subpopulations in 3D tumor cell cultures and about mechanisms of ECM-mediated virus resistance of tumor cells. It is clear that additional studies will be required to fully understand the mechanisms by which the ECM mediates increased HSV-1 resistance of tumor cells in 3D cultures and to assess the clinical relevance of information collected in these cultures. However, our observations suggest that the experimental platform provided by 3D tumor cultures will be invaluable for studies aimed at the improvement and preclinical evaluation of viral oncolytic agents similarly to its usefulness in the case of chemotherapeutic agents and radiation therapy.

Conflict of interest

The authors declare no conflict of interest.

Acknowledgements

This work was supported by fellowship grants to SD, SKK, SB, and AV by the Rosztoczy Foundation and by Public Health Service grant EY10457 to RF. RF is currently with Oakland University William Beaumont School of Medicine.

References

1 Guo SZ, Thorne SH, Bartlett DL. Oncolytic virotherapy: molecular targets in tumor-selective replication and carrier cell-mediated delivery of oncolytic viruses. *Biochim Biophys Acta* 2008; **1785**: 217–231.
2 Liu TC, Kirn D. Gene therapy progress and prospects cancer: oncolytic viruses. *Gene Ther* 2008; **15**: 877–884.
3 Latchman DS. Herpes simplex virus-based vectors for the treatment of cancer and neurodegenerative disease. *Curr Opin Mol Ther* 2005; **7**: 415–418.
4 MacKie RM, Stewart B, Brown SM. Intralesional injection of herpes simplex virus 1716 in metastatic melanoma. *Lancet* 2001; **357**: 525–526.
5 Shen Y, Nemunaitis J. Herpes simplex virus 1 (HSV-1) for cancer treatment. *Cancer Gene Ther* 2006; **13**: 975–992.
6 Varghese S, Rabkin SD. Oncolytic herpes simplex virus vectors for cancer virotherapy. *Cancer Gene Ther* 2002; **9**: 967–978.
7 Chiocca EA. The host response to cancer virotherapy. *Curr Opin Mol Ther* 2008; **10**: 38–45.
8 Benecia F, Courreges MC, Fraser NW, Coukos G. Herpes virus oncolytic therapy reverses tumor immune dysfunction and facilitates tumor antigen presentation. *Cancer Biol Ther* 2008; **7**: 1194–1205.
9 Fukuhara H, Todo T. Oncolytic herpes simplex virus type 1 and host immune responses. *Curr Cancer Drug Targets* 2007; **7**: 149–155.
10 Miller CG, Fraser NW. Requirement of an integrated immune response for successful neuroattenuated HSV-1 therapy in an intracranial metastatic melanoma model. *Mol Ther* 2003; **7**: 741–747.
11 Toda M, Rabkin SD, Kojima H, Martuza RL. Herpes simplex virus as an in situ cancer vaccine for the induction of specific anti-tumor immunity. *Hum Gene Ther* 1999; **10**: 385–393.
12 Guzman G, Oh SD, Shukla D, Valyi-Nagy T. Nectin-1 expression in the normal and neoplastic human female gynecologic tract. *Arch Pathol Lab Med* 2006; **130**: 1191–1195.
13 Guzman G, Oh SD, Shukla D, Engelhard HH, Valyi-Nagy T. Expression of entry receptor nectin-1 of Herpes simplex virus 1 and/or Herpes simplex virus 2 in normal and neoplastic human nervous system tissues. *Acta Virol* 2006; **50**: 59–66.
14 Kolodkin-Gal D, Zamir G, Edden Y, Pikarsky E, Pikarsky A, Haim H *et al*. Herpes simplex virus type 1 preferentially targets human colon carcinoma: role of extracellular matrix. *J Virol* 2008; **82**: 999–1010.
15 McKie TD, Grandi P, Mok W, Alexandrakis G, Insin N, Zimmer JP *et al*. Degradation of fibrillar collagen in a human melanoma xenograft improves the efficacy of an oncolytic herpes simplex virus vector. *Cancer Res* 2006; **66**: 2509–2513.
16 Nagano S, Perentes JY, Jain RK, Boucher Y. Cancer cell death enhances the penetration and efficiency of oncolytic herpes simplex virus in tumors. *Cancer Res* 2008; **68**: 3795–3802.
17 Rueger MA, Winkeler A, Miletic H, Kaestle C, Richter R, Schneider G *et al*. Variability in infectivity of primary cell cultures of human brain tumors with HSV-1 amplicon vectors. *Gene Ther* 2005; **12**: 588–596.
18 Yu Z, Adusumilli PS, Eisenberg DP, Darr E, Ghossein RA, Li S *et al*. Nectin-1 expression by squamous cell carcinoma is a predictor of herpes oncolytic sensitivity. *Mol Ther* 2007; **15**: 103–113.
19 Yun CO. Overcoming the extracellular matrix barrier to improve intratumoral spread and therapeutic potential of oncolytic virotherapy. *Curr Opin Mol Ther* 2008; **10**: 356–361.
20 Abbott A. Biology's new dimension. *Nature* 2003; **424**: 870–872.
21 Friedrich MJ. Studying cancer in 3 dimensions. *JAMA* 2003; **290**: 1977–1979.

22 Ghosh S, Spagnoli GC, Martin I, Ploegert S, Demougin P, Heberer M *et al*. Three-dimensional culture of melanoma cells profoundly affects gene expression profile: a high density oligonucleotide array study. *J Cell Physiol* 2005; **204**: 522–531.
23 Smalley KS, Lioni M, Herlyn M. Life isn't flat: taking cancer biology to the next dimension. *In vitro Cell Dev Biol Anim* 2006; **42**: 242–247.
24 Nelson CM, Bissell MJ. Modeling dynamic reciprocity: engineering three-dimensional culture models of breast architecture, function, and neoplastic transformation. *Semin Cancer Biol* 2005; **15**: 342–352.
25 Xu F, Burg KJL. Three-dimensional polymeric systems for cancer cell studies. *Cytotechnology* 2007; **54**: 135–143.
26 Schmeichel KL, Bissell MJ. Modeling tissue-specific signaling and organ function in three dimensions. *J Cell Sci* 2003; **116**: 2377–2388.
27 Schmidmaier R, Baumann P. Anti-adhesion evolves to a promising therapeutic concept in oncology. *Curr Med Chem* 2008; **15**: 978–990.
28 Wang F, Weaver VM, Petersen OW, Larabell CA, Dedhar S, Briand P *et al*. Reciprocal interactions between beta1-integrin and epidermal growth factor receptor in three-dimensional basement membrane breast cultures: a different perspective in epithelial biology. *Proc Natl Acad Sci USA* 1998; **95**: 14821–14826.
29 Weaver VM, Petersen OW, Wang F, Larabell CA, Briand P, Damsky C *et al*. Reversion of the malignant phenotype of human breast cells in three-dimensional culture and *in vivo* by integrin blocking antibodies. *J Cell Biol* 1997; **137**: 231–245.
30 Jacks T, Weinberg RA. Taking the study of cancer cell survival to a new dimension. *Cell* 2002; **111**: 923–925.
31 Vescio RA, Redfern CH, Nelso TJ, Udoretz S, Stern PH, Hoffman RM. *In vivo*-like drug responses of human tumors growing in three-dimensional gel-supported primary culture. *Proc Natl Acad Sci USA* 1987; **84**: 5029–5033.
32 Shimony N, Gorodetsky R, Marx G, Gal D, Rivkin R, Ben-Ari A *et al*. Fibrin microbeads (FMB) as a 3D platform for kidney gene and cell therapy. *Kidney Int* 2006; **69**: 625–633.
33 Valyi-Nagy K, Folberg R, Valyi-Nagy T, Maniotis AJ. Susceptibility of uveal melanoma to herpes simplex virus type 1: the role of tumor invasiveness, the extracellular matrix and chromatin sequestration. *Exp Eye Res* 2007; **84**: 991–1000.
34 Folberg R, Hendrix MJ, Maniotis AJ. Vasculogenic mimicry and tumor angiogenesis. *Am J Pathol* 2000; **156**: 361–381.
35 Folberg R, Arbieva Z, Moses J, Hayee A, Sandal T, Kadkol S *et al*. Tumor cell plasticity in uveal melanoma—microenvironment directed dampening of the invasive and metastatic genotype and phenotype accompanies the generation of vasculogenic mimicry patterns. *Am J Pathol* 2006; **169**: 1376–1389.
36 Folberg R, Leach L, Valyi-Nagy K, Lin AY, Apushkin MA, Ai Z *et al*. Modeling the behavior of uveal melanoma in the liver. *Invest Ophthalmol Vis Sci* 2007; **48**: 2967–2974.
37 Folberg R, Maniotis AJ. Vasculogenic mimicry. *APMIS* 2004; **112**: 508–525.
38 Maniotis AJ, Folberg R, Hess A, Seftor EA, Gardner LMG, Pe'er J *et al*. Vascular channel formation by human melanoma cells *in vivo* and *in vitro*: vasculogenic mimicry. *Am J Pathol* 1999; **155**: 739–752.
39 Maniotis AJ, Valyi-Nagy K, Karavitis J, Moses J, Boddipali JV, Wang Y *et al*. Chromatin organization measured by Alu I restriction enzyme changes with malignancy and is regulated by the extracellular matrix and the cytoskeleton. *Am J Pathol* 2005; **166**: 1187–1203.
40 Desai P, Pearson S. Incorporation of the green fluorescent protein into the herpes simplex virus type 1 capsid. *J Virol* 1998; **72**: 7563–7568.
41 Akhtar J, Tiwari V, Oh M, Kovacs M, Jani A, Kovacs SK *et al*. HVEM and nectin-1 are the major mediators of herpes simplex virus 1 (HSV-1) entry into human conjunctival epithelium. *Invest Ophthalmol Vis Sci* 2008; **49**: 4026–4035.
42 Folberg R, Kadkol S, Frenkel S, Valyi-Nagy K, Jager MJ, Pe'er J *et al*. Authenticating cell lines in ophthalmic research laboratories. *Invest Ophthalmol Vis Sci* 2008; **49**: 4697–4701.
43 Weeks BS, Ramchandran RS, Hopkins JJ, Friedman HM. Herpes simplex virus type-1 and -2 pathogenesis is restricted by the epidermal basement membrane. *Arch Virol* 2000; **145**: 385–396.
44 Weaver VM, Lelievre S, Lakins JN, Chrenek MA, Jones JC, Giancotti F *et al*. Beta4 integrin dependent formation of polarized three-dimensional architecture confers resistance to apoptosis in normal and malignant mammary epithelium. *Cancer Cell* 2002; **2**: 205–216.
45 Preston CM. Repression of viral transcription during herpes simplex virus latency. *J Gen Virol* 2000; **81**: 1–19.
46 Valyi-Nagy T, Shukla D, Engelhard HH, Kavouras J, Scanlan P. Latency strategies of alphaherpesviruses: herpes simplex virus and varicella-zoster virus latency in neurons. In: Minarovits J, Gonczol E, Valyi-Nagy T (eds). *Latency Strategies of Herpesviruses*. Springer: New York, 2007. pp 1–36.